UNIVERSIDAD DE CHILE
FACULTAD DE CIENCIAS FÍSICAS Y MATEMÁTICAS
DEPARTAMENTO DE GEOLOGÍA

GEOCRONOLOGÍA DEL BASAMENTO PALEOZOICO DEL CENTRO-SUR DE CHILE, IMPLICANCIAS EN LA EVOLUCIÓN TECTÓNICA DE GONDWANA OCCIDENTAL

TESIS PARA OPTAR AL GRADO DE MAGISTER EN CIENCIAS,
MENCIÓN GEOLOGÍA

RURIK ANDRÉS ROMERO NÚÑEZ

PROFESOR GUÍA:
FERNANDO BARRA PANTOJA

PROFESOR CO-GUÍA:
JOSÉ MARÍA GONZÁLEZ-JIMÉNEZ

MIEMBROS DE LA COMISIÓN:
MARTIN REICH MORALES
DIEGO MORATA CÉSPEDES

Este trabajo ha sido financiado por los Proyectos FONDECYT 1110345, FONDECYT DE INICIACION 11140005, y Núcleo Milenio Trazadores de Metales NC130065

SANTIAGO DE CHILE
2017

RESUMEN DE TESIS PARA OPTAR AL GRADO DE MAGÍSTER EN CIENCIAS MENCIÓN GEOLOGÍA
POR: Rurik Romero Núñez
FECHA: 13 de Marzo de 2017
PROFESOR GUÍA: Dr. Fernando Barra P.

GEOCRONOLOGÍA DEL BASAMENTO PALEOZOICO DEL CENTRO-SUR DE CHILE, IMPLICANCIAS EN LA EVOLUCIÓN TECTÓNICA DE GONDWANA OCCIDENTAL

Se presentan dataciones U-Pb en circones detríticos de la Serie Occidental del Basamento Metamórfico del centro-sur de Chile y el Complejo Piedra Santa (CPS) en Argentina, como también en las zonas de reacción entre las rocas ultramáficas de La Cabaña (~38°30'S) y en las cromititas encontradas en la misma zona.

Se detectan tres poblaciones características de circones detríticos dentro del área de estudio.

La primera se caracteriza por tener edades máximas de depósito en el Carbonífero Temprano, ausencia de circones devónicos y un alto aporte de circones ordovícicos (~470 Ma), además de circones meso-proterozoicos entre los 1000-1200 Ma. Este patrón se encuentra en las metapelitas de la Serie Oriental y en la sección norte de la Serie Occidental hasta las peridotitas de La Cabaña, como también en el CPS. Se presenta también una edad U-Pb de 301.9±2.6 Ma en un granitoide del Complejo Plutónico Chachil que intruye a esta última unidad.

La segunda población se caracteriza por un aporte casi exclusivo de edades pérmicas (260-298 Ma) las cuales definen su edad máxima de depósito. Estas poblaciones se encuentran en las localidades al sur de los 39°S hasta los 40°S.

La tercera población tiene principalmente circones devónicos (360-380 Ma) y edades máximas de depósito carboníferas. Esta se encuentra en los metasedimentos al sur-oeste de La Cabaña y al norte de los 39°S.

Tanto la distribución de estas edades como la intrusión del Batolito de la Costa y su continuidad con el Complejo Plutónico Chachil y los cuerpos carboníferos del Macizo Nordpatagónico, permiten concluir que existe una yuxtaposición de distintos bloques del basamento a través de la Zona de Falla Mocha-Villarrica, donde el bloque que alberga La Cabaña corresponde al bloque mejor conservado de la Serie Occidental. Por lo anterior se sugiere el uso del término Complejo Metamórfico de La Cabaña para referirse al basamento entre la Zona de Falla Lanalhue y Mocha-Villarrica.

Por otra parte, tanto los circones encontrados en las zonas de reacción como en las cromititas poseen una distribución de edades y características morfológicas similares a los encontrados en los metasedimentos. Esto, sumado a la presencia de circones metamórficos de ca. 285 Ma en ambas litologías, permiten concluir que fluidos provenientes desde los metasedimentos removilizaron circonio y posiblemente fragmentos de circones de estos últimos dentro de las rocas ultramáficas, constriñendo la edad a la que se incorporan las rocas ultramáficas al complejo metamórfico.

Agradecimientos

Primero, agradecer el apoyo de los proyectos Fondecyt 110345 y Fondecyt de Iniciación 11140005 a cargo del Dr. Fernando Barra y Dr. José María González, respectivamente, cuyo financiamiento permitió el desarrollo de este trabajo de tesis. Por supuesto también destacar el apoyo financiero y humano otorgado por el Núcleo Milenio Trazadores de Metales (NC130065) y el Centro de Excelencia en Geotermia de Los Andes (FONDAP 15090013).

Amplios agradecimientos los miembros de la comisión evaluadora, cuyos comentarios y correcciones han mejorado sustantivamente la calidad del trabajo presentado. Especiales agradecimientos a los profesores Fernando Barra y José María González cuyos aportes, discusiones y calidez humana fueron indispensables tanto para llevar adelante este trabajo como también para martillar piedras y maravillarme con las fuerzas de la naturaleza. Muchas gracias por depositar su confianza en mí por todos estos años, que han sido varios. Efectivamente, vi de qué están hechos los cerros.

Gran parte de este trabajo se realizó con la colaboración de Mathieu Leisen en el laboratorio de espectrometría de masas, por lo cual agradezco su disposición de enseñarme del extraño mundo de los laboratorios y la sinergia para combatir contra los caprichos de Caprichosa (que también tiene un lugar en mi corazón). También destacar el aporte de Verónica Rodríguez en cuanto al cariñoso rigor entregado en estos años, sin duda, la mejor jefa. Agradecimientos también para A. Tassara (UDEC) por la invitación a terreno al Complejo Piedra Santa.

Por supuesto, agradecer a mis padres por apoyarme en el mundo del postgrado y a mi familia, en especial a mi hermana que ya dejó de ser un ser individual y ahora pasó a ser la portadora de Silvestre. También agradecer ampliamente a Katia Rossel por el amplio apoyo brindado que me convenció día tras día de trabajar, y lo logró, obviamente sin ella esto salía para un par de años más.

Obviamente agradezco a todos aquellos que de una u otra forma aportaron a este trabajo. Los miembros de la Sala Milenio: E. Salazar, J. Rivera, F. Orellana (QEPD), L. Garrido, G. Palma (Giselita), I. Maureira, A. Gómez (Negro), P. Rojas, A. Genot, S. Tassara, N. Román, C. Milojevic, J. Crespo, C. Johansson, A.P. Herazo. En especial destacar el aporte esencial para este trabajo de las tardes de tertulia conformadas por Eduardo “Salo” Salazar y Javier “Yayer” Rivera donde las misceláneas temáticas aportaron directamente al trabajo presentado, alinearon chakras y distendieron la amargura que año a año, con orgullo, he forjado.

Agradecer también a los socios de Triple Q: K. Rossel (KQ) y F. Riquelme (FQ), por sacar adelante el proyecto paralelo de producción de cerveza. Lo estamos haciendo bien, y se nota.

Por último destacar la disposición de Smashville y El Concilio para distraerme en los momentos más críticos, esa distención fue clave para las últimas fases de trabajo.

Tabla de Contenido

Índice de Anexos

1. Introducción

1.1. Planteamiento del Problema

El Basamento Paleozoico del centro sur de Chile aflora continuamente desde los 32°-42°S en el margen costero del país, constituyendo gran parte de la unidad morfoestructural de la Cordillera de la Costa.

Este complejo, conformado mayoritariamente por esquistos cuarzo-micáceos, ha sido clásicamente interpretado como un gran cinturón metamórfico pareado en un contexto acrecionario del margen gondwánico en el Paleozoico Tardío. La principal unidad tratada en este trabajo, la Serie Occidental, posee la particularidad de presentar una serie de cuerpos máficos y ultramáficos que, a grandes rasgos, fueron metamorfizados bajo condiciones de alta presión y baja temperatura junto a los metasedimentos (Willner, 2005).

Sin embargo, en los últimos años, diversos autores han detectado distintos dominios tectónicos en esta gran unidad aparentemente homogénea, ya sea por dataciones radiométricas de circones detríticos de los metasedimentos (e.g. Hervé et al., 2013), como también el análisis geoquímico detallado de las rocas máficas y ultramáficas que se emplazan en la Serie Occidental (e.g. González-Jiménez et al., 2016).

Regionalmente, Hervé et al. (2013) distingue dos dominios de la Serie Occidental marcados por la Zona de Falla Lanalhue (ZFL) aproximadamente a los 38°S (Glodny et al., 2008), donde los patrones de circones detríticos al norte de ésta presentan edades máximas de depósito carboníferas y al sur un abrupto cambio a edades pérmicas. A pesar de lo anterior, en este último trabajo no se presentan este tipo de datos en una amplia extensión desde la ZFL hasta los 40°S.

El estudio de circones detríticos entre los 38°-40°S es crítico, en vista de que en esta zona se encuentran una serie de cuerpos ultramáficos de variada magnitud y cuyo origen se discute hasta el día de hoy. En particular, la metaperidotita de La Cabaña (~38°30’S) constituye el mayor afloramiento conocido de rocas ultramáficas del basamento cristalino y ha sido ampliamente estudiado debido a que es el único cuerpo ultramáfico conocido con cromitita masiva en Chile.

Existe un consenso en cuanto a que la formación de la metaperidotita de La Cabaña corresponde a una ofiolita en un contexto de suprasubducción, pero el ambiente tectónico ha sido ampliamente discutido hasta el día de hoy, variando desde una posición de antearco (Hervé et al., 1976; Godoy, 1979), trasarco (Frutos y Alfaro, 1987, Rabbia et al., 1994; Hufmann y Massone 200; Hofer et al., 2001) o intra-arco (Barra et al., 1998; González-Jiménez et al., 2014; 2016).

Sumado a lo anterior, en vista de que no existe una caracterización geocronológica de los metasedimentos que hospedan las rocas ultramáficas de La Cabaña, no es posible acotar el momento de acreción del macizo al margen.

Es por ello que en el presente trabajo se plantea que una red de muestreo detallada de circones detríticos de los esquistos metapelíticos que conforman la Serie Occidental podría dar indicios de distintos dominios tectónicos dentro del basamento metamórfico y una posible paleogeografía del margen gondwánico. A su vez, la caracterización del bloque albergante de La Cabaña junto con circones dentro de estos cuerpos, podrían dar cuenta de los procesos metamórficos acrecionarios y sedimentarios pre-acrecionarios al que fue sometido este macizo.

1.2. Objetivos

1.2.1. Objetivo General

Establecer el contexto tectónico y temporalidad de la acreción de los sedimentos y del cuerpo ultramáfico de La Cabaña en la Serie Occidental en un modelo evolutivo del margen gondwánico durante el Paleozoico Tardío.

1.2.2. Objetivos Específicos

1. Determinar las variaciones poblacionales de edades U-Pb en circones detríticos de los metasedimentos de la Serie Occidental entre los 38°-40°S.

2. Definir la proveniencia sedimentaria de circones detríticos, reconociendo posibles paleorelieves característicos del continente en el momento de formación del complejo.

3. Caracterizar las morfologías e imágenes de catodoluminiscencia (CL), junto con edades U-Pb en circones de las zonas de reacción entre las rocas ultramáficas de La Cabaña y los metasedimentos, determinando si el significado de estas edades corresponde a procesos sedimentarios y/o metamórficos.

4. Obtener edades U-Pb de circones extraídos de las cromititas podiformes de La Cabaña, caracterizando morfologías e imágenes CL de los mismos.

5. Integrar la base de datos obtenida en las distintas litologías a datos previamente reportados y determinar las posibles relaciones entre estos marcadores geocronológicos.

1.3. Hipótesis de Trabajo

El análisis regional de circones detríticos de la Serie Occidental permitiría la distinción de bloques tectónicos acretados en diferentes momentos de la evolución del margen paleozoico tardío. Los circones eventualmente presentes en los cuerpos

ultramáficos de La Cabaña y su respectiva zona de reacción deberían ser distintos tanto en edad como tipología a los de la roca encajante, por lo tanto estos podrían registrar el momento en que ambas litologías comparten una misma trayectoria metamórfica.

1.4. Metodologías

Con el propósito de cumplir con los objetivos planteados anteriormente, brevemente se enumeran las metodologías aplicadas en este trabajo. Una descripción más extensa se encuentra en cada una de las secciones posteriores de esta Tesis de Magíster.

1. Separación estándar de circones detríticos de los esquistos metapelíticos y zonas de reacción por medio de molienda, separador magnético Frantz, mesa Gémini y líquidos densos. Laboratorio de Preparación de Muestras del Departamento de Geología, Universidad de Chile.
2. Separación de circones de cromititas podiformes de La Cabaña por medio de Selective Fragmentation (selFrag), líquidos densos y separador magnético Frantz. Laboratorio selFrag, GEMOC/CCFS, Department of Earth and Planetary Sciences, Universidad de Macquarie, Sydney.
3. Obtención de imágenes de backscatter de las cloritas de la zona de reacción de Lavanderos (NE de La Cabaña) y CL de circones de los esquistos metapelíticos por medio de un microscopio electrónico de barrido (SEM) FEI Quanta 250. Laboratorio de microscopía electrónica, Centro de Excelencia en Geotermia Andina (CEGA), Departamento de Geología, Universidad de Chile. Las imágenes de CL de los circones obtenidos en las cromititas de La Cabaña fueron obtenidas con un equipo Zeiss EVO MA15. Geochemical Analysis Unit (GAU), GEMOC/CCFS, Department of Earth and Planetary Sciences, Universidad de Macquarie, Sydney.
4. Datación U-Pb de circones detríticos de los metasedimentos, realizadas en un espectrómetro de masas multicolector (MC-ICPMS) modelo Neptune Plus con un sistema de ablación láser excimero de ArF, modelo Analyte G2, pertenecientes al Laboratorio de Geología Isotópica, CEGA, Universidad de Chile. El análisis de circones más pequeños obtenidos de las cromititas fueron analizados por medio de un equipo SHRIMP II del John de Laeter Centre for Isotope Research, Universidad de Curtin, Perth.

1.5. Presentación y organización de tesis

El cuerpo principal de esta Tesis lo constituyen tres capítulos, dos capítulos corresponden a artículos científicos en vías de ser enviados para su publicación en el transcurso del año 2017.

El capítulo 1 corresponde a la introducción en la cual se presentan los antecedentes sobre el estado del conocimiento y la problemática a tratar, los objetivos generales y específicos del presente trabajo, la hipótesis y metodología, así como la estructura del cuerpo de tesis y una breve contextualización común para ambos trabajos.

El capitulo 2 corresponde al primero de los artículos y se titula "Sedimentary provenance of detrital zircons from Late Paleozoic basement of South Central Chile and Argentina between 37°S and 40°S and its implications for the evolution of the Paleozoic Gondwana margin". En este capítulo se presentan datos geocronológicos de circones detríticos de metasedimentos de Chile y Argentina, que son usados para establecer un modelo tectónico regional del basamento paleozoico tardío en el centro sur de Chile.

El capítulo 3 presenta los resultados e interpretaciones recogidas en el segundo de los artículos y se titula "Timing of the tectonic juxtaposition of ultramafic rocks and metasediments in the southern section of the coastal accretionary complex of Central Chile". En este capítulo se reportan datos originales de mineralogía y geocronología de circones de las rocas ultramaficas, zonas de reacción metasomática entre éstas y los esquistos encajantes, asi como de éstos últimos en el área de La Cabaña. Estos datos, permiten definir por primera vez, y a partir de métodos de gecronología absoluta, la edad del emplazamiento de las rocas ultramáficas en los metasedimentos del complejo acrecionario de la Cordillera de la Costa de Chile.

El cuerpo de tesis se completa con las conclusiones generales alcanzadas en el presente trabajo para optar al Grado de Magister en Geología.

1.6. Marco Geológico

Entre las latitudes 32°S y 42°S, el Basamento Metamórfico del centro sur de Chile aflora continuamente en el margen oeste del país (Fig. 1). Diversos autores (Hervé, 1988; Aguirre et al., 1972; Glodny et al., 2005) asocian esta unidad a un complejo acrecionario con dos sub-unidades asociables a un cinturón metamórfico pareado (*sensu* Miyashiro, 1961) definidas como Serie Oriental y Serie Occidental (Aguirre, 1972).

1.6.1. Serie Occidental

La Serie Occidental está conformada por esquistos micáceos de protolito psamopelítico, metacherts, metabasitas, escasas rocas ultramáficas serpentinizadas (Hervé, 1988) y escasos cuerpos de cromititas podiformes en las metaperidotitas de La Cabaña (Vergara, 1970; Alfaro, 1980; Barra et al., 1998). Este arreglo litológico representaría una mezcla de aportes sedimentarios continentales con porciones superiores de corteza oceánica desmembrada (Hervé et al., 2007) en un contexto de zona de acreción basal (Willner, 2005).

El metamorfismo de esta unidad correspondería a condiciones de alta presión (HP) y baja temperatura (LT) (Fig. 2). Metamorfismo en facies de esquistos verdes es predominante (7-9.3 kbar, 380-400°C) y se asocia al metamorfismo final de exhumación del complejo acrecionario, sin embargo, bloques aislados de esquistos azules conservados indican condiciones metamórficas de mayor presión a 9.5-10.7 kbar y 350-385°C (Willner, 2005). Recientemente, minerales de ultra-alta presión (Ti-clinohumita y Ti-condrodita) se han reportado en La Cabaña indicando condiciones metamórficas de mayor grado (González-Jiménez et al., aceptado)

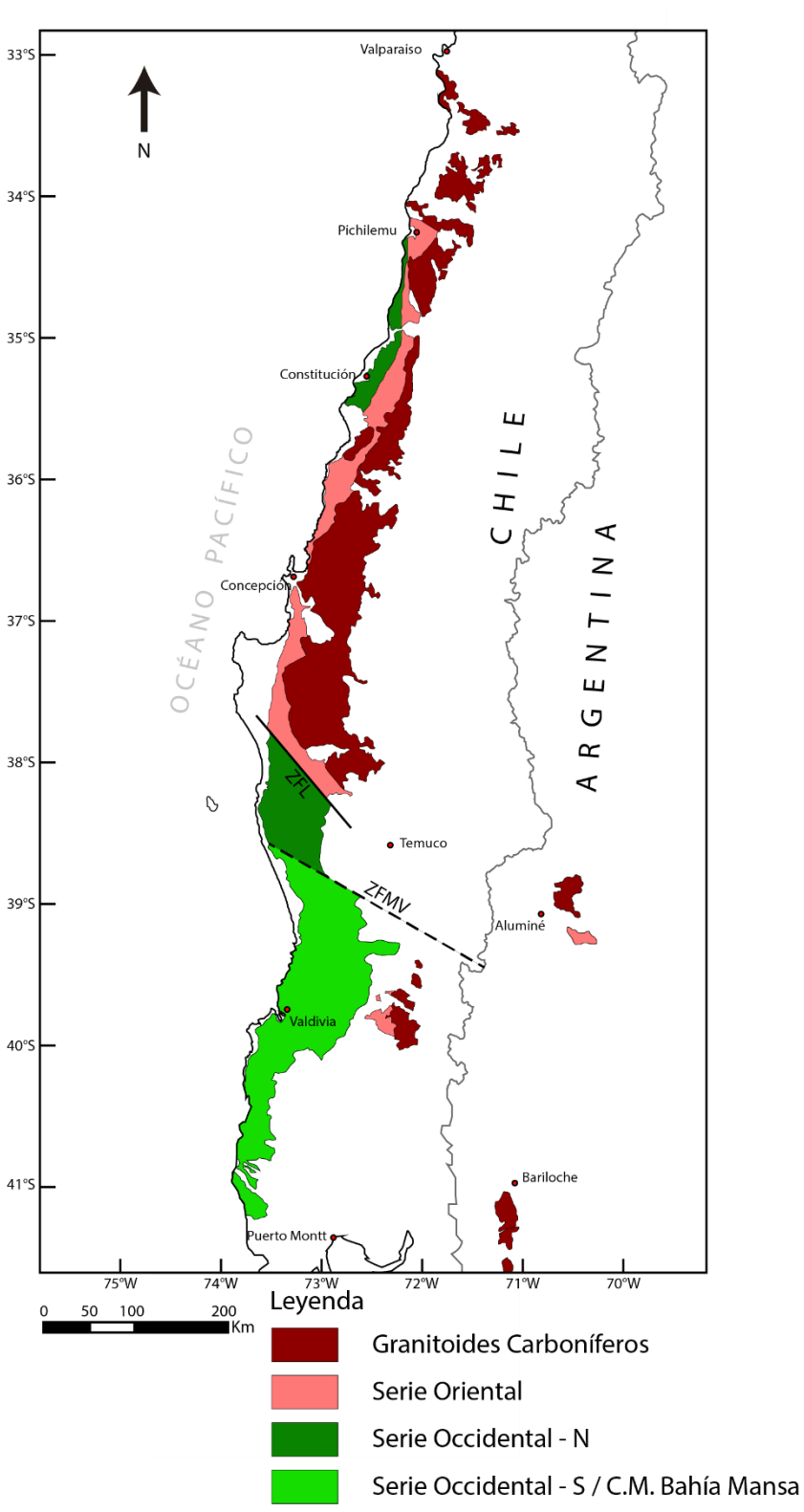

Fig. 1. Mapa geológico del Basamento metamórfico de centro-sur de Chile con sus principales divisiones (modificado de SERNAGEOMIN 2001). ZFL: Zona de Falla Lanalhue, ZFMV: Zona de Falla Mocha-Villarrica.

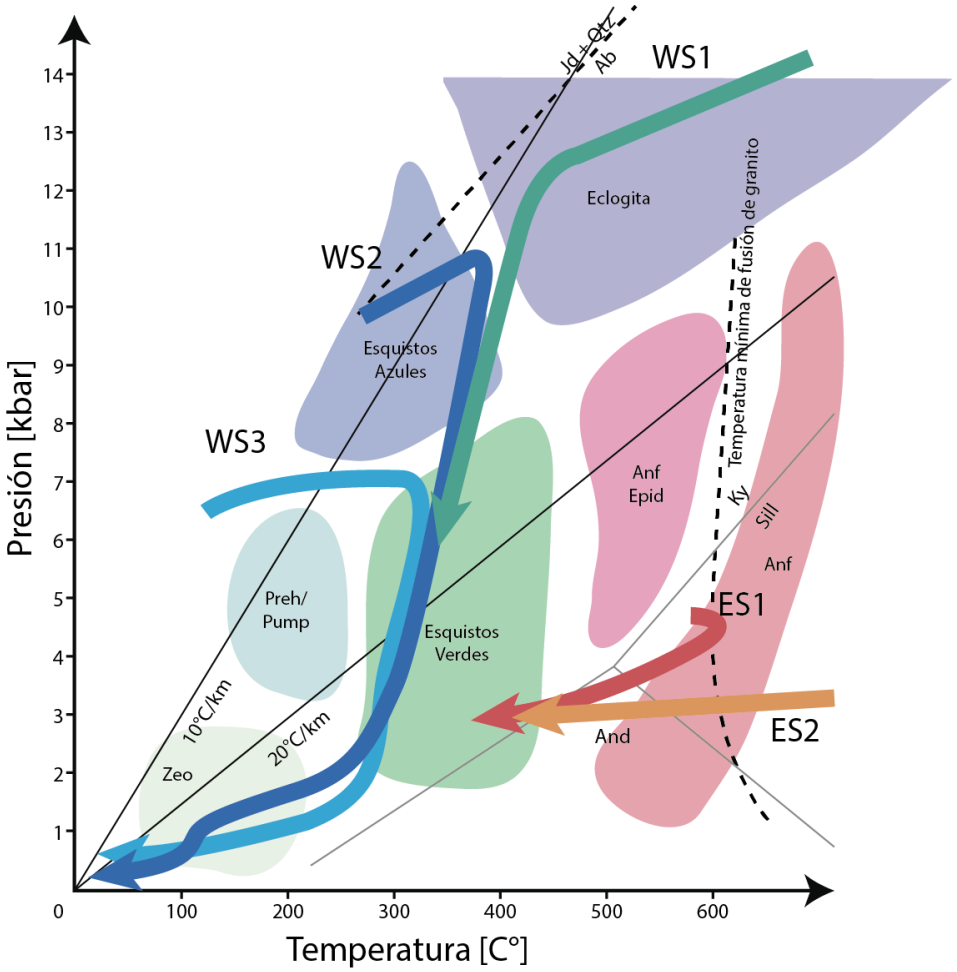

Fig. 2. Trayectorias P-T-t para las distintas unidades presentes en el Complejo Acrecionario Paleozoico Tardío de Chile central. Las curvas WS denotan trayectorias de la Serie Occidental (WS1 = bloque exótico; WS2 = Esquisto Verde; WS3 = Esquisto Azul), mientras que las ES corresponden a la Serie Oriental. Figura modificada de Hervé et al. (2007).

Las edades radiométricas más relevantes que constriñen los procesos metamórficos de la Serie Occidental son principalmente edades de enfriamiento de micas con el método $^{40}Ar/^{39}Ar$. Este proceso de enfriamiento se llevaría a cabo entre los 290-319 Ma (Willner et al., 2005) en las latitudes de 32-35°30'S. Contrastantemente más jóvenes son las edades al sur de los 39°S, donde estas fluctúan desde los 240-250 Ma (Duhart et al., 2001). Una sola edad radiométrica K-Ar en fuschitas se ha reportado para la zona de La Cabaña, dando una edad de 282 ± 6 Ma (Hofer et al., 2001).

1.6.2. Serie Oriental

La Serie Oriental está formada principalmente por metareniscas y metapelitas con moderada deformación que permite preservar algunas estructuras sedimentarias originales (González-Bonorino, 1971; Hervé, 1988) que son menos claras en la sección este de la unidad, cercano al Batolito de la Costa donde el grado metamórfico aumenta debido a la

intrusión de este mismo (Willner et al., 2005) principalmente en tiempos pennsylvanianos entre los 300-320 Ma (Hervé et al., 1988; Lucassen et al., 2004; Deckart et al., 2014).

1.6.3. Relaciones de contacto

El contacto entre ambas series es transicional en las cercanías de Constitución hacia el sur, mientras que en la porción norte se asocia a la falla Pichilemu-Vichuquén, de carácter frágil, cuya traza es menos clara hacia el sur (Willner, 2005). A su vez existe otra transición abrupta en el contacto de ambas series a los 38°S donde la Zona de Falla Lanalhue (Fig. 1) de orientación NW-SE, yuxtapone la unidad de acreción basal con la frontal debido a un aparente movimiento sinestral (Glodny et al., 2008) y marcaría la transición entre esquistos con circones de edades máximas de depósito carbonífera al norte de esta, contrastado con circones de edades máximas pérmicas al sur (Hervé et al., 2013).

1.6.4. Batolito de la Costa

El Batolito de la Costa de Chile Central (Muñoz Cristi, 1962) se compone principalmente de granitoides calcoalcalinos con edades que fluctúan en el Carbonífero Tardío. Este se extiende aproximadamente hasta el 38°S hacia el sur e intruye las rocas correspondientes a la Serie Oriental. A los 40°S existe un aparente movimiento hacia el este del batolito, aflorando en el cordón principal de la Cordillera de los Andes, conocido también como Batolito Futrono-Riñihue, ubicándose en el flanco norte del Lago Ranco (Rodríguez et al., 1998). La temporalidad y características del Batolito de la Costa serían concordantes con aquellas reportadas por Pankhurst et al. (2006) para una serie de afloramientos orientados de forma NW-SE al sur del Batolito Futrono-Riñihue, el cual propone una posible continuidad de este magmatismo en territorio argentino en lo que correspondería al Batolito Nordpatagónico.

2. Sedimentary provenance of detrital zircons from Late Paleozoic basement of South Central Chile and Argentina between 37°S and 40°S and its implications for the evolution of the Paleozoic Gondwana margin

Rurik Romero, Fernando Barra, Mathieu Leisen, Eduardo Salazar, José María González-Jiménez, Martin Reich

Department of Geology and Andean Geothermal Center of Excellence (CEGA), FCFM, Universidad de Chile, Plaza Ercilla 803, Santiago, Chile.

Submitted

to

___

*Corresponding author: Rurik Romero

Address: Universidad de Chile, Departamento de Geología,

Plaza Ercilla # 803, Santiago de Chile, Chile

Phone: +56 2 978 06 43

E-mail: rurikrom@gmail.com

Abstract

U-Pb detrital zircon patterns are presented for eight samples from metapelites of the Metamorphic Basement of South-Central Chile between the 37-40°S, along with a sample from the Piedra Santa Metamorphic Complex and a single U-Pb crystallization age of the Chachil Plutonic Complex located in Argentina.

The metamorphic basement on the studied area has two sub-units. The Eastern series is composed mainly of weakly deformed metasedimentary rocks superimposed with high temperature and low pressure metamorphism. The Western Series comprises metasedimentary rocks, metabasites and ultramafic rocks, and is typically mapped as a single and uniform unit between 38-40°S.

Two main distinct zircon populations are identified along the metamorphic basement. The first has Carboniferous maximum ages of deposition, a remarkable population of Ordovician zircons relatively close to a ~470 Ma age peak and widespread presence of Meso-proterozoic ages (1000 - 1200 Ma). The second group is drastically different, with Permian maximum ages of deposition (250 – 290 Ma) which concentrates the main population of these samples, secondary contribution of Pensylvanian and devonian-age zircons.

Our results shows that the distribution of each population is controlled by the Mocha-Villarrica Fault Zone, where metapelite samples north from this lineament shows patterns from the first described group including the Piedra Santa Complex, Argentina, which in fact is intruded by the Chachil Plutonic complex at 301.9±2.6 Ma. We postulate that the Piedra Santa Complex is part of the same accretional process as the metamorphic basement of Chile.

On the other hand, most samples south from the fault shows patterns from the second group, showing a sharp transition between an older Western Series-N and a younger Western Series-S (or Bahía Mansa Metamorphic Complex).

The present dislocation of blocks with different age would be product from a continental-scale dextral strike-slip tectonics along the Huincul Fault Zone which continues in westward direction as the Mocha Villarrica Fault Zone.

Keywords: Metamorphic Basement, Detrital Zircons, Western Series

1. Introduction

The Late Paleozoic metamorphic basement of south-central Chile crops out continuously from 32° to 42°S in the Coastal Cordillera of central Chile, and has been traditionally interpreted as a paired metamorphic belt in an accretionary context of the Gondwana continent western margin (e.g., Hervé, 1988). The basement has been divided in two geologic units: an Eastern and Western Series. The Eastern Series comprises metasedimentary rocks characterized by high temperature and low pressure (HT-LP) conditions (González-Bonorino, 1971; Hervé, 1988; Willner, 2005). The Western Series includes micaschists, metabasites, and serpentinized ultramafic rocks (Hervé, 1988). The unit is characterized by high pressure and low temperature (HP-LT) conditions within greenschist facies (Willner, 2005).

Typically, the Western Series have been mapped as a single and uniform unit of the metamorphic complex due to a fairly homogeneous lithological arrangement, mostly highly foliated ‘greyschists’ of metapelitic origin. Previous geochronological approaches on this unit have detected very different cooling ages of this unit (Duhart et al., 2001; Willner et al., 2005) and very different detrital zircon patterns (Hervé et al., 2013) depending mainly on the geographical location of the studied sample. This last observation lead the interpretation that the Lanalhue Fault Zone (LFZ; Glodny et al., 2008) was the tectonic limit between the older Northern Western Series (WS-N) and a younger Southern Western Series (WS-S) (Hervé et al., 2013).

Nevertheless, there are no reported detrital zircon data between the LFZ and the 40°S, which is critical due the presence of a series of mafic and ultramafic bodies which origin is still debated on this date. In this work we propose that a detailed characterization of the

metasedimentary basement of south central Chile between the 37°-40°S, focused on detrital zircon data, can reveal and constrain different domains within the Western Series.

Here we provide new geochronological data for several metasedimentary samples located in the Western and Eastern Series in order to develop a tectonic model for the western margin of Gondwana during the Late Paleozoic, and provide insights on the evolution of the Paleozoic basement of south-central Chile, integrating new elements to this tectonic framework as the La Cabaña metaperidotites (~38°30'S) and the Piedra Santa Formation in Argentina.

We present new detrital U-Pb ages for nine samples from the metasedimentary rocks of the metamorphic basement between 37°S and 40°S, identifying the main population ages from the metamorphic belt, mainly from the Western Series, and correlate them with the various tectonic processes in the western margin of South America during the Paleozoic. Additionally, we provide a U-Pb crystallization age for the Chachil Plutonic Complex, Argentina, which intrudes the Piedra Santa Formation to check a possible continuity of the chilean Coastal Batholith on a eastern location or a potential sedimentary source for the metasedimentary metamorphic basement.

2. Geological Background

The metamorphic basement of south-central Chile has been interpreted as a paired metamorphic belt (*sensu* Miyashiro, 1961) formed within an accretionary complex setting (Aguirre et al, 1972; Hervé, 1988; Willner et al, 2001; Glodny et al, 2005). On the other hand, other authors have interpreted that the metamorphic basement formed within a back-arc basin during the Late Carboniferous (Frutos and Alfaro 1987; Rabbia et al. 1994; Hufmann and Massonne 2000; Höfer et al. 2001). More recently, González-Jiménez et al. (2014) proposed that the accretionary complex formed in a marginal basin setting in a suprasubduction context.

Aguirre et al. (1972) divided the basement in two geologic units: an Eastern and Western Series. The Eastern Series comprises mainly metasandstones and metapelites with moderate deformation (González-Bonorino, 1971; Hervé, 1988). This geologic unit is characterized

by high temperature and low pressure (HT-LP) conditions, with higher temperature conditions related to the intrusion of the Coastal Batholith (Willner, 2005).

The Western Series includes micaschists of psamopelitic protoliths, metabasites, serpentinized ultramafic rocks (Hervé, 1988) with podiform chromitites in La Cabaña area (Vergara, 1970; Alfaro, 1980; Barra et al., 1998). The Western Series represents a mixture of continental sedimentary contributions with upper portions of oceanic crust (Hervé et al., 2007) within the context of basal accretion processes (Willner, 2005).

Overall, the unit is characterized by high pressure and low temperature (HP-LT) conditions within greenschist facies with peak metamorphic conditions at 7.0-9.3 kbar and 380°-420°C between 34° and 35°S (Willner, 2005), 250°-<500°C on Cr-spinel alteration from La Cabaña metaperidotites (Barra et al., 2014), 6-8 kbar and 270°-370°S at Bahia Mansa (Willner et al., 2001), and 8-9 kbar and 420°C near Valdivia (Glodny et al., 2005).

The Western Series has been divided in a northern and southern section, i.e., WS-N and WS-S, respectively, based on different detrital zircons sources (Hervé et al. 2013) and a tectonic control imposed by the Lanalhue Fault Zone (LFZ). The LFZ (Fig. 1) located at ca. 38°S, is a sinistral NW–SE-striking fault system that juxtaposes the Eastern and Western Series (Glodny et al., 2008).

3. Previous Geochronological Data

A limited number of studies have reported radiometric ages for the Late Paleozoic basement of south-central Chile. The Coastal Batholith at the latitudes of the study area, was dated using the Rb-Sr isochron method in samples from the Nahuelbuta range. The obtained whole rock isochron yielded an age of 294±24 Ma (MSWD = 1.3; n = 5; Hervé et al., 1988). A similar Rb-Sr isochron age of 306±6 Ma (MSWD = 2.3; n = 4) was obtained from a dioritic intrusion near the city of Concepción (Lucassen et al., 2004). More recently, Deckart et al. (2014) reported U-Pb zircon ages from six localities within the Coastal Batholith, constrained between 300 and 320 Ma.

Cooling ages of the metasedimentary WS-N at 32°-35°30'S were estimated using $^{40}Ar/^{39}Ar$ thermochronology with plateau ages in phengite yielded ages between 290-320 Ma

(Willner et al., 2005). Additionally, in the La Cabaña Massif area, located at ca. 38°30'S, a K-Ar fuchsite age of 282±6 Ma indicates a slightly younger cooling event (Höfer et al., 2001). Further south, in the WS-S, $^{40}Ar/^{39}Ar$ white mica ages are ~50 Ma younger, i.e., 243±4 Ma in Mehuín, ~245 Ma in Morro Bonifacio, and ~248 Ma in Hueicolla (Duhart et al., 2001).

4. Previous Detrital Zircon Studies

4.1. Late Paleozoic Basement of South-Central Chile

Willner et al. (2008) reported U-Pb detrital zircon ages for two samples from Pichilemu and Constitución, obtaining maximum depositional ages of 438 and 368 Ma, respectively. More recently, Hervé et al. (2013) presented U-Pb zircon ages for 10 samples collected from both the Eastern and the Western Series distributed between 34-41°S. These authors concluded that their ages point to distinct provenances controlled by the LFZ. North of the LFZ, samples show Carboniferous maximum ages of deposition, a lack of Devonian zircons and a significant contribution of zircons from early Paleozoic orogens, i.e., the Pampean and Famatinian orogens (500-570 Ma and 420-500 Ma, respectively). On the other hand, south of the LFZ Early Permian peaks are prominent, minor Devonian peaks are present and the contribution of Proterozoic zircons is practically nonexistent (Fig. 2).

4.2 Piedra Santa Complex

The Piedra Santa Complex is a metamorphic unit located on the Neuquén Province (Argentina) which is composed mainly from metapelites and metagreywackes, this unit is also intruded by the Chachil Plutonic Complex which its crystallization age is not well constrained. Lithological features and deformational history suggests a possible association with the Late Paleozoic Metamorphic in Chile. Franzese (1995) reported a series of K-Ar radiometric data yielding ages between 299-311 Ma on metapelitic schists.

In the other hand, the Chachil Plutonic Complex has yielded Permian K-Ar (281±4 Ma; Sillitoe, 1977) and Rb-Sr (285±5 Ma; Varela et al., 1994) ages. In more recent studies, the Voluntad Porphyry, which is closely related to this complex, yielded Late Carboniferous Re-Os molibdenite ages between 312-316 Ma (Garrido et al., 2008).

4.3 Paleozoic Sedimentary Sequences of Argentina

Similar detrital zircon patterns of the Chilean metamorphic basement have been found on other locations of South America. In Argentina, the Ventania System is a sedimentary succession located in the Sierras Australes on the eastern margin of South America (Fig. 3), interpreted as a fold-thrust complex developed as part of the Cape Fold System in South Africa (Ramos, 2008; Ramos et al., 2014). The Tunas Fm. is the upper member of this succession, and comprises a succession of sandstones intercalated with tuff levels. This formation has a detrital zircon pattern similar to the reported for the Chilean metamorphic basement. The lower section of the Tunas Fm. has a Carboniferous maximum deposition age, and an important input of Ordovician zircons as well as a significant contribution of Proterozoic zircons (Ramos et al., 2014), similar to the age pattern found in the Balcarce Fm. (Rapela et al., 2007) and Suri Fm. (Rapela et al., 2011) (Fig 4).

On the other hand, the upper section of the Tunas Fm. Has a markedly different age pattern with a main Permian population with minor Devonian peaks (Ramos et al., 2014; Fig. 4).

Farther south of the inferred limits of Patagonia, the sedimentary Sierra Grande Fm. shows a predominance of Early Paleozoic zircons mainly of Ordovician and Cambrian ages, and a minor presence of Proterozoic zircons (Pankhurst et al., 2006; Uriz et al., 2011; Fig. 4).

5. Tectonic Overview

Sedimentary sources for the units studied here would have originated from accretionary orogens formed during the Paleozoic era. The Early Cambrian Pampean Orogeny (~550-500 Ma) resulted from the collision of the Pampia Terrane with the Rio de la Plata Craton (Rapela et al., 1998). This event is represented in Argentina and is relatively continuous from 32°S to ~38°S.

The Famatinian Orogeny (500-420 Ma) is represented by extensive magmatic and metamorphic activity in the Gondwana margin due to the subduction and collision between Pampia and Cuyania (or Precordillera) terranes. The main period of magmatic activity occurred between 490 and 470 Ma (Pankhurst et al., 1998; 2000; Sims et al., 1998; Stuart-Smith et al., 1999; Rapela et al, 2001).

The North Patagonian Massif (NPM) is a continental block whose origin and relationship with the rest of Gondwana are not well constrained. It extends from Rio Negro, Argentina (~38°S), where the EW trending Huincul Fault Zone (HFZ) defines its northern limit, to the Deseado Massif (43°S) to the south.

The continuity of the Early Paleozoic orogenies south of the Huincul Fault Zone, where Ramos (1984, 2008) proposed a Carboniferous-Permian suture between Patagonia and Gondwana, is widely discussed. South of the Rio Negro, Ordovician granitoids have been reported in the area of Sierra Grande that could represent an extension of the Famatinian orogeny on the NPM (Pankhurst et al., 2006). Furthermore, in the same area, a Pampean deformation event is detected (Dickerson, 2004). Gravimetric and aeromagnetic studies along the Huincul Fault Zone show a truncation of NS trending structures formed during the Early Paleozoic (Chernicoff and Zapettini, 2004). High density rocks such as mafic and ultramafic rocks are expected to be present in a collisional suture and should be recognized using magnetic studies, however neither of these lithologies have been found along the entire fault zone.

On the other hand, this discontinuity has also been interpreted as a shear zone between blocks in the context of escape tectonics, at least for the Sierra Grande area (Gregori et al., 2008). Paleomagnetic poles in the clastic units of the Sierra Grande Formation are closely related to those of South America (Rapalini, 1998), which contrasts with a model of a far traveled allochthonous terrane accreted during the Carboniferous-Permian as postulated by Ramos (1984).

6. Methods

Due to intense meteoric alteration and thick forest cover, rock samples were collected from road cuts, and along the Chilean coastline. The sampled rocks are mostly micaschists from the Late Paleozoic metamorphic basement from central Chile and from the Piedra Santa Metamorphic Complex, Argentina.

Zircons were separated using traditional methods at the Sample Preparation Laboratory, Department of Geology, Universidad de Chile. About 5-10 kg of samples were crushed and

milled. The heavy mineral fraction was obtained using a Gemini water table and zircons were concentrated by means of a Frantz isodynamic separator and heavy liquids. Zircons were later mounted in epoxy resin along with Plešovice reference zircon (Sláma et al., 2008). Cathodoluminescense (CL) images were obtained using a FEI Quanta 250 scanning electron microscope (SEM) with a Centaurus sensor for CL detection at the SEM Laboratory of the Andean Geothermal Centre of Excellence (CEGA), Department of Geology, Universidad de Chile.

U-Pb dating of zircons was performed at the Isotopic Geology Laboratory of the Andean Geothermal Centre of Excellence (CEGA) using a laser ablation system coupled to a multicollector mass spectrometer with inductively coupled plasma (LA-MC-ICPMS). The laser ablation system is the Analyte G2 193 nm ArF excimer laser manufactured by Photon Machines with a double volume HelEx ablation cell that allows for a He atmosphere ablation. The MC-ICPMS used in this study is the Neptune Plus, manufactured by ThermoFisher Scientific. The instrument has six Faraday detectors and six ion counters (CCD). The laser diameter used for ablation was 30 microns and the 'sample bracketing' method was used to correct for mass bias. The Plešovice zircon was used as the primary standard and 91500 (Wiedenbeck et al., 1995; 2004) or Sri Lanka-2 (SL-2) (Gehrels et al., 2008) as a secondary standard. Data reduction was performed with Iolite software (Paton et al., 2011). A detailed description of the methods and equipment employed in this study can be found in Leisen et al. (2016).

The subsequent statistical data evaluation of the U-Pb ages was performed with Isoplot 4.0 (Ludwig, 2010) and Age Pick (Gehrels, 2009).

7. Results

7.1. Detrital Zircon Ages

All data is reported in Table SMXX, and probability density plots are shown in Fig. 5 and Fig. 6. A brief description of the results (main age populations, maximum depositional age) obtained for each of the localities is presented here.

7.1.1. Yobilo (ES-N)

The Yobilo sample (YOB-D2b) has a U-Pb age distribution centered on the Early Paleozoic, with two main age peaks at 448 Ma (Ordovician) and 492 Ma (Cambrian). Lower Proterozoic ages are present with a minor peak at 857 Ma and a spread of ages ranging from 600 to 1200 Ma.

The youngest zircon in this sample has a 326 Ma age, but the youngest cluster of at least three analyses is at ~375 Ma.

7.1.2. Tirúa (WS-N)

The Tir-14-1 sample shows two large populations, one Missisipian-Early Cambrian (~330-662 Ma) and the second with a large population of Grenvillian-age zircons that dominates the sample (~1000 to 1300 Ma).

Grenvillian-age peaks are at 1099 and 1152 Ma. A similar contribution is detected at 500 and 627 Ma followed by peaks at 454 and 423 Ma. The maximum age of deposition is at 423 Ma, but some zircons cluster at ~350 Ma, which is consistent with the populations found in other basement rocks of the south-central Chile.

7.1.3. Contulmo (WS/ES-N)

The Cot-14-1 sample shows a similar pattern to the Tir-14-1 sample, with two age populations, i.e., Missisipian-Early Cambrian and Grenvillian.

The main age peak is at ~464 Ma, followed by peaks at 519 and 420 Ma. Minor peaks are recorded in the Grenvillian, with probabilistic highs at 1042 and 1128 Ma.

The maximum age of deposition is ~420 Ma, but an underestimation of younger populations is suspected, with the youngest zircon showing an age of 343 Ma.

7.1.4. Piedra Santa Micaschists (PS Fm.)

The pattern from the Piedra Santa schists is mainly Proterozoic, with an age cluster from 953 to 1368 Ma, which represents ~70% of the analyzed zircons. Additionally, an early

Paleozoic cluster is represented by a notorious peak at 457 Ma which is close to the youngest reliable zircon age of 434 Ma.

7.1.5. Quitratúe (WS-S)

The sample of Quitratúe (QE-D3) shows a slightly different distribution to all other samples. Age populations are distributed between 292 and 890 Ma, the contribution of Grenvillian sources is negligible, with only one zircon within this range.

The main probability peak is at 585-606 Ma, followed by peaks at 540, 489, and 471 Ma. Younger contributions are fairly minor and are concentrated at 321 and 306 Ma. The youngest recorded ages are ca. 270 Ma.

7.1.6. Gorbea (WS-S)

In Gorbea (GRB1-D4), zircon ages cluster at the 283-298 Ma peak, with almost half of the analyzed zircons. Secondly, a Devonian peak at 393 Ma is recognized, followed by peaks at 435 and 500 Ma. Older populations are virtually nonexistent, with only a few occurrences including one Grenvillian age.

7.1.7. Los Lagos (WS-S)

The sample from Los Lagos (LLG-14-1) has a Permian-age peak (~266 Ma) concentrating most of the analyses. Secondary peaks at 281 and a younger peak at 255 Ma have also been recognized. The ~255 Ma peak is considered the maximum reliable age of deposition.

There is also a significant Carboniferous contribution with peaks at 300 and 324 Ma (Pennsylvanian), and other peaks at 374 Ma (Devonian) and 437 Ma (Silurian).

Younger zircons without statistical significance are reported at 150 and 198 Ma.

7.1.8. Valdivia, ‘PA’ (WS-S)

A low number of zircons were recovered from sample PA-DA, near the city of Valdivia, regardless the overall age pattern is similar to those observed in other samples from the WS-S. Permian and Carboniferous ages were obtained, with a main Permian age peak at

266 Ma and a maximum age of deposition of 253 Ma. In addition, secondary peaks at 286, 338, and 358 Ma were obtained, where the latter is the oldest statistically significant age.

7.1.9. Valdivia, 'Dos Lucas' (WS-S)

In Valdivia, 'Dos Lucas' sector, two populations were obtained, a main population cluster of Permian-Carboniferous age between 265 and 346 Ma, and a smaller Early Carboniferous-Devonian peak (356-456 Ma). Pre-Devonian zircons are nonexistent. The maximum age of deposition in this area is ~270 Ma.

7.2. U/Th ratios

U/Th ratios (Fig. 7) are used to discriminate between igneous and metamorphic zircons. Expected U/Th ratio values in igneous zircons are less than 10, while higher values indicate a metamorphic origin for the analyzed zircon (Rubatto, 2002)

The largest number of metamorphic zircons is found in sample DL-D4 with four out of 57 analyzed zircons, representing 7% of the total. These metamorphic zircons cluster around 400 Ma (Early Devonian). Overall, there is a very small metamorphic component in the analyzed samples.

7.3 Igneous U-Pb ages

A sample from the Chachil Plutonic Complex (RRPS-1), which intrudes the Piedra Santa Fm Argentina, was also analyzed. The weighted average U-Pb age yielded 301.9±2.6 Ma with a MSWD=7.7. Concordia and Tera-Wasserburg diagrams are plotted in Fig. 8.

8. Discussion

8.1. Sedimentary Provenance

Several potential sources of detrital zircons can be identified in eastern locations of South America for the metasedimentary rocks of the Western Series of south-central Chile.

Proterozoic Zircons

The oldest age cluster found in samples north of 39°S is between 1000 and 1200 Ma, corresponding to 'Grenvillian' ages, typically representing the basement of accreted terranes during the Early Paleozoic (e.g., Precordillera). In the vicinity of the studied area, Grenvillian rocks are found in the Cordon del Portillo, San Rafael Block and Las Matras Block, Argentina (Sato et al., 2000 and references therein). The collisional evolution of the margin of Gondwana probably exhumed some of these blocks at the time of deposition of the Late Paleozoic metasedimentary basement and constitutes a potential source of eroded debris. These blocks are possibly the primary source of zircons.

Zircons with ages between 600-550 Ma age are present in several samples from the northern sector (e.g. YOB-D2, COT-14-1 and TIR-14-1), however this peak is not observed south of 39°S, with the exception of sample QE-D3 (Quitratúe). We interpret this 600-530 Ma age population as related to the Brasiliano orogeny, related to the igneous and metamorphic rocks of the Ventania System (e.g., Cerro Corral, San Mario and Cerro Colorado Granites; Ramos et al., 2014 and references therein).

An alternative source for Brasiliano and Grenvillian zircons can be the erosion of Ordovician metasedimentary sequences as found the Eastern Sierras Pampeanas (33°S), where Rapela et al. (2016) reports detrital zircon data of these rocks with relevant presence of Grenvillian-age zircons as well as Brasiliano-age populations.

Early Paleozoic

Recurring peaks of ~520 Ma and associated populations are clearly traceable to igneous intrusions associated with the Pampean Orogeny, with main age peaks representing the period of highest magmatic activity. Outcrops of this age are found in the Sierras Pampeanas, but minor outcrops are found up to 38°S (Ramos et al., 2010).

Large populations of Ordovician zircons are found north of 39°S, with a main age peak of ~470 Ma. These Ordovician zircons are clearly related to the Famatinian Orogeny. Magmatic bodies of this age are also found in the Sierras Pampeanas, in southern localities (~38°S) and are also present on Patagonian domains on the Sierra Grande Area (Pankhurst

et al., 2006). These bodies are clearly the most probable source of sediments of these ages and dominate the provenance of detritus for sedimentary rocks north of 39°S.

Devonian

Minor Devonian peaks at 370 and 390 Ma are identified in the southern part of the Paleozoic basement, which can be related to the erosion of the discontinuous NW-SE belt of Devonian intrusives present in Argentina, represented by the San Martin de los Andes Tonalites and Colan Conhue among others (Pankhurst et al., 2006). Some authors have suggested that this Devonian magmatic belt was formed by subduction (Varela et al., 2005), while others alleged a terrane collision between Antonia (Antarctica and Patagonia) and the NPM at 380-360 Ma (Martinez Dopico et al., 2011) or Chilenia with the NPM between 390-350 Ma (Martinez et al., 2012). To date, none of the above hypothesis can be disregarded, however independent of the origin of these bodies they remain as the most suitable source of Devonian sediments for the southern part of the basement. Despite being ubiquitous in samples between 39°S and ~40°S, the Devonian zircon population is rather small, which is contrary to the possible presence of a large and extensive range at these latitudes.

Late Paleozoic

In Yobilo and Tirua (samples YOB-D2b and TIR-14-1), located in the northern area, zircons of Mississipian age are recognized. There are no identified outcrops of igneous or metamorphic rocks of Early Carboniferous age in the area. However a series of granitic intrusive bodies associated with a subduction margin is described in the Sierras Pampeanas as an early stage of the subduction process on the Gondwana margin (Alasino et al., 2012 and references therein). If subduction was also present at the studied latitudes as a continuous magmatic arc, these rocks would be the most viable candidate for the Early Carboniferous zircons found in the micaschists.

Samples north of the 39°S have no record of Late Carboniferous zircons, whereas metasediments at southern latitudes have a significant population of this age. Late Carboniferous ages are associated with the Chilean Coastal Batholith, and the Late

Carboniferous bodies of the North Patagonian Batholith in Argentina between 41°S and 42°S (Pankhurst et al., 2006) which are oriented NW-SE in patagonian domains (Fig. 3). Our results show that the Coastal Batholith was exposed at the time of deposition of the protolith and contributed sediments, at least between 39°S and 40°S.

The main age population in samples south from the 39°S (samples GRB1-D5, LLG-14-1, PA-D4, DL-D4) is Permian with zircon peak ages that range between 250 and 290 Ma. The main candidate for a sedimentary source is the Choiyoi Magmatic Province, with U-Pb ages ranging between 286 and 247 Ma (Sato et al., 2015), and the Permian granitic occurrences of the North Patagonian Batholith (Pankhurst et al., 2006; 2014), which can be related with the former. Based on the fact that the Tunas Fm. indicates a sediment provenance from a S-SE direction, high rates of subsidence and its upper section is mainly dominated by Permian detrital zircons (Ramos et al., 2014), we can infer that the North Patagonian Batholith was an important topographic high, and the same depositional process is represented on the western flank of this topographical barrier in the sediments of the WS-S.

8.2. Sedimentary Considerations

8.2.1. Redefinition of the Northern and Southern Western Series

In general, all the metasedimentary samples from the metamorphic basement can be grouped on two groups based on their distribution of detrital zircons.

The first group has Carboniferous maximum ages of deposition, is devoided from Devonian zircons, its main population is around a ~470 Ma peak and has an important input of Mesoproterozoic zircons. This ‘signature’ is widely found on other metamorphic ocurrences in Chile (e.g. Pankhurst et al., 2006; Alvarez et al., 2011; Hervé et al., 2013; Maksaev et al., 2015)

The second group has a mainly Permian population which is also the maximum age of deposition, has relative Devonian inputs and scarse Mesoproterozoic ages.

These differences have been related to the Lanalhue Fault Zone (LFZ, Hervé et al., 2013), however, the new data provided here shows that the WS-N extends even further south than

previously thought. Samples from Contulmo and Tirúa (~38°25'S) have statistically the same populations of detrital zircons than those observed in the rest of samples from the WS-N and ES.

Therefore, we interpret that the LFZ can represents a contact zone with similar characteristics than the Pichilemu-Vichuquén fault (Willner et al., 2009) located north of 35°30'S, and that defines a sharp boundary between the HT/LT (ES) and LT/HP micaschists (WS). This is in contrast to the model presented by Glodny et al. (2008) in which the LFZ yuxtaposes both ES and WS-S by means of a transform fault.

In the other hand, the northernmost sample with Permian maximum deposition ages is the Gorbea sample (~39°10'S), helping to constrain the transition between both populations.

Given these two boundaries, the separation between the WS-N and WS-S appears to be contrained to the ~39°S. Interestingly, in this latitude a remarkable topographical discontinuity of the morphological unit of the Coastal Cordillera is evident where its elevation changes from approximately 490 to 30 masl. The Mocha-Villarrica Fault Zone (MVFZ) (as in Melnick et al., 2009; Cembrano and Lara, 2009; Figs. 1,9) is the most fitting fault detected in the area and could be responsible of yuxtaposing two metamorphic units with similar lithological features but different ages of deposition. This observation is also supported, as the K-Ar 282±6 Ma age reported in La Cabaña fuchsites (Hofer et al., 2001) is considerably older than the $^{40}Ar/^{39}Ar$ cooling ages reported in white mica by Duhart et al. (2001) in southern locations.

Based on our observations, the lithological assemblage that comprises Carboniferous metamorphosed pelites, metabasites, massive sulfide mineralization (Collao and Alfaro, 2000) and the serpentinized peridotites with podiform chromite from La Cabaña, between the LFZ and the MVFZ, should be considered as a new metamorphic unit, La Cabaña Metamorphic Complex (LCMC), interpreted as a unit of the Northern Western Series, which corresponds to the best preserved extension of the paleomargin on carboniferous-early permian times, as most part of the Western Series is tectonically eroded on northern locations (see Fig.1).

Detrital zircon analysis from the Piedra Santa complex (sample RRPS-2) and the crystallization age obtained from the Chachil Plutonic Complex (sample RRPS-1) in Argentina, show a similar tectonic setting than those occurred on the older units of the Paleozoic basement of Chile. The detrital zircon age pattern from Piedra Santa resembles the Ordovician dominated patterns from the Chilean metamorphic basement, the only different feature is a lack of Carboniferous zircons which changes the maximum age of deposition. Nevertheless, this absence is also detected in Chile, in the Contulmo area (sample COT-14-1) and both samples (samples 02CH11 and 02CH31) analyzed by Willner et al. (2008).

The crystallization age at 301.9±2.6 Ma of the granitic Chachil Plutonic Complex, which intrudes the Piedra Santa Complex, is very similar to the interval of U-Pb ages previously reported for the Coastal Batholith (eg. Deckart et al., 2013). Also, the K-Ar ages reported in the Piedra Santa Micaschists (Franzese, 1995) match with the intrusion of the Coastal Batholith in the northern section of the Metamorphic Basement in Chile (Willner et al., 2005). Our new U-Pb data supports a continuation of the paired metamorphic on an eastern location than the current Andean Range

Assuming the continuity of the Coastal Batholith on the Chachil Plutonic Complex, the truncation of the magmatic arc is also compatible with the proposed MVFZ as an ancient transform fault and, in fact, makes more evident the spatial correlation with the transcontinental Huincul Ridge (Fig. 9). The paleozoic-triassic dextral strike-slip fault activity of the Huincul Ridge (Turner and Baldis, 1978) and the possible continuation into the MVFZ can explain the variations of the detrital zircon patterns found on the western margin.

In this context, the pelitic schists with Permian maximum ages of deposition and its intermingled serpentinites southern than the MVFZ, such as Quitratúe ultramafic rocks and similar rocks, corresponds to a younger accretionary complex cooled down on Early Triassic times. Therefore, the schists analyzed on these latitudes, known as WS-S, fits on the definition of Duhart et al. (2001) of the Bahía Mansa Metamorphic Complex,

8.2.2. Depositional Constrains

The allochthony of the North Patagonian Massif has been discussed by several authors (e.g. Pankhurst et al., 2006, Ramos et al., 2008, Gregori et al., 2008, among others). The comparative analysis of detrital zircons from the lower section of the Tunas Fm. in the Ventania System (Ramos et al., 2014), the Sierra Grande Formation (Pankhurst et al., 2006.; Uriz et al., 2011), and the Eastern/Western Series-N (Hervé et al., 2013;. Willner et al., 2008; this study) shows that there is a common source of sediments for both the eastern and western flanks of South America, which is the Ordovician Famatinian Orogen and an Early Carboniferous unknown source.

The only range which has every element found on the detrital zircon patterns from de ES/WS-N is well represented in the Sierras Pampeanas between 28-33°S, given the consistent presence of granitoids of ~470 Ma, the widespread presence of sedimentary sequences containing zircons of Cambrian and Grenvillian ages (Rapela et al., 2016 and references therein), and calc-alkaline Early Carboniferous granitoids (Alasino et al., 2012 and references therein). We support that this range was also present on southern latitudes, probably unexhumed in present days.

As an overview of the WS-S, detrital zircon patterns are statistically similar among them. The main contributions are Permian, similar to the Upper Tunas Fm. from the Ventania System (Ramos et al., 2014). Both patterns can be related to the existence of a continental Permian topographic high, probably located also in the northern belt of the North Patagonian Batholith, which provides sediments to the Tunas Fm. as their paleocurrents indicate a southern provenance (Ramos et al., 2014). Similar depositional process, but in a SW direction, would be the main source of detritus of the WS-S where paleocurrents are obviously not conserved.

This topography, or extensive Permian covering, is also responsible for depriving early Paleozoic and Proterozoic zircons to the south-western oceanic basin were the WS-S was deposited. This configuration allows us to explain the abrupt change of ages along the Western Series.

Pennsylvanian contributions are present in WS-S samples and show that the CB and NPB's Carboniferous granitoids were exhumed at the time of deposition and were a relatively

important source of sediments, especially in Quitratúe (sample QE). We interpret that this sample was deposited between the formation of the ES/WS-N and the WS-S.

A small population of Devonian zircons in the WS-S was observed in our samples, but only in Dos Lucas (sample DL-D4), near Valdivia, it is statistically significant. A minor Devonian population was also detected in Gorbea (sample GRB). The sparse presence of Devonian zircons indicates that small isolated intrusions of this age were exposed during the Late Carboniferous to Early Permian because these ages are not present in any of the samples from the ES or WS-N (Willner et al., 2008; Hervé et al., 2013; this study).

8.3. Tectonic Model

Based on our new detrital zircon ages for micaschists from the Western Series of the metamorphic basement of south-central Chile and Piedra Santa Complex, a tectonic model is presented here for the western margin of Gondwana during the Paleozoic (Fig. 10).

As mentioned, the NPM apparently was not separated by a large oceanic basin from the rest of South America at least in carboniferous times. However, the series of E-W tectonic discontinuities and, especially, the dextral movement of the Huincul Ridge allow us to infer that the position of the NPM was farther east, at least at the time of the intrusion of the Chilean Coastal Batholith and Chachil Plutonic Complex. Hence, the Carboniferous magmatic arc formed along the coastline of Chile and continues in the Chachil Plutonic Complex Argentina at ca. 39°S, probably on a NW-SE trend. The southern continuation of the arc is represented by the Carboniferous granitoids located at Ranco lake, Chile, then continues south-east into Argentina with the Cordón del Serrucho, El Bolson and El Maitén (Pankhurst et al., 2006). Thus, we estimate a dextral displacement of the carboniferous arc of at least 130 km to reach their current position along the MVFZ lineament, an extension of the Huincul Fault Zone to the west.

The source of the sediments of the Eastern Series and Western Series-N (or simply *sensu stricto* Western Series) is fairly uniform, despite being north or south than the MVFZ (Hervé et al., 2013). This suggests that a large Ordovician range associated with the Famatinian orogeny (~470 Ma) with a superimposed missisipian age magmatism, similar to

the subduction related magmatic bodies from the Sierras Pampeanas (Alasino et al., 2012), provided most of the sediments to both western and eastern margins of South America as recorded in the detrital zircon patterns from Tunas Fm., a range that probably extended to the 40°S in the Sierra Grande area.

After this magmatic event, sediments from the Ordovician range and the recently formed Mississipian magmatic arc were deposited at the Gondwana margin, forming the Eastern Series. The sample from the Piedra Santa Complex, Argentina (sample RRPS-2) might have been deposited at this time, however it lacks a Mississipian age peak, alternatively it could have been deposited at an earlier time.

The sediments of the Western Series-N were deposited synchronically or shortly after the Eastern Series due their statistically similar detrital zircon patterns and their youngest zircon ages.

The emplacement of the Coastal Batholith occurred during the Late Carboniferous, imposing a HT/LP metamorphism on the host rocks. A LT/HP metamorphism was superimposed on these rocks, which have been dated at 290-280 Ma (Willner et al., 2005; Hofer et al., 2001). This LT/HP is represented in the Western Series by outcrops from Pichilemu to La Cabaña (Carahue). The natural limit between the Eastern and Western series is represented by the Pichilemu-Vichuquén and Lanalhue Fault Zones, supported by the $^{40}Ar/^{39}Ar$ ages of fault activity at 280-270 Ma (Glodny et al., 2008) representing early stages of cooling. It is unclear if this first phase of continental growth extended further south, but sample QE-D3 (Quitratúe) shows a detrital zircon pattern that can represent a transition between the WS-N and the WS-S (or Western Series and Bahía Mansa Metamorphic Complex) with a Pennsylvanian youngest zircon age, and zircon contributions from Ordovician and Panafrican sources.

Deposition of sediments from the WS-S occurred during Permian-Early Triassic. The main source of sediments was probably the Choiyoi Magmatic Province. Most of the magmatism of this province has U-Pb ages ranging 286-247 Ma (Sato et al., 2015 and references therein), but recent radiometric data from a granite at 28°S in the Quebrada del Carrizo (292±6 Ma, zircon U-Pb; Maksaev et al., 2015) and a series of granitoids on the NPB yield

older Permian ages (Pankhurst et al., 2006) with significant crustal residence time (Fanning et al., 2011), suggesting an early Permian magmatic event. Isotopic analysis on Early Permian zircons from other metasedimentary complexes in southern locations can support a subduction-related magmatic arc in Patagonia (Castillo et al., 2015).

The Permian magmatism deprives the western margin of the continent from Early Paleozoic zircons due to its topographical barrier and/or overlaying older potential sources with volcanoclastic sediments. Deposition and accretion of Permian sediments to the western margin is evident south of 39°S, where the accretion took place against the older accretionary prism (ES and WS?). The accretion of sediments in northern latitudes is not corroborable because a great extent of the Late Paleozoic Basement (specifically the Western Series) is visibly tectonically eroded (Fig. 1). During this time, detritus from the Choiyoi Magmatic Province and early stages of Permian magmatism provided most of the sedimentary contributions, with secondary inputs from the Coastal Batholith and Devonian zircons which were probably exhumed during this period. The sediments were finally accreted and cooled at approximately 240 Ma (Duhart et al., 2001).

The probable setting in this stage is an old accretionary prism formed by early carboniferous deposited sediments that cooled off during the Early Permian (ES and WS-N) and another accretionary prism on a western position composed of Permian sediments that cooled off during the Triassic (WS-S or Bahía Mansa). The current distribution of fragments of these accretionary prisms is explained by dextral strike-slip tectonics along the Mocha-Villarrica Fault Zone, the westernmost extension of the Huincul Ridge, probably at Triassic times.

The Andean Range is responsible for the apparent ‘dislocation’ of blocks. The continuity of the Coastal Batholith and the ‘old prism’ from the 38°15’S to the 39°15’S is not exhumed due to the absence of contractional tectonics (Folguera and Ramos, 2009) capable to exhume these rocks and the extensive volcanics in the Andean Range, in the same fashion as between the 40°S and 41°30’S. The Neogene shallowing of the Nazca plate in the northern segment of the metamorphic basement (Kay and Mpodozis, 2002) deformed and tectonically eroded the continental margin, orientating most of the metamorphic basement

in a north-south trend making less observable the original orientation of the accretionary prisms and Coastal Batholith which was probably NW-SE.

9. Conclusions

The detrital zircons from metasedimentary rocks of the Late Paleozoic Basement of south-central Chile have two main characteristic patterns. The first, has a Carboniferous maximum deposition age, a mainly Ordovician provenance and relatively large presence of Grenvillian age zircons, whereas the second pattern has a Permian maximum deposition age and virtually no Proterozoic zircons. The first group indicates a provenance from a source similar to the Sierras Pampeanas range, which its southern extension is probably unexhumed in present days, and the second group corresponds to a depositional stage where the Choiyoi Magmatic Province was the predominant source of sediments.

The first group has been detected in the Western Series in southern latitudes from the Lanalhue Fault Zone near the peridotites from La Cabaña Massif (Fig. 1; 8). Since the sedimentary host rocks of this ultramafic body can be associated with a similar depositional environment as rocks from northern locations of the basement, we conclude that the massif was accreted in the continental margin in similar timing than the Western Series in northern locations, and possibly, more ultramafic rocks were accreted in northern latitudes, but have been eroded tectonically.

In Argentina, a similar tectonic setting than in the metamorphic basement of Chile is identified in the Piedra Santa Complex and the Chachil Plutonic Complex, via U-Pb ages of both units. The Piedra Santa Complex has a detrital zircon pattern similar to the Eastern Series and Western Series-North and is intruded by a Pennsylvanian granitoid (301.9±2.6 Ma) which is the timing of crystallization of the Coastal Batholith. This leads to a continuity of the Chilean metamorphic basement on Argentina at the 39°S.

The Western Series abruptly changes the detrital zircon pattern at the 39°S where the MVFZ is located. Almost every sample has permian maximum deposition ages from this fault to southern latitudes, forming part of a younger accretionary complex.

It is proposed that the MVFZ is the westernmost continuation of the Huincul Ridge, where a dextral strike tectonic explains the dislocation of blocks of different accretionary complexes where no lithological differences can be detected but can be revealed with radiometric data.

10. Acknowledgements

This research has been financially supported by Fondecyt Grant #1110345, entitled “Origin and evolution of the Coastal Cordillera ophiolite complex, Central Chile” to Fernando Barra. Additional funding was provided by FONDAP project 15090013 “Centro de Excelencia en Geotermia de los Andes, CEGA”. The authors acknowledge support through the MSI “Millennium Nucleus for Metal Tracing Along Subduction” (NC130065).

Figures

Figure.1 Geological map of the main units of the Metamorphic Basement of South Central Chile (Modified from SERNAGEOMIN, 2003). Location of each sample is indicated along with their respective maximum age of deposition, except for the sample RRPS-1 correspondant to a magmatic crystallization age. Detrital zircon data from Willner et al., 2008 (prefix "02") and Hervé et al., 2013 (prefix "FO") are also included. LFZ: Lanalhue Fault Zone, MVFZ: Mocha-Villarrica Fault Zone.

Figure.2 Probability density plots from previously reported samples by Willner et al., 2008 and Hervé et al., 2013.

Figure.3 Relative locations of Late Paleozoic sedimentary sequences in Argentina and the Metamorphic Basement in Chile. Also, carboniferous magmatism is indicated in the western flank of the continent.

Figure.4 Probability density plots from previously reported detrital zircon data from the Ventania System (a,b) and Sierra Grande Formation.

Figure.5 Probability density plots from samples in a northern position than the MVFZ. Representative peaks are highlighted.

Figure.6 Probability density plots from samples in a southern position than the MVFZ. Representative peaks are highlighted.

Figure.7 U/Th ratios for every analyzed zircon in this study

Figure.8 Concordia and Tera-Wasserburg diagrams from igneous zircon ages for the granitic sample RRPS-1

Figure.9 Detailed geological map showing the spatial relationship of the domains identified in this work. Same legend as Figure 1 is used. The possible continuity of the Coastal Batholith and the Chachil Plutonic Complex, as well as the Coastal Batholith and the Carboniferous magmatism on the North Patagonian Massif, is indicated with red dots. Main structural features are also mapped. LFZ: Lanalhue Fault Zone; MVFZ: Mocha-Villarrica Fault Zone; HRS: Deformational area of the Huincul Rift System (as in Ramos, M., et al., 2014); LCMC: La Cabaña Metamorphic Complex.

Figure.10 Proposed tectonic setting for the formation of the Paleozoic Basement of South Central Chile. (a) Deposition of the sedimentary protolith of the Eastern Series, Piedra Santa Complex and Western Series-N from a southern extension of the Sierras Pampeanas Range. (b) Intrusion of the Coastal Batholith and Chachil Plutonic Complex on the Eastern Series and Piedra Santa Complex and early metamorphism of the Western Series-N. (c) Cooling ages of the Western Series-N while the protolith of the Western Series-S (Bahía Mansa Metamorphic Complex) is deposited from erosion of early stages of the Choiyoi Magmatic Province. (d) Present day disposition of the metamorphic basement, dextral

dislocation along the Huincul and Mocha-Villarrica Fault systems and superimposed Andean Range.

References

Aguirre, L., Hervé, F., Godoy, E., 1972. Distribution of metamorphic facies in Chile, an outline. Kristalinikum 9: 7–19.

Alasino, P., Dahlquist, J., Pankhurst, R., Galindo, C., Casquet, C., Rapela, C., Larrovere, M., Fanning, C., 2012. Early Carboniferous sub- to mid-alkaline magmatism in the Eastern Sierras Pampeanas, NW Argentina: A record of crustal growth by the incorporation of mantle-derived material in an extensional setting. Gondwana Research 22: 992–1008.

Alfaro, G., 1980. Antecedentes preliminares sobre la composición y génesis de las cromitas de La Cabaña (Cautín). Revista Geológica de Chile 11: 29-41.

Alvarez, J, Mpodozis, C., Arriagada, C., Astini, R., Morata, D., Salazar, E., Valencia, V., Vervoort, J., 2011. Detrital zircons from late Paleozoic accretionary complexes in north-central Chile (28°-32°S): Possible fingerprints of the Chilenia terrane. Jounral of South American Earth Sciences 32: 460-476.

Barra, F., Rabbia, O., Alfaro, G., Miller, H., Höfer, C., Kraus, S., 1998, Serpentinitas y cromititas de La Cabaña, Cordillera de la Costa, Chile central: Revista Geológica de Chile 25: 29-44.

Barra, F., Gervilla., F.,Hernández, E., Reich, M., Padrón-Navarta, J., González-Jiménez, J.M., 2014. Alteration patterns of chromian spinels from La Cabaña peridotite, south-central Chile. Miner Petrol 108: 819-836.

Castillo, P., Fanning, C., Hervé, F., Lacassie, J., 2015. Characterisation and tracing of Permian magmatism in the south-western segment of the Gondwanan margin; U–Pb age, Lu–Hf and O isotopic compositions of detrital zircons from metasedimentary complexes of northern Antarctic Peninsula and western Patagonia. Gondwana Research 36: 1-13. http://dx.doi.org/10.1016/j.gr.2015.07.014

Cembrano, J., Lara, L. 2009. The link between volcanism and tectonics in the southern volcanic zone of the Chilean Andes: A review. Tectonophysics 471: 96-113.

Chernicoff, C., Zappetinni, E., 2004. Geophysical evidence for terrane boundaries in south-central Argentina. Gondwana Research 7: 1105-1116.

Collao, S., Alfaro, G., 2000. Paleozoic massive sulphide orebodies of the Nahuelbuta and Queule mountains, south-central Chile: Results of geothermobarometry and sulphur isotope studies. In: Sherlock, R.L. and Logan, M.A. (eds) Volcanogenic massive sulphide deposits of Latin America. Geological Association of Canada, Mineral Deposits Division, Special Publication 2: 629-641.

Deckart, K., Hervé, F., Fanning, M., Ramírez, V., Calderón, M., y Godoy, E., 2014. U-Pb geochronology and Hf-O isotopes of zircons from the pennsylvanian coastal batholith, south central Chile. Andean Geology 41: 49-82.

Dickerson, P., 2004. Pampean Orogen: an intraplate component of Early Paleozoic deformation. Gondwana Research 7: 115–124.

Duhart, P., McDonough, M., Muñoz, J., Martin, M., y Villaneuve, M., 2001. El Complejo Metamórfico Bahía Mansa en la Cordillera de la Costa del centro-sur de Chile (39°30'-42°S): Geocronología K-Ar, 40Ar/39Ar y U-Pb e implicancias en la evolución del margen sur-occidental de Gondwana. Revista Geológica de Chile 28: 179-208.

Fanning, M., Hervé, F., Pankhurst, R., Rapela, C., Kleiman, L., Yaxley, G., Castillo, P., 2011, Lu-Hf isotope evidence for the provenance of Permian detritus in accretionary complexes of western Patagonia and the northern Antarctic Peninsula región. Journal of South American Earth Sciences 32 : 485-496.

Franzese, J, 1995. El Complejo Piedra Santa (Neuquén, Argentina): parte de un cinturón metamórfico neopaleozoico del Gondwana suroccidental. Revista Geológica de Chile 22: 193-202.

Frutos J., Alfaro, G., 1987. Metallogenetic and tectonic chracteristics of the Paleozoic ophiolitic belt of the southern Chile coast cordillera. Geologische Rundschau 76: 343–356.

Folguera, A., Ramos, V. 2009. Collision of the Mocha fracture zone and a <4 Ma old wave of orogenic uplift in the Andes (36°-38°S). Lithosphere 1: 364-369.

Garrido, M., Barra, F., Domínguez, E., Ruiz, J., Valencia, V., 2008. Late Carboniferous porphyry copper mineralization at La Voluntad, Neuquén, Argentina: Constraints from Re–Os molybdenite dating. Mineralium Deposita 43: 591-597.
Gehrels, G., Valencia, V., Ruiz, J. 2008. Enhanced precision, accuracy, efficiency, and spatial resolution of U-Pb ages by laser ablation–multicollector–inductively coupled plasma–mass spectrometry. Geochemistry Geophysics Geosystems (G3) 9.

Gehrels, G. 2009. Arizona LaserChron Center analysis tools for U-Th-Pb geochronologic data. From: http://www.geo.arizona.edu/alc: http://docs.google.com/View?id=dcbpr8b2_7c3sgpxft

Glodny, J., Lohrmann, J., Echtler, H., Gräfe, K., Seifert, W., Collao, S., Figueroa, O., 2005. Internal dynamics of a paleoaccretionary wedge: Insights from combined isotope tectonochronology and sandbox modelling of the south-central Chilean forearc. Earth and Planetary Science Letters 231: 23–39.

Glodny, J., Echtler, H., Collao, S., Ardiles, M., Burón, P., Figueroa, O., 2008. Differential Late Paleozoic active margin evolution in South-Central Chile (37°S-40°S) - the Lanalhue Fault Zone. Journal of South American Earth Sciences 26: 397-411.

González-Bonorino F., 1971. Metamophism of the crystalline basement of Central Chile. Journal of Petrology 12: 149-175.

González-Jiménez J.M., Barra, F., Walker, R., Reich, M., Gervilla, F., 2014. Geodynamic implications of ophiolitic chromitites in the La Cabaña ultramafic bodies, Central Chile. International Geology Review 56: 1466-1483.

Gregori, D., Kostadinoff,J., Strazzere, L., Raniolo, A., 2008. Tectonic significance and consequences of the Gondwanide orogeny in northern Patagonia, Argentina. Gondwana Research 14: 429–450.

Hervé, F., 1988. Late Paleozoic Subduction and Accretion in Southern Chile. Episodes 11: 183-188.

Hervé, F., Munizaga, F., Parada, M., Brook, M., Pankhurst, R., Snelling, N., Drake, R., 1988. Granitoids of the Coast Range of central Chile: geochronology and geologic setting. Journal of South American Earth Sciences 1: 185-194.

Hervé, F., Faundez, V., Calderón, M., Massone H.J., Willner, A.P., 2007. Metamorphic and plutonic basement complexes. In: Moreno, T., Gibbons, W. (Eds). The Geology of Chile. The Geological Society, London. pp. 5-19.

Hervé, F., Calderón, M., Fanning, C.M., Pankhurst, R.J., Godoy, E., 2013. Provenance variations in the Late Paleozoic accretionary complex of central Chile as indicated by detrital zircons. Gondwana Research 23: 1122-1135.

Höfer, C., Kraus, S., Miller, H., Alfaro, G., and Barra, F., 2001. Chromite-bearing serpentinite bodies within an arc–backarc metamorphic complex near La Cabaña, south Chilean Coastal Cordillera. Journal of South American Earth Sciences 14: 113–126. doi:10.1016/S0895-9811(01)00011-6.

Hufmann, L., Massonne, H., 2000. Ancient arc/back-arc and N-MORB volcanics incorporated in the Late Palaeozoic/Early Mesozoic metamorphic complex of the Coastal Cordillera of Chiloé, Southern Central Chile, in Congreso Geológico Chileno, No. 9: Actas, Puerto Varas, Chile, Tomo 2:738–741.

Kay, J., Mpodozis, C. 2002. Magmatism as a probe to the Neogene shallowing of the Nazca plate beneath the modern Chilean flat-slab. Journal of South American Earth Sciences 15: 39-57.

Leisen, M., Barra, F., Romero, R., Morata, D., Reich, M., 2015. Geocronología U-Pb de Circones Mediante Ablación Láser Acoplado a un ICP-MS Multicolector: Metodología Utilizada en el Laboratorio de Geoquímica Isotópica del Centro Fondap CEGA, Universidad de Chile. In: Congreso Geológico Chileno 14, La Serena, Chile.

Lucassen, F., Trumbull, R., Franz, G., Creixell, C., Vásquez, P., Romer, R., y Figueroa, O., 2004. Distinguishing crustal recycling and juvenile additions at active continental margins: the Paleozoic to recent compositional evolution of the Chilean Pacific margin. Journal of South American Earth Sciences 17: 103-119.

Ludwig, K., 2010. Isoplot/Ex version 4.1, a geochronological toolkit for Microsoft Excel. Berkeley Geochronology Center, Special Publication n. 4.

Maksaev, V., Arancibia, J., Munizaga, F., Tassinari, C., 2015. Detrital-zircon U-Pb geochronology of the Quebrada del Carrizo Metamorphic Complex and El Jardín Schists and spatially-related granitoids of the Sierra Castillo Batholith. Andean Geology 42: 285-312.

Martínez, J., Dristasa, J., Massone, H., 2012. Palaeozoic accretion of the microcontinent Chilenia, North Patagonian Andes: high-pressure metamorphism and subsequent thermal relaxation. International Geology Review: 54: 472-490.

Martínez Dopico, C., Lopez de Luchi, M., Rapalini, A., Kleinhanns, I., 2011. Crustal segments in the North Patagonian Massif, Patagonia: An integrated perspective based on Sm/Nd isotope systematics. Journal of South American Earth Sciences 31: 324–341.

Melnick, D., Echtler, H.P., 2006. Morphotectonic and geologic digital map compilations of the south-central Andes (36–42°S). In: Oncken, O., Chong, G., Franz, G., Giese, P., Götze, H.-J., Ramos, V.A., Strecker, M., Wigger, P. (Eds.), The Andes – Active Subduction Orogeny. Frontiers in Earth Science Series, Vol. 1. Springer-Verlag, Berlin, Heidelberg, New York, pp. 565–568.

Miyashiro A.,1961. Evolution of metamorphic belts. Journal of Petrology 2: 277-311.

Pankhurst, R., Rapela, C., Saavedra, J., Baldo, E., Dahlquist, J., Pascua, I., Fanning, C., 1998. The Famatinian magmatic arc in the southern Sierras Pampeanas, In: Pankhurst, R., Rapela, C., (Eds,), The Proto-Andean Margin of Gondwana. Geological Society of London, Special Publications 142, 343-367.

Pankhurst, R., Rapela, C., Fanning, C., 2000. Age and origin of coeval TTG, I-S-type granites in the Famatinian belt of NW Argentina. Transactions of the Royal Society of Edinburgh: Earth Sciences 91, 151-168.

Pankhurst. R., Rapela. C., Fanning, C., Márquez, M., 2006. Gondwanide continental collision ant the origin of Patagonia. Earth-Science Reviews 76: 235-257.

Pankhurst, R., Rapela, C., López de Luchi, M., Rapalini, A., Fanning, C., Galindo, C., 2014. The Gondwana connections of northern Patagonia. Journal of the Geological Society, London 171: 313-328. http://dx.doi.org/10.1144/jgs2013-081

Paton, C., Hellstrom, J., Paul, B., Woodhead, J., Hergt, J., 2011. Iolite: Freeware for the visualisation and processing of mass spectrometric data. Journal of Analytical Atomic Spectrometry 26:2508-2518.

Rabbia, O.M., Alfaro, G., Barra, F., 1994. Presencia de espilitas metasomatizadas en el cinturón serpentinítico de la Cordillera de la Costa. In: II Jornada de Mineralogía,

Petrografía y Metalogénesis de rocas Ultrabásicas. Tomo 3: pp. 607–615. Buenos Aires, Argentina.

Ramos, V., 1984. Patagonia: Un continente paleozoico a la deriva?. In: 9° Congreso Geológico Argentino (Bariloche), Actas 2, pp. 311-325.

Ramos, V., 2008. Patagonia: A paleozoic continent adrift?. Journal of South American Earth Sciences 26: 235-251.

Ramos, V., Vujovich, G., Martino, R., y Otamendi, J., 2010. Pampia: A large cratonic block missing in the Rodinia supercontinent. Journal of Geodynamics 50: 243-255.

Ramos, V., Chemale, F., Naipauer, M., Pazos, P., 2014. A provenance study of the Paleozoic Ventania System (Argentina): Transient complex sources from Western and Eastern Gondwana. Gondwana Research 26: 719-740.

Ramos, M., Folguera, A., Fennell, L., Giménez, M., Litvak, V., Dzierma, Y., Ramos, V., 2014. Tectonic evolution of the North Patagonian Andes from field and gravity data (39–40°S). Journal of South American Earth Sciences 51: 59-75.

Rapalini, A., 1998. Syntectonic magnetization of the mid-Palaeozoic Sierra Grande Formation: further constraints of the tectonic evolution of Patagonia. Journal of the Geological Society of London 155: 105–114.

Rapela, C., Pankhurst, R., Casquet, C., Baldo, E., Saavedra, J., Galindo, C., 1998. Early evolution of the Proto-Andean margin of South America. Geology 26: 707–710.

Rapela, C., Pankhurst, R., Baldo, E., Casquet, C., Galindo, C., Fanning, C., y Saavedra, J., 2001. Ordovician metamorphism in the Sierras Pampeanas: New U-Pb SHRIMP ages in the central-east Valle Fértil and the Velasco batholith. In: III South American Symposium on Isotope Geology, pp. 616-619. Cautín, Chile.

Rapela, C., Pankhurst, R., Casquet, C., Fanning, C., Baldo, E., González-Casado, J., Galindo, C, Dahlquist, J., 2007. The Río de la Plata craton and the assembly of SW Gondwana. Earth-Science Reviews 83: 49-82.

Rapela, C., Fanning, C., Casquet, C., Pankhurst, R., Spalleti, L, Poiré, D., Baldo, E., 2011. The Rio de la Plata craton and the adjoining Pan-African/brasiliano terranes: Their origins and incorporation into south-west Gondwana. Gondwana Research 20: 673-690.

Rapela, C., Verdecchia, S., Casquet, C., Pankhurst, R., Baldo, E., Galindo, C., Murra, J., Dahlquist, J., Fanning, M., 2016. Identifying Laurentian and SW Gondwana sources in the Neoproterozoic to Early Paleozoic metasedimentary rocks of the Sierras Pampeanas: Paleogeographic and tectonic implications. Gondwana Research 32: 193-2012.

Rubatto, D., 2002. Zircon trace element geochemistry: partitioning with garnet and the link between U–Pb ages and metamorphism. Chemical Geology 184: 123-138.

Sato, A., Tickyj, H., Llambías, E., Sato, K., 2000. The Las Matras tonalitic–trondhjemitic pluton, central Argentina: Grenvillian-age constraints, geochemical characteristics, and regional implications. Journal of South American Earth Sciences 13: 587-610.

Sato, A., Llambías, E., Basei, M., Castro, C., 2015. Three stages in the Late Paleozoic to Triassic magmatism of southwestern Gondwana, and the relationships with the volcanogenic events in coeval basins. Journal of South American Earth Sciences 63: 48-69. http://dx.doi.org/10.1016/j.jsames.2015.07.005

SERNAGEOMIN, 2003. Mapa Geológico de Chile: version digital, publicación geológica digital, No. 4, 2003. CDROM, versión 1.0, 2003. Base Geológica escala 1:1.000.000. Gobierno de Chile, Servicio Nacional de Geología y Minería, Subdirección Nacional de Geología.

Sillitoe, R., 1977, Permo-Carboniferous, upper Cretaceous and Miocene porphyry copper type mineralization in the Argentinian Andes. Economic Geology 72: 99-103.

Sims, J., Ireland, T., Camacho, A., Lyons, P., Pieters, P., Skirrow, R., Stuart-Smith, P., Miró, R., 1998. U-Pb, Th-Pb and Ar-Ar geochronology from the southern Sierras Pampeanas, Argentina: implications for the Palaeozoic tectonic evolution of the western Gondwana margin. Geological Society of London, Special Publication 142: 259-281.

Sláma, J., Košler, J., Condon, D., Crowley, J., Gerdes, A., Hanchar, J., Horstwood, M., Morris, G., Nasdala, L., Norberg, N., Schaltegger, U., Schoene, B., Tubrett, M., Whitehouse, M., 2008. Plešovice zircon — A new natural reference material for U–Pb and Hf isotopic microanalysis. Chemical Geology 249: 1-35.

Stuart-Smith, P., Camacho, A., Sims, J., Skirrow, R., Pieters, P., Black, L. and Miró, R., 1998. U-Pb, Th-Pb and Ar-Ar geochronology from the southern, 1999. Uranium-Lead dating of felsic magmatic cycles in the southern Sierras Pampeanas, Argentina: Implications for the tectonic development of the proto-Andean Gondwana margin. In: Ramos, V., Keppe, J. (Eds): Laurentia Gondwana connections before Pangea, Special Paper 336: 87-114. Geological Society of America. Boulder Colorado.

Turner, J., Baldis, B., 1978. La estructura transcontinental del límite septentrional de la Patagonia. In: VII Congreso Geológico Argentino, pp. 225–238. Neuquén, Argentina.

Uriz, N., Cingolani, C., Chemale, F., Macambira, M., Armstrong, R., 2011. Isotopic studies on detrital zircons of Silurian–Devonian siliciclastic sequences from Argentinean North Patagonia and Sierra de la Ventana regions: comparative provenance. International Journal of Earth Sciences (Geologische Rundschau) 100: 571–589.

Varela, R., Teixeira, W., Cingolani, C., Dalla Salda, L., 1994. Edad Rubidio-Estroncio de granitoides de Aluminé-Rahue, Cordillera Norpatagónica, Neuquén, Argentina. In VII Congreso Geológico Chileno, Actas, p. 1254-1258. Concepción.

Varela, R., Basei, M., Cingolani, C., Siga, O., Passarelli, C., 2005. El basamento cristalino de los Andes norpatagónicos en Argentina: geocronología e interpretación tectónica. Revista Geológica de Chile 32: 167-187.

Vergara, L. 1970. Prospección de yacimientos de cromo y hierro en La Cabaña, Cautín. Bachelor's thesis, Universidad de Chile. 96 p.

Wiedenbeck, M., Allé, P., Corfu, F., Griffin, W.L., Meier, M., Oberli, F., von Quadt, A., Roddick, J.C. and Spiegel, W. 1995. Three natural zircon standards for U-Th-Pb, Lu-Hf, trace element and REE analyses. Geostandards Newsletter 19: 1-23.

Wiedenbeck, M., Hanchar, J., Peck, W., Sylvester, P., Valley, J., Whitehouse, M., Kronz, A., Morishita, Y., Nasdala, Lutz., Fiebig, J., Franchi, I., Girard, J.-P., Greenwood, R., Hinton, R., Kita, N., Mason, P., Norman, M., Ogasawara, M., Piccoli, P., Rhede, D., Satoh, H., Schulz-Dobrick, B., Skår, Ø., Spicuzza, M., Terada, K., Tindle, A., Togashi, S., Vennemann, T., Xie, Q., Zheng, Y. 2004. Further Characterisation of the 91500 Zircon Crystal. Geostandards and Geoanalytical Research 28: 9-39

Willner, A., Pawlig, S., Massonne, H-J., Hervé, F. 2001. Metamorphic evolution of spessartine quartzites (coticules) in the high-pressure, low-temperature complex at Bahia Mansa, Coastal Cordillera of south-central Chile. Canadian Mineralogist 39: 1547–1569.

Willner A.P., 2005. Pressure-Temperature Evolution of a Late Palaeozoic Paired Metamophic Belt in North-Central Chile (34°-35°30'S). Journal of Petrology 46: 1805-1833.

Willner, A.P., Thompson, S., Kröner, A., Wartho, J., Wijbrans, J., Hervé, F., 2005. Time markers for the evolution and exhumation history of a Late Palaeozoic Paired Metamorphic Belt in North-Central Chile (34°-35°30'S). Journal of Petrology 46: 1835-1858.

Willner, A.P., Gerdes, A., Massone, H.J., 2008. History of cristal growth and recycling at the Pacific convergent margin of South America at latitudes 29°-36°S revealed by a U-Pb and Lu-Hf isotope study of detrital zircon from late Paleozoic accretionary systems. Chemical Geology 253: 114-129.

Willner, A.P., Richter, P., Ring, U., 2009. Structural overprint of a late Paleozoic accretionary system in north-central Chile (34°-35°S) during post-accretional deformation. Andean Geology 36: 17-36.

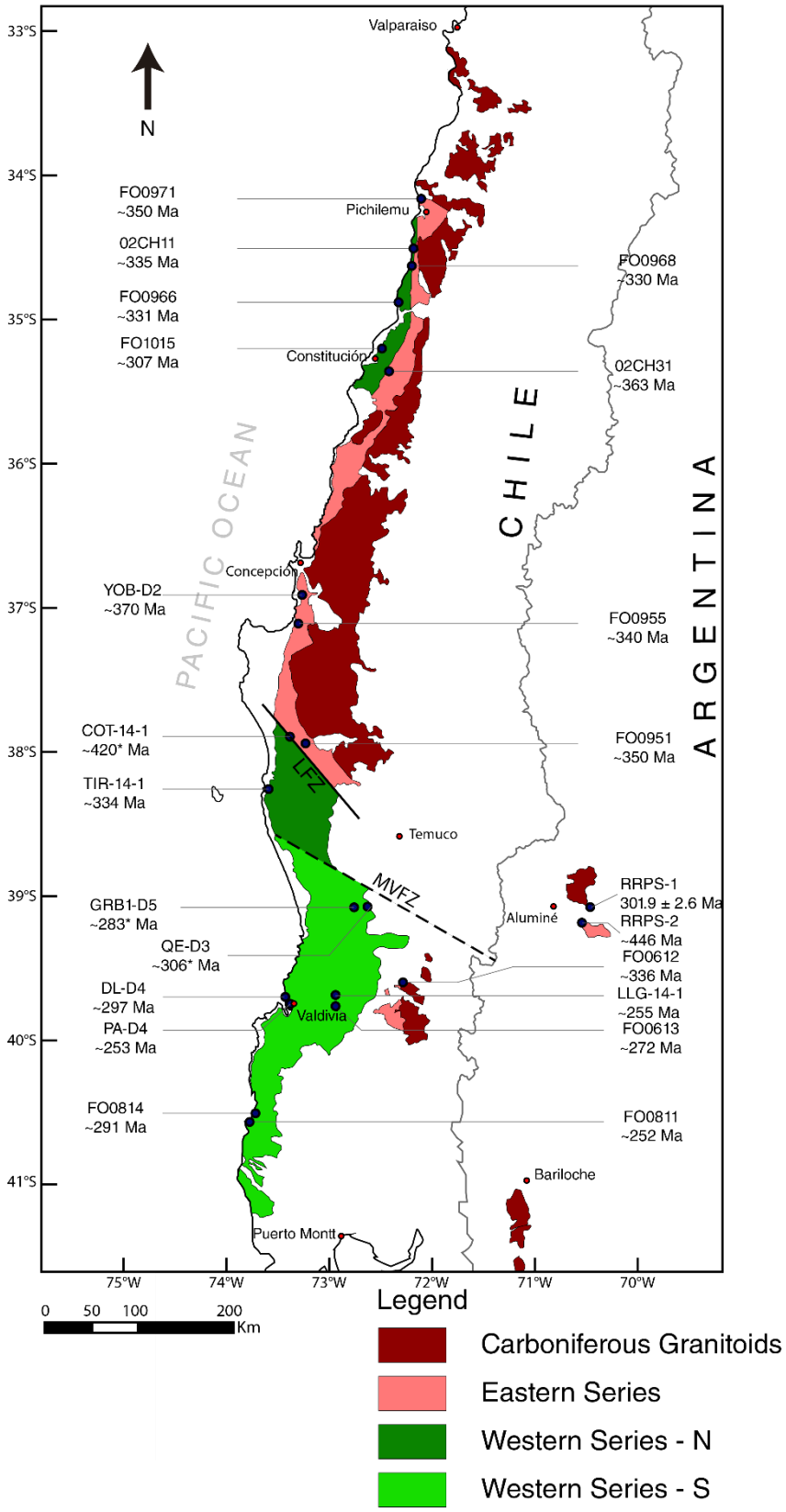

FIGURE 1. ROMERO ET AL.

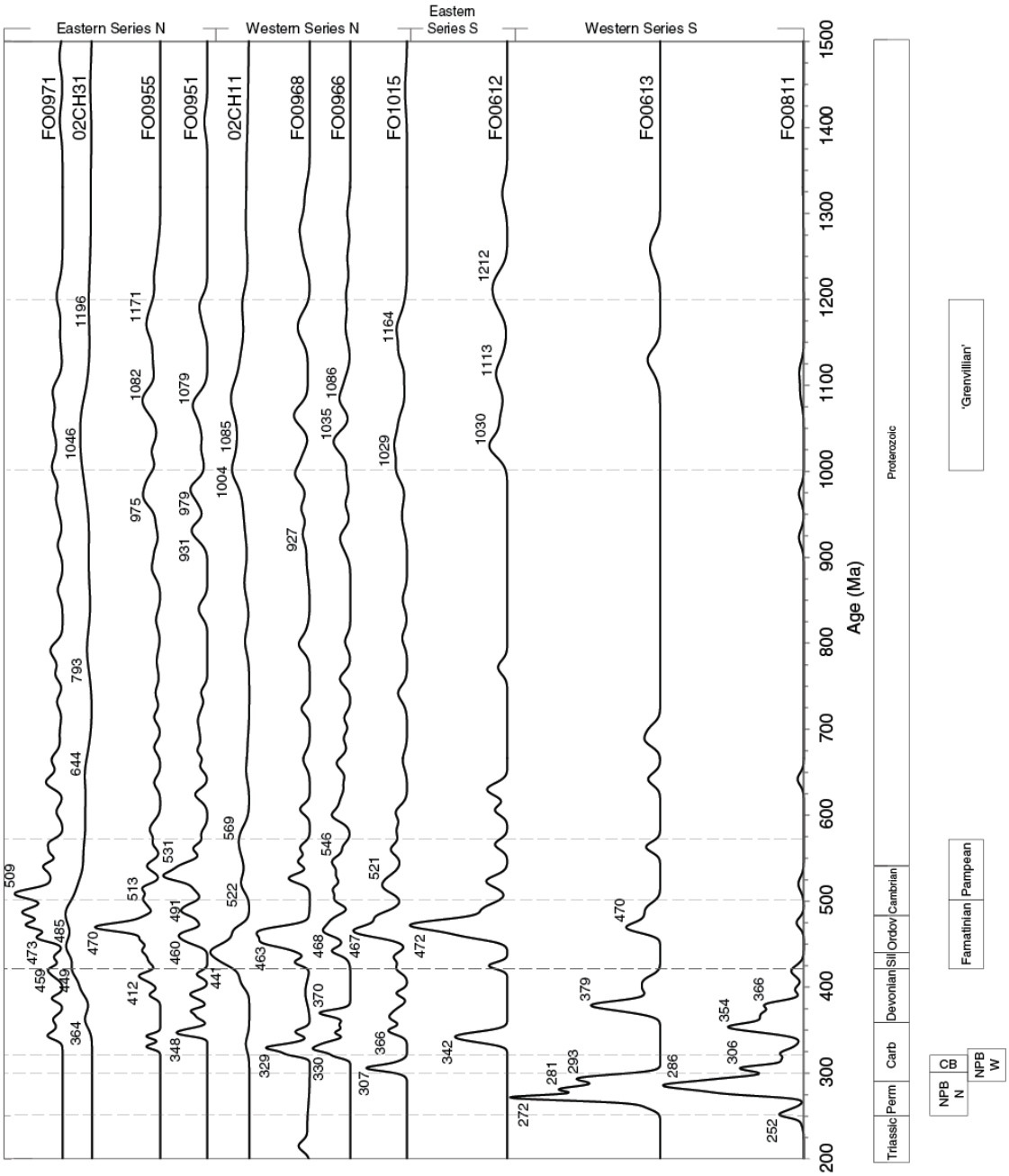

FIGURE 2. ROMERO ET AL.

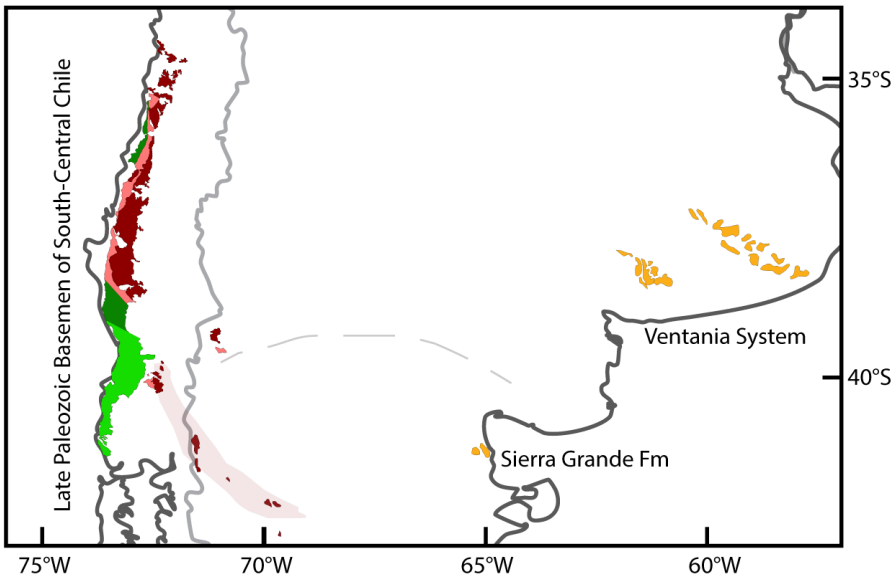

FIGURE 3. ROMERO ET AL.

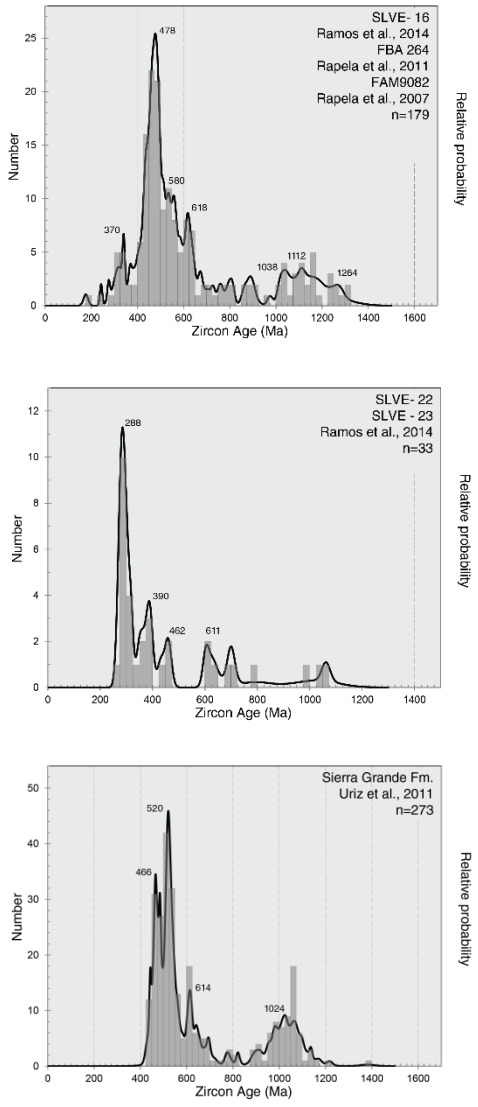

FIGURE 4. ROMERO ET AL.

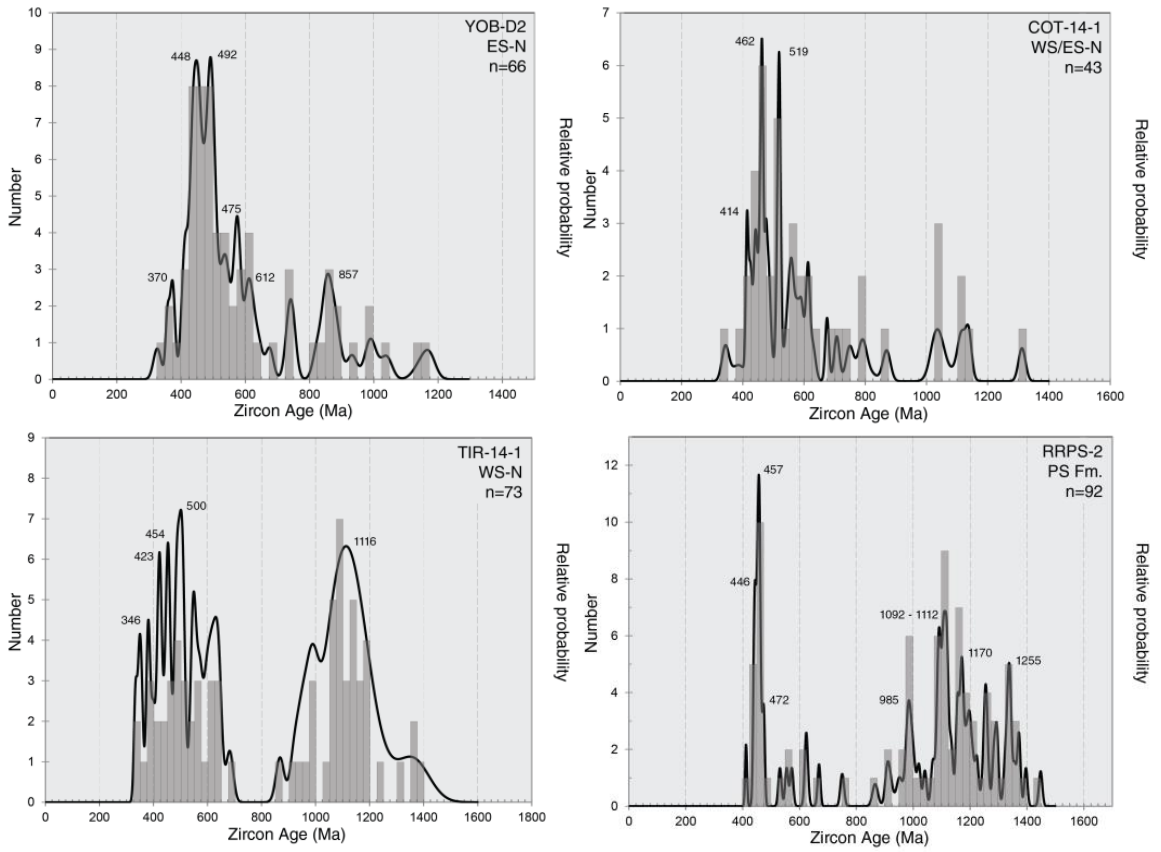

FIGURE 5. ROMERO ET AL.

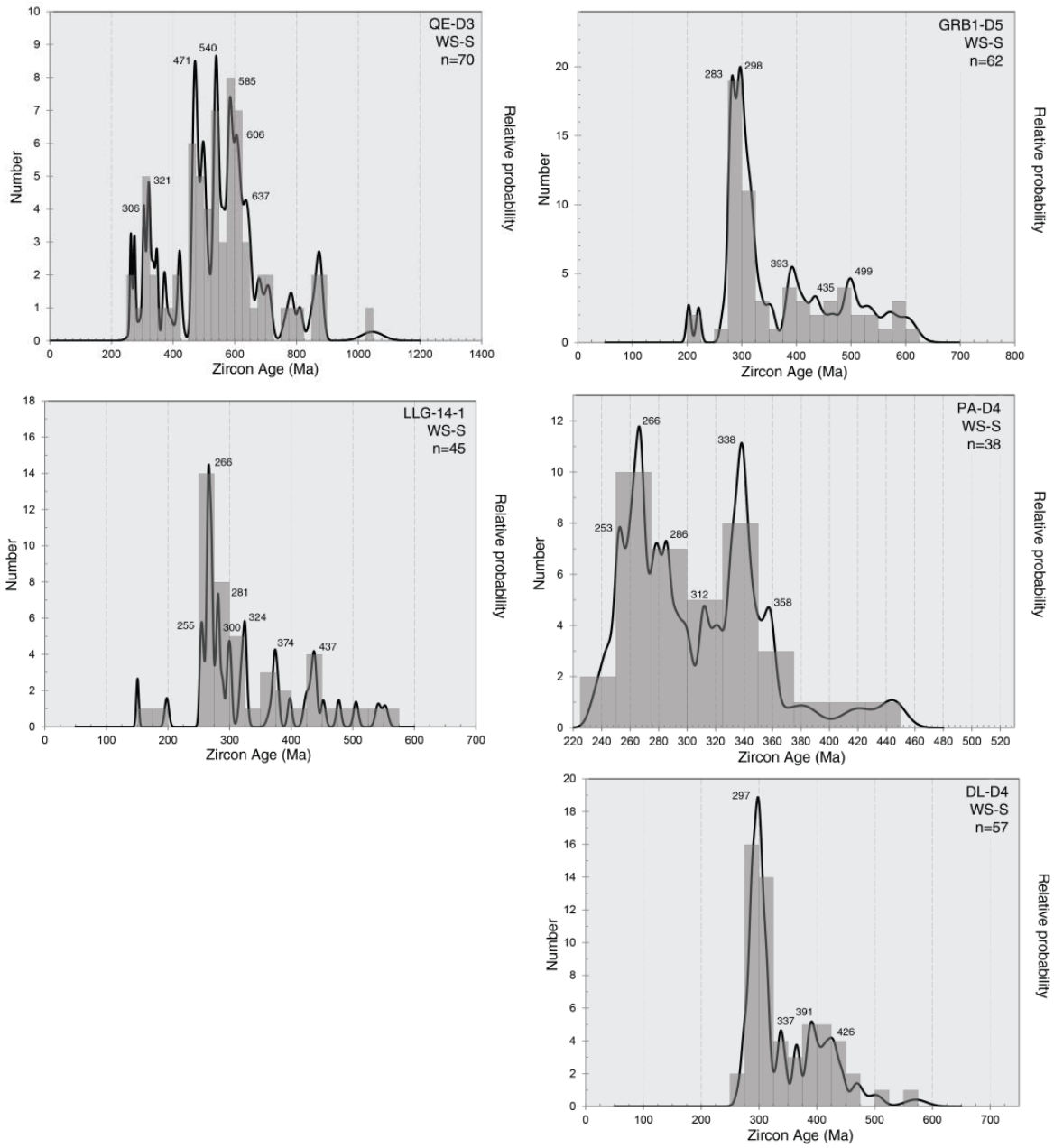

FIGURE 6. ROMERO ET AL.

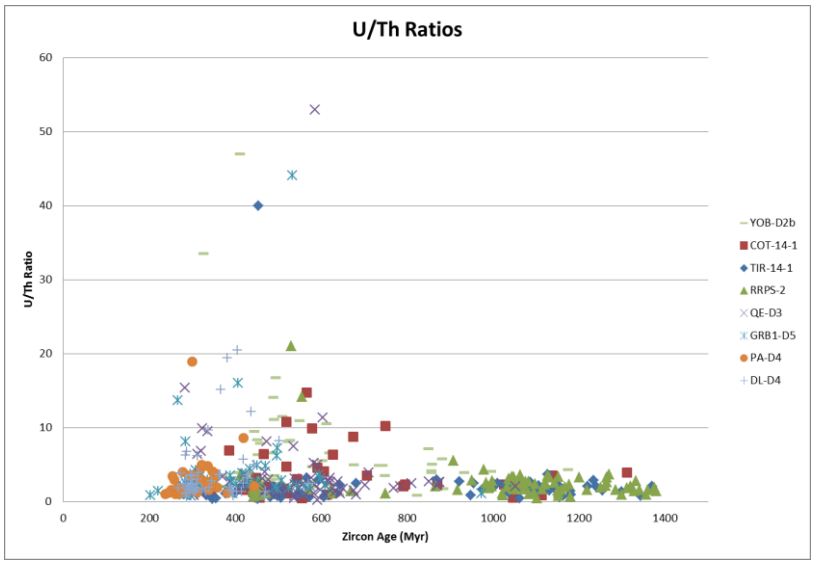

FIGURE 7. ROMERO ET AL.

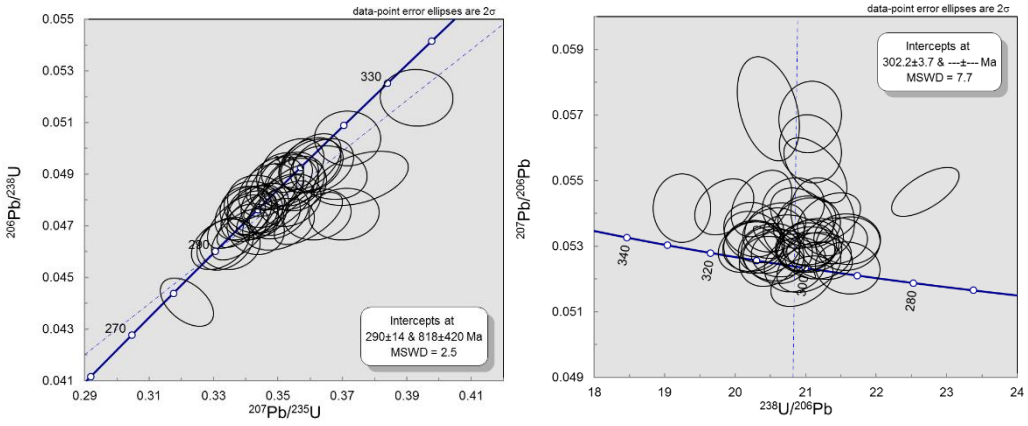

FIGURE 8. ROMERO ET AL.

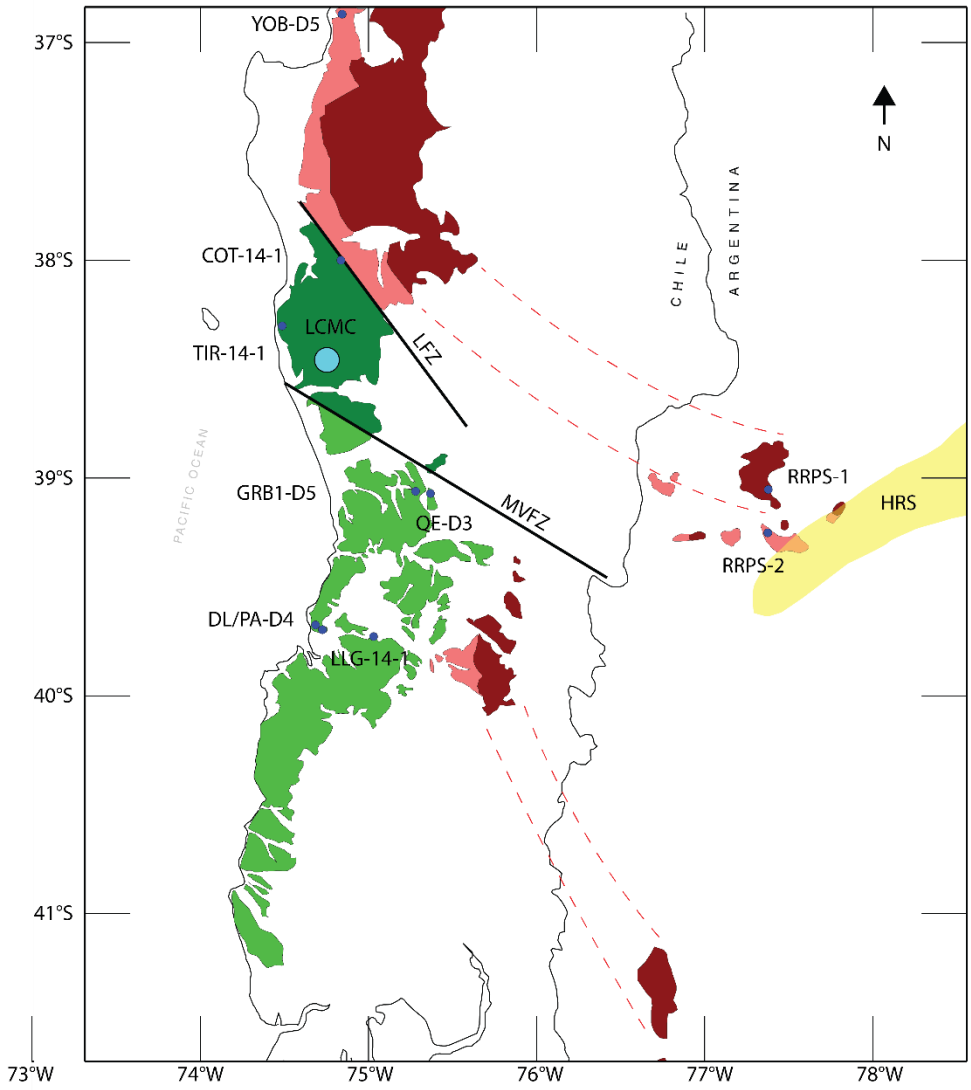

FIGURE 9. ROMERO ET AL.

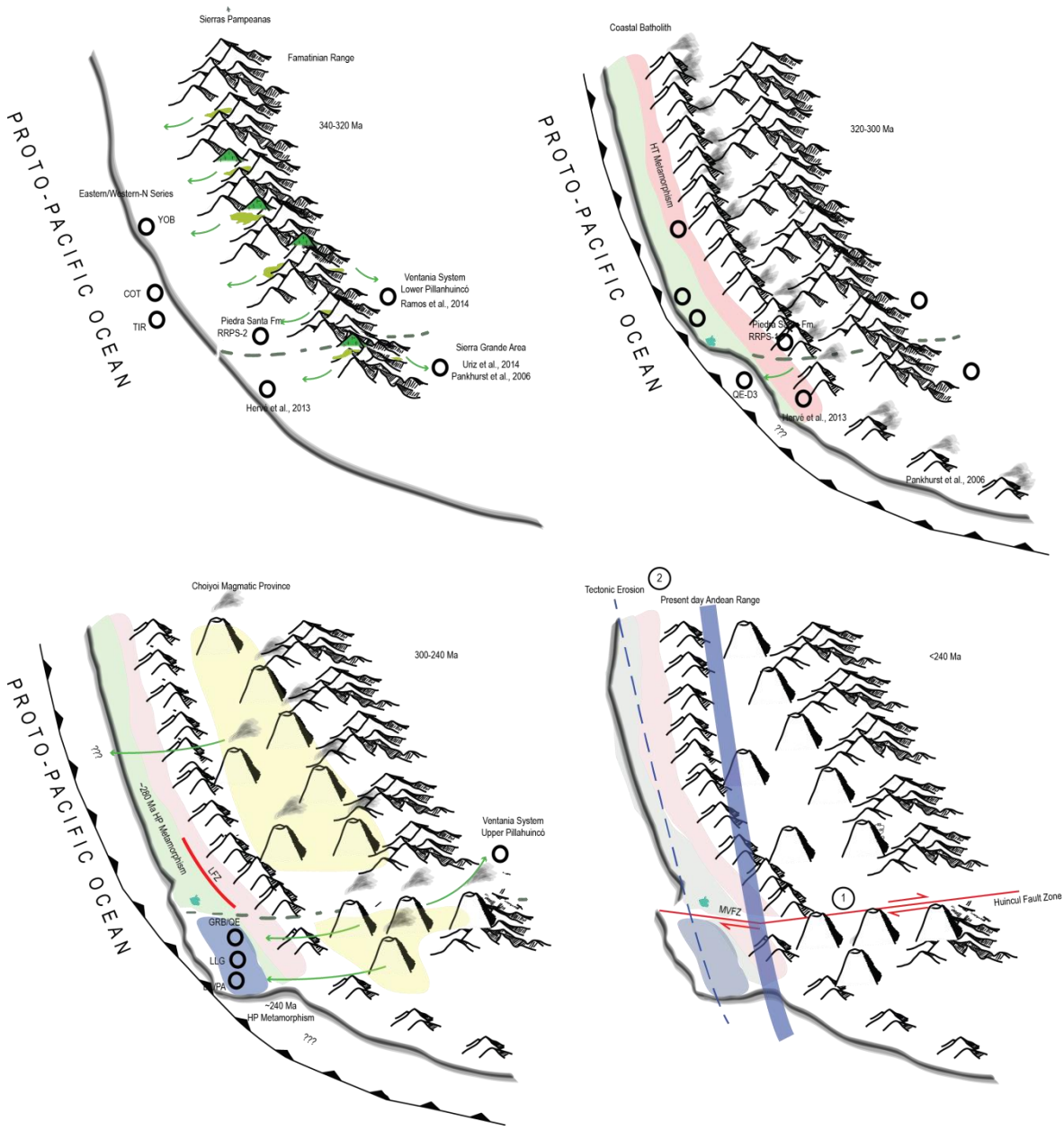

FIGURE 10. ROMERO ET AL.

3. Timing of the tectonic emplacement of ultramafic rocks and metasediments in the southern section of the coastal accretionary complex of Central Chile

Rurik Romero[a], José M. González-Jiménez[a], Fernando Barra[a], Mathieu Leisen[a], Leonardo N. Garrido[a], Cristina Talavera[b], Sarah Gain[d], William L. Griffin[d], Suzanne Y. O'Reilly[d], Martin Reich[a], Diego Morata[a]

a. Department of Geology and Andean Geothermal Center of Excellence (CEGA), FCFM, Universidad de Chile, Plaza Ercilla 803, Santiago, Chile.
b. Department of Physics and Astronomy, Curtin University, Perth, WA 6102, Australia
c. Centre for Microscopy Characterization and Analysis, The University of Western Australia, Crawley, WA 6009, Australia

Submitted

To

International Geology Review

*Corresponding author: Rurik Romero

Address: Universidad de Chile, Departamento de Geología,

Plaza Ercilla # 803, Santiago de Chile, Chile

Phone: +56 2 978 06 43

E-mail: rurikrom@gmail.com

Abstract

New U-Pb ages are presented for ultramafic rocks and host micaschists of the La Cabaña area in the southern section of the coastal accretionary complex of Central Chile. Metasedimentary rocks of the Western Series hosting the ultramafic bodies, contain a main population of detrital zircons of Devonian age (365-380 Ma), very diferent from neighbouring areas where Devonian zircons are scarse. On the other hand, zircon ages from metasomatic rocks (albitites and chlorites) produced along the disequibrium-contact between the metasediments and the ultramafic bodies, are mainly Ordovician (~478 Ma) and deprived from devonian zircons, which resembles a typical detrital zircon pattern from other locations of the Western Series. A population of zircons from the chloritite wall rock of the small body of Lavanderos, the easternmost ultramafic body in La Cabaña, is in textural equilibrium with metamorphic ilmenite. These zircons yield an age peak of 285 ± 10 Ma (n =3) identical, within error, to the previously reported K-Ar cooling age of fuchsite determined at 282 ± 6 Ma. Most zircons extracted from chromite pods have euhedral oscillatory-zoned growth patterns with a similar range of ages that those reported on northern host rocks (324 - 1090 Ma; n = 12), except for three cloudy zoned zircons with high U/Th ratios with a close age peak at 285.5 ± 7 Ma (n = 2).

The presence of early permian ages (~280-290 Ma) on all the studied rocks suggests the remobilization of Zr. This process would be triggered by metamorphic fluids as a result of the disequilibrium reaction when ultramafic rocks were emplaced with the metasediments within the accretionary complex. In this period, Paleozoic and mesoproterozoic zircons inherited from the metasedimentary host rocks were also mechanically incorporated in ultramafic rocks.

Keywords: Chromitites, zircon, metamorphism.

1. Introduction

La Cabaña metaperidotite is the largest known exposure of ultramafic rocks in the metamorphic basement of the Coastal Cordillera of central Chile. The metamorphic basement corresponds to an acretionary complex developed at the continental paleo-Pacific margin of Gondwana during Late Paleozoic times. The ultramafic rocks are exotic blocks that were incorporated into the metasedimentary rocks during the first stages of the acretionary complex formation (Hervé, 1988, Willner et al., 2005). As a result of the hot emplacement of these ultramafic rocks, the metasedimentary host schists developed local thermal metamorphism, leading to the formation of a well-developed meter-scale blackwall (Höfer et al., 2001). Detailed observations of the structure of this blackwall shows a clear zonation from the host rocks towards the serpentinized ultramafic rocks, and includes micaschists, biotitite, albitite, chloritite, tremolite-rich anfibolite, and silicified/talquitized serpentinite (Höfer et al., 2001). The aforementioned authors suggested that serpentinite, blackwall and micaschists preserve common syndeformational structures indicating that the blackwall marks the time of the emplacement of the ultramafic bodies into the host metasediments. However, there are no geochronological constrains for the age of formation of this blackwall, and therefore of the emplacement of the peridotite into the continental crust.

The only radiometric age available for the area is a K-Ar date of fuchsite collected at the contact between metabasites and metapelites with abundant Cr-tourmaline and fuchsite (Rabbia et al., 1997), which provided a cooling age of 282±6 Ma interpreted as the timing of cooling of Cr-rich muscovite. The latter crystallized from fluids which remobilized Cr from the serpentinites once they were emplaced into the host rocks. These ages are slightly younger than $^{40}Ar/^{39}Ar$ plateau ages obtained from white micas within metapelitic schists in the Western Series between 32-35°30'S (290-319 Ma; Willner et al., 2005), although significatively older than those obtained further south in micas from metapelites of the Bahia Mansa Complex (243±4 Ma in Mehuín, ~245 Ma in Morro Bonifacio, and ~248 Ma in Hueicolla; Duhart et al., 2001). Furthermore, fission-track ages on zircons from

metapelites between 32-35°30'S, also belonging to the Western Series, constrains an exhuming event of metasedimentary rocks between 206-232 Ma (Willner et al., 2005).

With the aim to better constrain the emplacement age of the La Cabaña ultramafic peridotites into the acretionary complex, we present the first U-Pb zircon ages from rocks of the metasomatic blackwall formed at the boundary between the La Cabaña ultramafic bodies and the host schists: a biotite-albitite schist (sample CA14-4) and a chloritite schist (sample LAV-14-5) in which both a zircon mount and zircons in a thick section were analyzed. In order to contextualize the age of the metasomatic blackwall within the framework of the tectonic evolution of the area we also performed U-Pb zircon dating of the host micaschist in La Cabaña (3 samples) . Additonally, we extracted zircon grains from four chromitite samples hosted within the serpentinites.

2. Geological setting

2.1. The Coastal Cordillera of central Chile

The metamorphic units of the Coastal Cordillera of central Chile crop out almost continuously between 32°S and 43°S in the Pacific coast of Chile (Fig. 1a), and constitutes the Metamorphic Basement of central Chile. The oldest unit of this basement is a paired metamorphic belt with two sub-units known as the Eastern and Western Series (Aguirre et al., 1972; Fig. 1a). The Eastern Series consist of metasandstones and metapelites weakly deformed (González-Bonorino, 1971) affected by high temperature and low-pressure metamorphism by the intrusion of the Coastal Batolith between 320-300 Ma (Willner, 2005; Deckart et al., 2013). The Western Series consists of micaschists of psamopelitic protoliths of continental origin, metabasites (metagabbros and metavolcanic rocks) and highly serpentinized peridotites, which were interpreted by Hervé (1974) as remmants of a dismembered ophiolite complex. There is a general consensus that this type of ophiolite may form in a suprasubduction zone (*sensu* Dilek and Furnes, 2011), although the hypothesis on the position within this tectonic environment varies from fore-arc (Hervé et al., 1976; Godoy, 1979), back-arc (Frutos and Alfaro 1987; Rabbia et al. 1994; Hufmann and Massonne 2000; Höfer et al. 2001) or intra-arc (Barra et al., 1998; González-Jiménez et al., 2014). Overall, the rocks of this unit are characterized by high pressure and low temperature (HP-LT) metamorphism. Greenschists facies (7-9.3 kbar and 380-400°C) are

widespread on the complex associated with final exhumation of the metamorphic rocks during development of an accretionary complex, nevertheless, isolated blocks of blueschists indicate higher pressure peak metamorphic conditions at 9.5-10.7 kbar and 350-385°C (Willner, 2005; González-Jiménez et al., accepted).

2.2. The ultramafic bodies of the La Cabaña area

La Cabaña area is located 60 km north-west of the city of Temuco (Fig. 1a), and comprises six known outcrops of metamorphosed ultramafic rocks, namely Centinela Bajo Norte, Centinela Bajo Sur, Encanto River, Loma Gúzman, Lavanderos and Mina de Talco (González-Jiménez et al., 2016a and references therein). Chromitite samples and rocks from the blackwalls were collected at Centinela Bajo Norte and Lavanderos (Fig. 1c). Centinela Bajo Norte is a small body of ~6 km long and 3 km wide that comprises isolated blocks of massive spinel-bearing and clinopyroxene-poor meta-dunites (< 60 % of olivine replaced by lizardite) embedded in a matrix of schistose, locally mylonitic, antigorite (Atg) serpentinites (Barra et al., 1998; Höfer et al., 2001; Barra et al., 2014; González-Jiménez et al., 2016a). Both lizardite-bearing metadunites and Atg-serpentinites display similar trace-element profiles that are enriched in Fluid Mobile Elements (FME: As, Sb, B, Li, Cs, Pb, U, Ba, Sr), a geochemical fingerprint that indicates hydration and subsequent serpentinization of the protholitic peridotites within a mantle wedge above a subducting slab (c.f. Deschamps et al., 2011).

According to González-Jiménez et al. (2016a), massive dunites experienced hydration at depths of 1.6-3.2 GPa and temperatures < 400ºC, which promoted the replacement of olivine by lizardite (Lz) ± magnetite (Mag). In contrast, schistose and mylonitic antigorite serpentinites experienced prograde metamorphism at much higher pressures (2-2.6 GPa) and temperatures (400-600ºC) associated with the development of a subduccion channel prior of the formation of the Paleozoic accretionary complex of the Chilean Coastal Cordillera (González-Jiménez et al., accepted). These metamorphic temperatures are in good agreement with those estimated for the metamorphic peak in the host metapelitic rocks (i.e., 380-420ºC at 0.7-0.9 GPa; Willner, 2005; Glodny et al., 2005). The emplacement of peridotites into the metasedimentary rocks as hot bodies was estimated to occur at 510-560ºC from metamorphic rims in chromite grains from the serpentinites and

chromitites as well as at 520-550ºC by the formation of metasomatic reaction (blackwall) zones (Höfer et al. 2001). The exhumation of the ultramafic bodies and their host rocks as a coherent block is registered by a common greenschist-facies overprint (300-400ºC, 0.3-0.4 GPa) recorded in serpentinites, associated chromitites and sulfide occurences, and metapelites (González-Jiménez et al., 2016a).

The blackwall zone comprises different lithological domains, where a biotite-albite schist is identified as the most proximal to the metasedimentary host rocks, and formed by Mg-rich solutions derived from the altered serpentinites. Most of this zone is composed of biotite with large porphyroclasts of albite and highly chloritized garnet (Höfer et al., 2001). An anfibolite/chlorite-rich domain is located closer to the ultramafic body and is dominated by large tremolite crystals coexisting with antigorite. K-Ar dating of a Cr-rich mica (fuchsite) from this domain yielded a cooling age of 286±2 Ma (Rabbia et al., 1997). Chloritite rocks are almost monomineralic Mg-chlorite but also contain accessory phases such as sphene, apatite, and zircons. Additionally, talc schist formed within fault zones comprises talc, and scarse amphibole and chlorite.

3. Sampling and analytical methods

Five to ten kg of sample of the different rock-types forming the blackwall, micaschists and chromitite boulders were collected from the Centinela Bajo Norte and Lavanderos ultramafic bodies in order to extract zircons for U-Pb dating. Additionally, we performed polished thick sections of an ilmenite-bearing chloritite from the blackwall of the Lavanderos outcrop to perform in-situ U-Pb zircon.

3.1. Zircon separation and concentration

Zircons from the host micaschist and chloritite were extracted at the sample preparation lab in the Geology Department, Universidad de Chile by crushing, Frantz separator, Gemini water table and heavy liquids. A fraction of zircons were mounted on epoxy resin for later U-Pb dating. Also, a thick section of the chloritite was prepared for in-situ U-Pb dating.

Five chromitites boulders found scattered in Centinela Bajo, were processed in order to extract zircons. About 10 kg of sample were processed, but zircons were recovered only in

four of these samples. An amphibolite on the eastern contact of Centinela Bajo was also sampled, but no zircons were obtained.

Zircons were concentrated using conventional methods, i.e., heavy liquids, and a Frantz magnetic separator in a selFrag laboratory. In an effort to recover the maximum number of zircon grains from the chromitite samples and the albitite biotitite schist, samples were processed at the SELFRAG Lab at the GEMOC/CCFS Centre, Department of Earth and Planetary Sciences, Macquarie University, Sydney, Australia. About 10 kg of sample were first put in a plastic bag and then crushed using an automatic press in order to reduce the rock size to about 3-4 cm. These small rock bits were disintegrated using the SELFRAG high voltage pulse power fragmentation system. The disintegration parameters were set at 10 mm gap, 200 pulses per cycle, 3 pulses per second frequency, and variable voltage (115kv – 140kv). The disaggregated sample was screened using 210μm disposable sieves and the <210 μm fraction panned with a Russian Lotok (pan) to remove the bulk of the sample including the fines and the light material fraction. The non-magnetic fraction was separated from the panned concentrate using a Frantz LB-1 Magnetic Barrier Separator set at 1.7A /ss=10^0 /fs=15^0 and then treated by heavy liquid separation using a sodium polytungstate solution with a density of ~3 g/cm^3 to produce the final zircon concentrate. Zircons were then hand-picked from the concentrate and mounted in epoxy resin for subsequent lapping, polishing, and analysis.

3.2. Mineral imaging

Prior to the isotopic analyses all zircon grains were imaged by Cathodoluminescence (CL) and by back-scatered electron (BSE) mode to examine their internal structure and relate it with possible chemical zoning. CL and BSE images of the zircons were obtained using two Scanning Electron Microscopy (SEM): (1) a FEI Quanta 250 at the Electron Microscopy Laboratory of the Andean Geothermal Centre of Excellence, CEGA-Universidad de Chile, and (2) a Zeiss EVO MA15 at the Geochemical Analysis Unit (GAU) of the GEMOC/CCFS Centre in the Department of Earth and Planetary Sciences, Macquarie University, Sydney.

3.3. U-Pb dating

Zircons with a grain-size less than 50μm recovered from the chromitite samples were mounted with TEMORA-2 standard (416.5 ± 0.22 Ma; Black et al., 2004) in 25 mm diameter epoxy disc and then polished and coated with gold. The analyses were performed over two sessions using a SHRIMP II instrument, in the John de Laeter Centre for Isotope Research, Curtin University, Perth, Australia, following standard operation procedures (Compston et al., 1984; Williams, 1998). During analytical runs, the primary (O_2^-) ion beam was 0.6 nA during the first session and 1.2 nA during the second session, with a spot size of 15 μm. The data were processed using the Squid and Isoplot programs (Ludwig, 2010). Common Pb was subtracted using the measured ^{204}Pb and common Pb composition determined using the Stacey and Kramers (1975) model.

U-Pb dating of zircons from the host rocks were performed at the Isotopic Geology Laboratory of the Andean Geothermal Centre of Excellence (CEGA) using a laser ablation system coupled to a multicollector mass spectrometer with inductively coupled plasma (LA-MC-ICPMS). The laser ablation system is an Analyte G2 193 nm ArF excimer laser manufactured by Photon Machines with a double volume HelEx ablation cell that allows for a He atmosphere ablation. The MC-ICPMS used in this study is the Neptune Plus, manufactured by ThermoFisher Scientific. The instrument has six Faraday detectors and six ion counters (CCD). The laser diameter used for ablation was 30 microns and the 'sample bracketing' method was used to correct for mass bias. The Plešovice zircon was used as the primary standard and 91500 (Wiedenbeck et al., 1995; 2004) or Sri Lanka-2 (SL-2) (Gehrels et al., 2008) as a secondary standard. Data reduction was performed with Iolite software (Paton et al., 2011). A detailed description of the methods and equipment employed in this study can be found in Leisen et al. (2016).

4. CL imaging and zircon geochronology

4.1. Host rocks— metasedimentary micaschits

Highly foliated metapelitic quartz-rich micaschists are the host rock enclosing the ultramafic bodies of the La Cabaña area. The three schists selected for this study (samples CA15-11, CA15-26 and CA15-13; Fig. 1b) consist of abundant white mica, quartz, biotite, albite porphyroblasts, occasionally retrograde chlorite altering biotite and possible organic

material (Fig. 2a). This mineral assemblage has been interpreted to be representative of a psammopelitic environment of deposition (Hervé, 1988).

Zircons recovered from these samples show CL images with the typical oscillatory zonation of grains crystallized from melts or fluids (Fig. 3). A total of 154 LA-MC-ICPMS analyses were performed on oscillatory cores and rims of zircons recovered from the three studied samples (Table SM1). Mostly all analyses cluster along the Concordia curve, except for sample CA-15-26, where Pb loss was detected. The cumulative plots show a clear predominance of Paleozoic ages (Fig. 4), ranging from Lower Carboniferous (~340-350 Ma) to Ordovician (~470 Ma) ages. Devonian peaks are dominant (e.g., 364, 369, and 381 Ma) and secondary peaks at 413 and 419 Ma are detected. Mesoproterozoic ages are also identified in the 1200-1000 Ma interval, but they do not define a clear peak age.

4.2. Blackwall— Biotite-albite schists

A biotite-albitite sample (CA-14-4) was colected along the western flank of the Centinela Bajo ultramafic body in contact with rodingitized metagabbros (Fig. 1c). The biotite-albitite rock comprises large albite porphyroblasts, partially chloritized biotite and quartz (Fig. 2b). Zircons recovered from this rock are euhedral with prismatic habits and concentric zoning in CL images (Fig. 3). A total of 15 U-Pb ages were obtained (Table SM2) which range from Archean (3693 Ma) to Upper Devonian (367 Ma), although most of the grains yielded ages between 600-400 Ma and Meso-proterozoic ages (~1080 Ma) (Fig. 4).

4.3. Blackwall—chloritite schist

The studied chloritite (sample LAV-14-5) contained an unusual number of zircons, which were analyzed using two different approaches. The first one used in-situ zircons found in an ilmenite-bearing vein observed in a polished thick block, whereas the second one used zircon grains extracted from the bulk-rock chloritite using conventional separation methods. The zircons were later mounted on a polished epoxy mount for LA-MC-ICPMS analysis at Universidad de Chile.

A particular thick section of the sample LAV-14-5 consists of >90% Mg-rich chlorite matrix (Fig. 2c) crosscut by a centimetric ilmenite vein with titanite rims and minor

occurrence of rutile within the ilmenite. Milimetric monacite-(Ce) and xenotime-(Y) grains grows on the contact of the ilmenite and chlorite matrix. Disseminated apatite and zircons ocurr in the chlorite matrix, mostly surrounding the ilmenite vein (Fig. 5). Electron backscattered images on these zircons show that most of them have sub-rounded shapes, "spongy" texture, intergrowth with chlorite, EDS spectrums with high-U regions and occurrence of high-Th inclusion, probably thorite ($(Th,U)SiO_4$), all of these clear signs of reabsorption or metamorphic growth (Corfu et al., 2003) in textural equilibrium with chlorite matrix (Fig. 5). 20 U-Pb ages were obtained from these zircons (Table SM3) which are highly discordant as shown on the Concordia plot (Fig. 6a), scattering from Late Devonian (396.5 ± 5 Ma) to Triassic (228 ± 8 Ma) ages (Fig. 6b). Peak ages were observed in cumulative-age probability plots, with minor age clusters at around ~241 and ~285 Ma, and older clusters at 350, 367 and 391 Ma (Fig. 6b).

The bulk rock sample, devoided of ilmenite veins, contains zircons predominantly euhedral with variable degree of fracturation, in CL images shows oscillatory-zonations (Fig. 2). Only a few grains show cloudy zonation and bright rims. U-Pb ages (Table SM4) of the euhedral zircons range from a 326 to 11262 Ma whereas two zircons yield younger ages at 206±8 Ma and 258±7 Ma. The probability density plot (Fig. 4) shows the youngest population represented as a peak at 337 Ma represented by four grains. The most important input is Ordovician, represented in a 478 Ma peak (n = 7), followed by Cambrian zircons at 505 and Upper Neo-Proterozoic peak ages at 556, 611 and 649 Ma, each one with at least four grains. Meso-proterozoic ages are scattered on this period with no major probabilistic peaks but distributed between the 1200-1000 Ma.

4.4. Chromitite boulders

Several authors have reported large boulders of chromitite in La Cabaña (Vergara, 1970; Barra et al., 1998; Höfer et al., 2001). These boulders consist of massive chromitite (>90% chromite) and has been interpreted as 'chromitite floaters' liberated mechanically from the ultramafic host rocks. At hand-specimen scale, most of these boulders have a secondary mineralogy on brittle fractures filled with kämmererite (Cr-rich chlorite) and a late generation of chrysotile and Mg-carbonates (Barra et al., 2014). In this work, we analyzed

zircons in four chromitite boulders (Samples CAB-71, CA14-39, CA14-41 and CA14-5). U-Pb ages are reported in Table SM5.

Sample CAB-71 is the one that most zircons were recovered (n =8). CL images shows sub-euhedral fractured zircons with concentrical CL zoning, no metamorphic growths or cloudy zonations were identified (Fig. 3). U-Pb analyses yielded between Silurian (442 Ma) to Mesoproterozoic ages (1090 Ma) and a single Paleoproterozoic age (1907 Ma) was also obtained (Fig. 7).

Only three zircons were extracted from sample CA14-41. Two of them are euhedral and show a concentric zoning in CL images, while the third one has an irregular CL zonation. U-Pb ages for this sample are: Lower Mississipian (355 ± 9 Ma), Lower Devonian (418 ± 9Ma), and Silurian (431 ± 6 Ma).

Sample CA14-39 also had three zircons. Two of these grains are subeuhedral and the other is anhedral. These three grains have irregular zoning or show no zoning in CL images. (Fig. 3). U-Pb data shows that the oldest grain is Upper Mississippian (324 ± 5 Ma), whereas the other two have a Pennsylvanian (309 ± 6Ma) and a Permian age (281 ± 7 Ma). These two last grains have a high U/Th ratio of 100 and 33, respectively.

Finally, from sample CA14-5 only one zircon was recovered. The zircon grain is anhedral with a cloudy zonation (Fig. 3), has a high U/Th ratio of 33 and yielded a Permian age (287 ± 4 Ma).

5. Discussion

5.1. Inherited zircons of detrital origin in micaschists, blackwall and chromitite boulders

Micaschist from this study, sampled roughly south-west of La Cabaña ultramafic bodies (samples CA15-11, CA15-13 and CA15-26 in Fig. 1b), show a predominance of Devonian age zircons (365-400 Ma). Is noteworthy that the typical features of the metasedimentary samples further north on the Paleozoic Basement are a widespread presence of ~470 Ma and Mesoproterozoic (1200-1000 Ma) ages, which are virtually nonexistent in this new data.

Devonian zircons from all the analyzed micaschist of this study when plotted cluster around a ~368 Ma peak (Fig. 8). These are majorly prismatic grains with concentric CL zoning, this observation is complemented with the low U/Th ratios which allows us to conclude a magmatic origin of those zircons.

The micaschists U-Pb detrital zircon age patterns are very different to those reported for micaschists located north of La Cabaña ultramafic bodies(samples COT14-1, TIR-14-1 in Fig. 1; Data in Romero et al., 2016), with main age peaks at ~470 Ma and at 1200-1000 Ma (Fig. 4). These patterns are devoided of Devonian zircons, a typical feature identified in metasedimentary rocks from Late Paleozoic metamorphic units of Chile and Argentina (Pankhurst et al., 2006; Alvarez et al., 2011; Hervé et al., 2013; Maksaev et al., 2015), and whose protoliths have been interpreted to be pelitic to continental sedimentary deposits in the margin of Gondwana with a provenance from a mountain range with similar features as the Sierras Pampeanas (as in Alasino et al., 2015) outcropping on Argentina.

The source of Devonian zircons in the neighbourhood of La Cabaña remains unknown because there are no reported intrusions of Devonian age at these latitudes. The nearest Devonian intrusion is the 395±4 Ma tonalite of San Martin de los Andes, Argentina, located ca. 40 ºS (Pankhurst et al., 2006). However, this unit is an unlikely source of Devonian zircons in La Cabaña, because this ca. 395 Ma age is poorly represented in the Devonian age peaks of La Cabaña rocks. Furthermore, the lack of a ~395 Ma age peak in the nearest metapelites from the Eastern Series at Ranco Lake (Hervé et al., 2013), suggests that this tonalite was probably not exposed at the time of sedimentation . Thus, the distribution of detrital zircon age populations around La Cabaña suggest the presence of a Devonian (365-380 Ma) intrusion on a western position from the sedimentary basin of the pelitic protolith, supporting an arc/backarc model as proposed by Frutos and Alfaro (1987) and later revised by other authors (Barra et al., 1998; González-Jiménez et al., 2014). This paleotectonic configuration could explain the zircon age patterns observed in the area, where sediments deposited in a proximal position to the continental margin are domined by Ordovician zircons, and zircons of a 365-380 Ma age derived from a magmatic body, presumably an oceanic arc, were deposited in a south-westernmost position in the sedimentary basin. In this case, La Cabaña massif represents a transition between both depositional environments.

Zircons from the biotite-albitite schists have Early Paleozoic ages, between ~604 and ~367, and Mesoproterozoic ages in the interval of 1200-1000 Ma. These zircons, like those magmatic zircons found in the micaschist host rock, exhibit prismatic forms, internal concentric zoning and low U/Th ratios (Table SM 2). Nevertheless, the number of recovered grains was limited, and does not allow for a proper comparison with the age pattern detemined for the metapelitic schists. Similarly to the biotite-albitite schists, many of the zircons from the bulk rock chloritite blackwall are prismatic with perfect oscillatory zoning and have low U/Th, as also recognized in magmatic zircons from the enclosing micaschist. The probability density plot obtained from zircons of magmatic origin in this chloritite is very similar to those obtained in the micaschists north of La Cabaña by Romero et al., 2016 (Fig. 1, 4) as well as in many other metasedimentary rocks from the northern section of the metamorphic basement (Willner et al., 2008; Hervé et al., 2013).

The observation that biotite-albitite and chloritite show similar detrital zircon patterns and, in turn, to those reported for rocks from the northern section of the metamorphic basement led us to suggest that these are zircons inherited from the host micaschists, which were not affected by the metasomatic reaction that formed the blackwall.

Chromitites hosted in serpentinites also contain prismatic zircons with concentric zoning and ages between 324-1090 Ma, similar to those of the micaschists host rocks. It is noteworthy that some grains obtained from sample CAB-71 have Proterozoic inherited cores with Ordovician magmatic/metamorphic rims (Fig. 2), expected for a zircon formed on the widespread Ordovician Famatinian orogeny which intrudes Mesoproterozoic (‘Grenvillian’) basement in South America. In this scenario, it is proposed that zircons from the host rocks were incorporated into the chromitite-bearing ultramafic bodies by fluids released during metamorphism (e.g., Belousova et al., 2015; Griffin et al., 2016). Interestingly, these chromitites are crosscut by late chlorite and chrisotile veins, which represent former fractures where fluids carrying zircons could infiltrate the peridotite. The observation that chlorite veins are comprised of Cr-rich chlorite identical to that intergrowth with secondary metamorphogenetic chromite rims in chromitite, cleary support the possible incorporation/recrystallization of these zircons by/from fluids of metamorphic origin.

We suggest that fluids saturated in Zr released from the host micaschists not only introduced the zircons but also contributed to crystallization of new ones.

5.2. Age of tectonic emplacement of ultramafic rocks into the acretionary prism

According to previously published structural, geochemical and petrological works (Höfer et al., 2001; González-Jiménez et al., 2016a) the genesis of blackwalls at the contact between ultramafic rocks and host micashists was associated with the hot intrusion of the former into the latter. Höfer et al. (2001) proposed that the formation of the blackwall reaction took place 282 ± 6 Ma ago on the basis of ^{40}K-^{40}Ar cooling age of fuchsite found in the tourmaline-rich contact between metabasites and metapelites near Lavanderos. This age matches very well with those obtained from a young population of metamorphic zircons identified in the ilmenite-bearing cloritite (285 ± 10 Ma weighted average; n= 3) and the anhedral cloudy zoned grains on chromitite which have U/Th ratios 30< (285.5 ± 7 Ma weighted average; n =2). The metamorphic origin of zircons within the chloritite is supported by the fact that they are in textural equilibrium with chlorite and rutile transformed to ilmenite (Fig. 4) as well as the cloudly internal structure and abundant inclusions of Th-rich minerals (thorite) (Fig. 4), typical of metamorphic zircons (Corfu, et al., 2003). According to Kohn et al. (2015) the dissolution of zircons takes place on prograde conditions where rutile grains are more stable and the later transformation of rutile to ilmenite marks the zircon growth rates proggresively on cooling conditions starting from 700°C. Therefore, the textural equilibrium between the zircons, xenotime/monacite and oxides intergrowth with chlorite clearly suggests the remobilization of zirconium and other REE by metamorphic fluids during the disequilibrium contact between the hot intruding ultramafic body and host metasediments. All these observation suggest that intrusion of the ultramafic bodies into the metasediments and the subsequent formation of the blackwall took place at least at ca. 285 Ma ago.

On the other hand, a triassic exhuming period has been proposed by Willner et al. (2005) as fission-track in zircons from metapelites from the Eastern and Western Series between 34-35°30'S suggests a later exhumation in a time span of 26 Ma, between 232 and 206 Ma. Indeed, this exhumation process could be represented on the reaction zone ilmenite-bearing chloritites, with the youngest metamorphic zircon U-Pb ages clustering at ~241 Ma (Fig.5)

but temperatures reached on this exhumation phase described by Willner et al., (2005) are between 300-200°C, temperatures which are very low to dissolve and reprecipitate zircon grains. A posible solution to this paradox is a complexation and of Zr in low temperature metamorphic fluids, as the ligant PO_4^{3-} can facilitate the mobilization of Zr at very low temperatures (<200°C) (Linnen et al., 2014), which is coherent with the presence of apatite, xenotime and monacite grains associated to the rutile/ilmenite vein with zircons on thick section.

Therefore, from the new data presented in this work we proposed that: (1) the age of 285 ± 10 Ma dates the late formation of the blackwall and hence the final emplacement of the ultramafic rocks in the host metasedimentary schists, after temperatures high enough to promote the formation of amphibolitites that age reflects a late crystallization of metamorphic zircons within the reaction zone and chromitite on retrograde conditions, and (2) the development of the aureole and intrusion of ultramafic rocks and exhumation persisted for ca. 45 Ma between 286 and 241 Ma.

6. Conclusions

The host rocks of La Cabaña metaperidotites have two distinct detrital zircon patterns, a classical pattern with mostly Ordovician ages, devoided of Devonian zircons and presence of mesoproterozoic ages, and another with mostly Devonian zircons and little presence of other ages. In the reaction zone, the chloritite and albitite-biotite members have similar patterns of U-Pb ages than the classic host rocks, which are interpreted as inherited zircons from the host rock micaschists within the reaction zone. Nevertheless, metamorphic zircons were also identified in a thick section of the chloritite which cluster at ~285 Ma.

U-Pb ages prismatic zircons from chromitites scatter on the same interval as the host rock metapelites, from Carboniferous to Mesoproterozoic ages, which is clear evidence for an infiltration of those zircons from the host rocks to ultramafic rocks.

On the other hand, a ~285 Ma cluster of anhedral zircons of the chromitites is closely related to the metamorphic zircons found on the chloritite. This reflects the timing of tectonic emplacement, where ultramafic and metapelitic rocks shared a common

metamorphic path on retrograde conditions, marking also the time where zircons with a wide variety of ages were physically incorporated on the ultramafic rocks.

7. Acknowledgements

This research has been financially supported by a Fondecyt Intiation Grant #11140005 to J.M. González-Jiménez entitled "*Decoding precious metals (platinum-group elements and gold) in upper mantle rocks of the Chilean Cordillera*" and Fondecyt Grant #1110345, entitled "Origin and evolution of the Coastal Cordillera ophiolite complex, Central Chile" to F. Barra. Additional funding was provided by FONDAP project 15090013 "*Centro de Excelencia en Geotermia de los Andes, CEGA*". The authors acknowledge support through the MSI "*Millennium Nucleus for Metal Tracing Along Subduction*" (NC130065).

Figures

Figure 1. (a) Distribution of the geological units of the Metamorphic Basement of central Chile and location of the study area, (b) Geologic sketch map of the studied area showing the location of regionally sampled micaschists, (c) Geologic map of La Cabaña including samples dated in this study. Modified from SERNAGEOMIN (2003) and Höfer et al. (2001).

Figure 2. Photomicrographs of studied samples. (a) Host rock micaschist, (b) Blackwall albitite-biotitite schist, (c) Blackwall chloritite and (d) Chromitite with chlorite alteration.

Figure 3. Representative CL images of zircon grains from micaschists, reaction zone chloritite and biotite-albitite schist, and chromitite boulders. $^{206}Pb/^{238}U$ ages and U/Th ratios are indicated on each grain.

Figure 4. Probability density plots of U-Pb zircon ages from host rock micaschists and blackwall units.

Figure 5. Electron microscope images of a section of the ilmenite bearing LAV-14-5 sample. (a) Backscatter image the ilmenite vein on the chlorite matrix, some of the numerous zircons are indicated in the image. (b) Detailed view of a single zircon grain in

the chlorite matrix with apatite grains. (c,d) representative zircon grains intergrowth with chlorite. Note the bright inclusions of Th-rich mineral. (e,f) CL images of zircons from figs. c and d.

Figure 6. In-situ U-Pb ages of Lavanderos ilmenite-bearing chloritite. (a) Concordia plot. (b) Probability density plot of $^{206}Pb/^{238}U$ ages.

Figure 7. U- Pb concordia diagrams for the zircon data obtained on each chromitite-ore.

Figure 8. Probability plots of the two different zircon age populations found on the host rock micaschists of La Cabaña Metamorphic Complex, main peak of each population is indicated. Metamorphic zircons of the reaction zone chloritites and from chromitite ores are indicated in the green area as well as the fuschite K-Ar age reported by Hofer et al. (2001).

References

Aguirre, L., Hervé, F., Godoy, E., 1972, Distribution of metamorphic facies in Chile, an outline: Kristalinikum, v. 9, p. 7–19.

Alasino, P., Dahlquist, J., Pankhurst, R., Galindo, C., Casquet, C., Rapela, C., Larrovere, M., Fanning, C., 2012, Early Carboniferous sub- to mid-alkaline magmatism in the Eastern Sierras Pampeanas, NW Argentina: A record of crustal growth by the incorporation of mantle-derived material in an extensional setting: Gondwana Research, v. 22, p. 992–1008.

Barra, F., Rabbia, O., Alfaro, G., Miller, H., Höfer, C., Kraus, S., 1998, Serpentinitas y cromititas de La Cabaña, Cordillera de la Costa, Chile central: Revista Geológica de Chile v. 25, p. 29-44.

Belousova, E., González-Jiménez, J.M., Graham, I., Griffin, W., O'Reilly, S., Pearson, N., Martin, L., Craven, S., Talavera, C., 2015, The enigma of crustal zircons in upper-mantle rocks: Clues from the Tumut ophiolite, southeast Australia: Geology, v. 43, p. 119-122.

Black, L.P., Kamo, S.L., Williams, I.S., Mundil, R., Davis, D.W., Korsch, R.J., Foudoulis, C., 2003, The application of SHRIMP to phanerozoic geochronology: a critical appraisal of four zircon standards: Chemical Geology, v. 200, p. 171-188.

Compston, W., Williams, I., Meyer, C., 1984. U-Pb geochronology of zircons from Lunar Breccia 73217 using sensitive high mass-resolution ion microprobe. Journal of Geophysical Research, v. 89, p. 525-534.

Corfu, F., Hanchar, J., Hoskin, P., Kinny, P., 2003, Atlas of Zircon Textures: Reviews in Mineralogy and Geochemistry, v. 53, p. 469-500.

Deckart, K., Hervé, F., Fanning, M., Ramírez, V., Calderón, M., y Godoy, E., 2014, U-Pb geochronology and Hf-O isotopes of zircons from the pennsylvanian coastal batholith, south central Chile: Andean Geology, v. 41, p. 49-82.

Deschamps, F., Guillot, S., Godard, M., Andreani, M., Hattori, K., 2011, Serpentinites act as sponges for fluid-mobile elements in abyssal and subduction zone environments: Terra Nova, v. 23, p. 171–178.

Dilek, Y., Furnes, H., 2011, Ophiolite genesis and global tectonics: Geochemical and tectonic fingerprinting of ancient oceanic lithosphere. GSA Bulletin, v. 123, p. 387-411.

Duhart, P., McDonough, M., Muñoz, J., Martin, M., y Villaneuve, M., 2001, El Complejo Metamórfico Bahía Mansa en la Cordillera de la Costa del centro-sur de Chile (39°30'-42°S): Geocronología K-Ar, $^{40}Ar/^{39}Ar$ y U-Pb e implicancias en la evolución del margen sur-occidental de Gondwana: Revista Geológica de Chile, v. 28, p. 179-208.

Frutos J., Alfaro, G., 1987, Metallogenetic and tectonic characteristics of the Paleozoic ophiolitic belt of the southern Chile coast cordillera: Geologische Rundschau, v. 76, p. 343–356.

Gehrels, G., Valencia, V., Ruiz, J., 2008, Enhanced precision, accuracy, efficiency, and spatial resolution of U-Pb ages by laser ablation–multicollector–inductively coupled plasma–mass spectrometry. Geochemistry Geophysics Geosystems (G3), v. 9.

Glodny, J., Lohrmann, J., Echtler, H., Gräfe, K., Seifert, W., Collao, S., Figueroa, O., 2005, Internal dynamics of a paleoaccretionary wedge: Insights from combined isotope tectonochronology and sandbox modelling of the south-central Chilean forearc: Earth and Planetary Science Letters, v. 231, p. 23–39.

Godoy, E., 1979, Metabasitas del basamento metamórfico, *in* Congreso Geológico Chileno: Actas, p. 133–144.

González-Bonorino F., 1971, Metamophism of the crystalline basement of Central Chile: Journal of Petrology, v. 12, p. 149-175.

González-Jiménez J.M., Barra, F., Walker, R., Reich, M., Gervilla, F., 2014, Geodynamic implications of ophiolitic chromitites in the La Cabaña ultramafic bodies, Central Chile: International Geology Review, v. 56, p. 1466-1483.

González-Jiménez, J.M., Barra, F., Garrido, L., Reich, M., Satsukawa, T., Romero, R., Salazar, E., Colás, V., Orellana, F., Rabbia, O., Plissart, G., Morata, D., 2016, A secondary precious and base metalmineralization in chromitites linked to the development of a Paleozoic accretionary complex in Central Chile: Ore Geology Reviews, v. 78, p. 14-40.

González-Jimenez, J.M., Plissart, G., Garrido, L., Padrón-Navarta, J., Romero, R., Marchesi, C., Reich, M., Barra, F., Morata, D., 2016. Ti-clinohumite and Ti-chondrodite in antigorite serpentinites from Central Chile: mineralogical evidence for deep and cold subduction. European Journal of Mineralogy, accepted.

Griffin, W., Afonso, J., Belousova, E., Gain, S., Gong, X., González-Jiménez, J.M., Howell, D., Huang, J-X., McGowan, N., Pearson, N., Satsukawa, T., Shi, R., Williams, P., Xiong, Q. Yang, J-S., Zhang M. and O'Reilly S., 2016, Mantle recycling: Transition-Zone metamorphism of Tibetan ophiolitic peridotites and its tectonic implications: Journal of Petrology, v. 57, p. 655-684.

Hervé, F., 1974, Petrology of the Crystalline Basement Nahuelbuta Mountains, South-Central Chile [Ph.D. thesis]: Hokkaido, Hokkaido University.

Hervé, F., Godoy, E., Del Campo, M., Ojeda, J., 1976, Las metabasitas del basamento metamórfico de Chile Central y Austral. *in* I Congreso Geológico Chileno, Actas, p. 175–187.

Hervé, F., 1988, Late Paleozoic Subduction and Accretion in Southern Chile. Episodes, v. 11, p. 183-188.

Höfer, C., Kraus, S., Miller, H., Alfaro, G., and Barra, F., 2001, Chromite-bearing serpentinite bodies within an arc–backarc metamorphic complex near La Cabaña, south Chilean Coastal Cordillera: Journal of South American Earth Sciences, v. 14, p. 113–126. doi:10.1016/S0895-9811(01)00011-6.

Hufmann, L., Massonne, H., 2000, Ancient arc/back-arc and N-MORB volcanics incorporated in the Late Palaeozoic/Early Mesozoic metamorphic complex of the Coastal Cordillera of Chiloé, Southern Central Chile, *in* IX Congreso Geológico Chileno, Actas, Puerto Varas, Chile, p. 738–741.

Kohn, M., Corrie, S., Markley, C., 2015, The fall and rise of metamorphic zircon. American Mineralogist, v. 100, p. 897-908.

Leisen, M., Barra, F., Romero, R., Morata, D., Reich, M., 2015, Geocronología U-Pb de Circones Mediante Ablación Láser Acoplado a un ICP-MS Multicolector: Metodología Utilizada en el Laboratorio de Geoquímica Isotópica del Centro Fondap CEGA, Universidad de Chile. In: Congreso Geológico Chileno 14, La Serena, Chile.

Linnen R., Samson, I., Williams-Jones, A., Chakhmouradian A., 2014, Geochemistry of the rare-earth element, Nb, Ta, Hf, and Zr deposits. In Holland H, Turekian K (eds) Treatise on geochemistry, second edition, vol 13: 543-568.

Ludwig, K., 2010, Isoplot/Ex version 4.1, a geochronological toolkit for Microsoft Excel: Berkeley Geochronology Center, Special Publication n. 4.

Paton, C., Hellstrom, J., Paul, B., Woodhead, J., Hergt, J., 2011, Iolite: Freeware for the visualisation and processing of mass spectrometric data: Journal of Analytical Atomic Spectrometry, v. 26, p. 2508-2518.

Petrus, J., Kamber, B., 2012. VizualAge: A Novel Approach to Laser Ablation ICP-MS U-Pb Geochronology Data Reduction. Geostandards and Geoanalytical Research 36: 247-270.

Rabbia, O.M., Alfaro, G., Barra, F., 1994, Presencia de espilitas metasomatizadas en el cinturón serpentinítico de la Cordillera de la Costa, *in* II Jornada de Mineralogía, Petrografía y Metalogénesis de rocas Ultrabásicas, actas, p. 607–615. Buenos Aires, Argentina.

Rabbia, O., Hernández, L., Miller, H., Alfaro, G., 1999. Química mineral de la asociación: Turmalina-Cr, Mica-Cr, Cromita, Cuarzo, presente en el Basamento Metamórfico del centro sur de Chile. VIII Congreso Geológico Chileno (Antofagasta), Actas, pp. 1468-1472.

Romero, R., Barra, F., Leisen, M., Salazar, E., González-Jimenez, J.M., Reich, M., 2016. Sedimentary provenance of detrital zircons from Late Paleozoic basement of South Central

Chile and Argentina between 37°S and 40°S and its implications for the evolution of the Paleozoic Gondwana margin. To be submitted to Journal of Geological Society.

Sláma, J., Košler, J., Condon, D., Crowley, J., Gerdes, A., Hanchar, J., Horstwood, M., Morris, G., Nasdala, L., Norberg, N., Schaltegger, U., Schoene, B., Tubrett, M., Whitehouse, M., 2008, Plešovice zircon — A new natural reference material for U–Pb and Hf isotopic microanalysis: Chemical Geology, v. 249, p. 1-35.

SERNAGEOMIN, 2003. Mapa Geológico de Chile: version digital. publicación geológica digital, No. 4, 2003. CDROM, versión 1.0, 2003. Base Geológica escala 1:1.000.000.Gobierno de Chile, Servicio Nacional de Geología y Minería, Subdirección Nacional de Geología.

Stacey, J., Kramers, J. 1975. Approximation of Terrestrial Lead Isotope Evolution by a 2-Stage Model. Earth and Planetary Science Letters, v. 26, p. 207-221.

Vergara, L. 1970. Prospección de yacimientos de cromo y hierro en La Cabaña, Cautín. Bachelor's thesis, Universidad de Chile. 96 p.

Wiedenbeck, M., Allé, P., Corfu, F., Griffin, W.L., Meier, M., Oberli, F., von Quadt, A., Roddick, J.C. and Spiegel, W., 1995, Three natural zircon standards for U-Th-Pb, Lu-Hf, trace element and REE analyses. Geostandards Newsletter, v. 19, p. 1-23.

Wiedenbeck, M., Hanchar, J., Peck, W., Sylvester, P., Valley, J., Whitehouse, M., Kronz, A., Morishita, Y., Nasdala, Lutz., Fiebig, J., Franchi, I., Girard, J.-P., Greenwood, R., Hinton, R., Kita, N., Mason, P., Norman, M., Ogasawara, M., Piccoli, P., Rhede, D., Satoh, H., Schulz-Dobrick, B., Skår, Ø., Spicuzza, M., Terada, K., Tindle, A., Togashi, S., Vennemann, T., Xie, Q., Zheng, Y., 2004, Further Characterisation of the 91500 Zircon Crystal. Geostandards and Geoanalytical Research, v. 28, p. 9-39.

Williams,I., 1998. U-Th-Pb geochronology by ion microprobe. In. Mckibben, M. (ed.) Understanding Mineralizing Processes. Society of Economic Geologists. Reviews in Economic Geology, v. 7, p. 1-35.

Willner A.P., 2005, Pressure-Temperature Evolution of a Late Palaeozoic Paired Metamophic Belt in North-Central Chile (34°-35°30'S): Journal of Petrology, v. 46, p. 1805-1833.

Willner, A.P., Thompson, S., Kröner, A., Wartho, J., Wijbrans, J., Hervé, F., 2005, Time markers for the evolution and exhumation history of a Late Palaeozoic Paired Metamorphic Belt in North-Central Chile (34°-35°30'S): Journal of Petrology, v. 46, p. 1835-1858

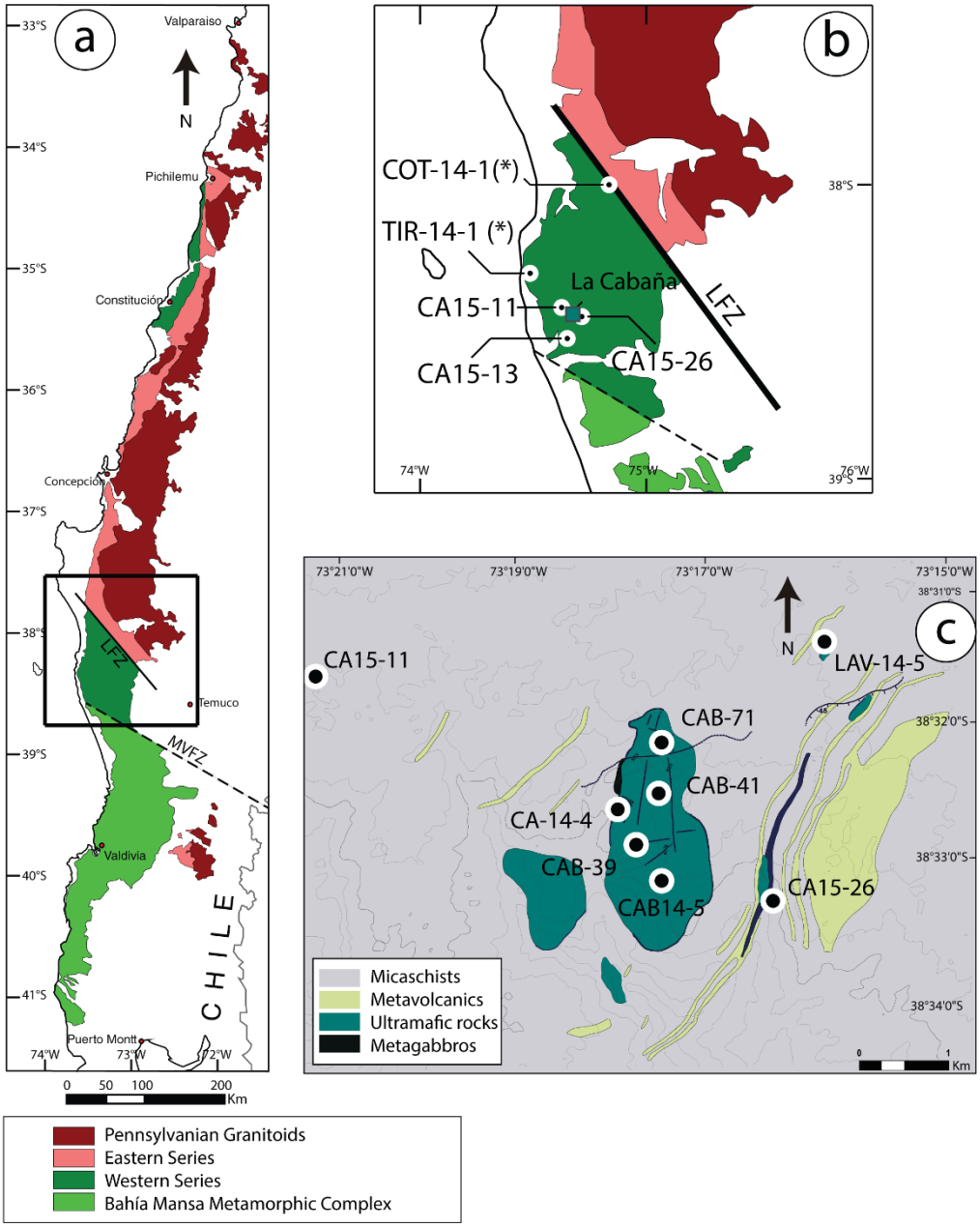

FIGURE 1. ROMERO ET AL.

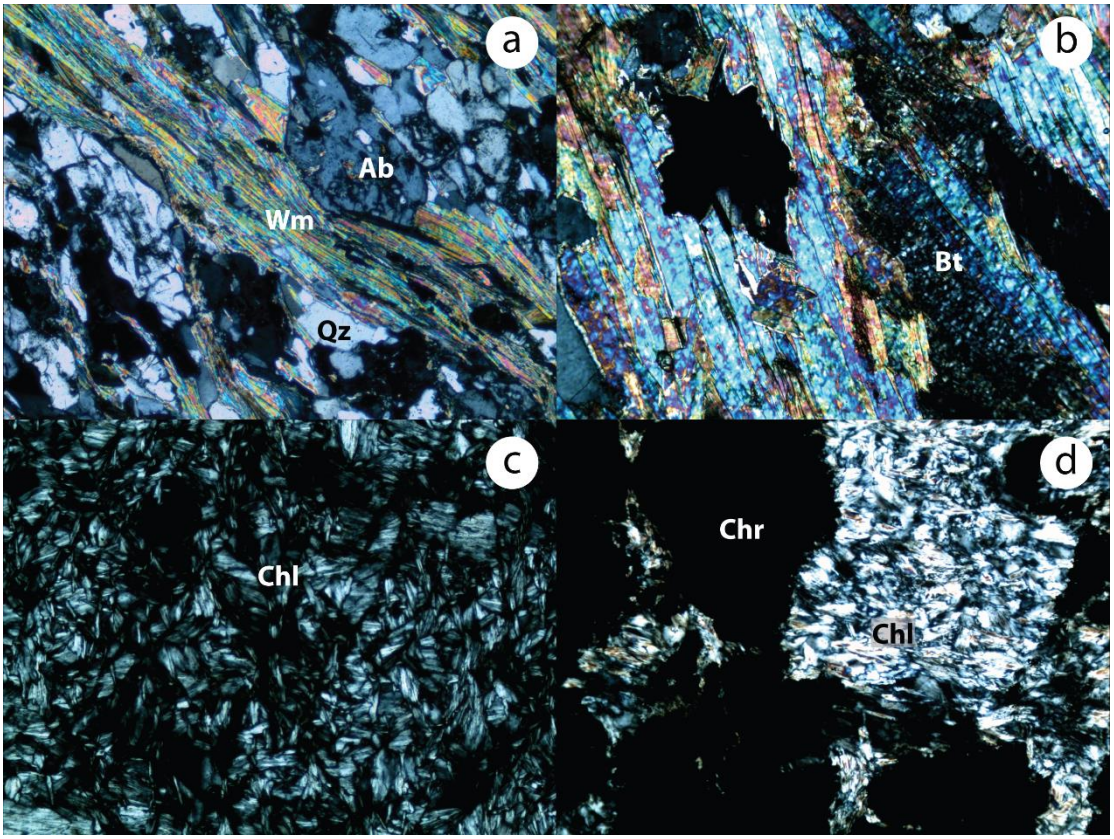

FIGURE 2. ROMERO ET AL.

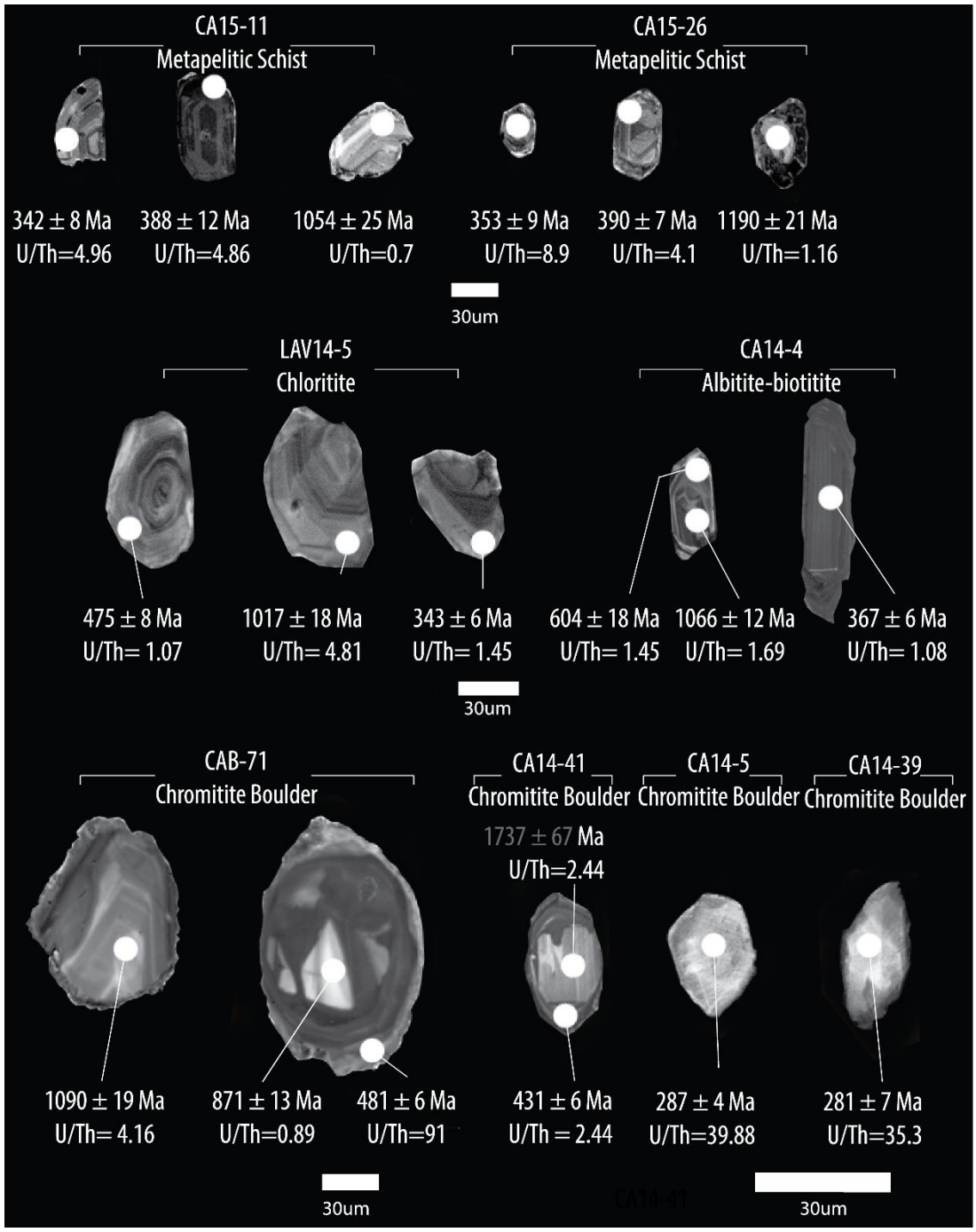

FIGURE 3. ROMERO ET AL.

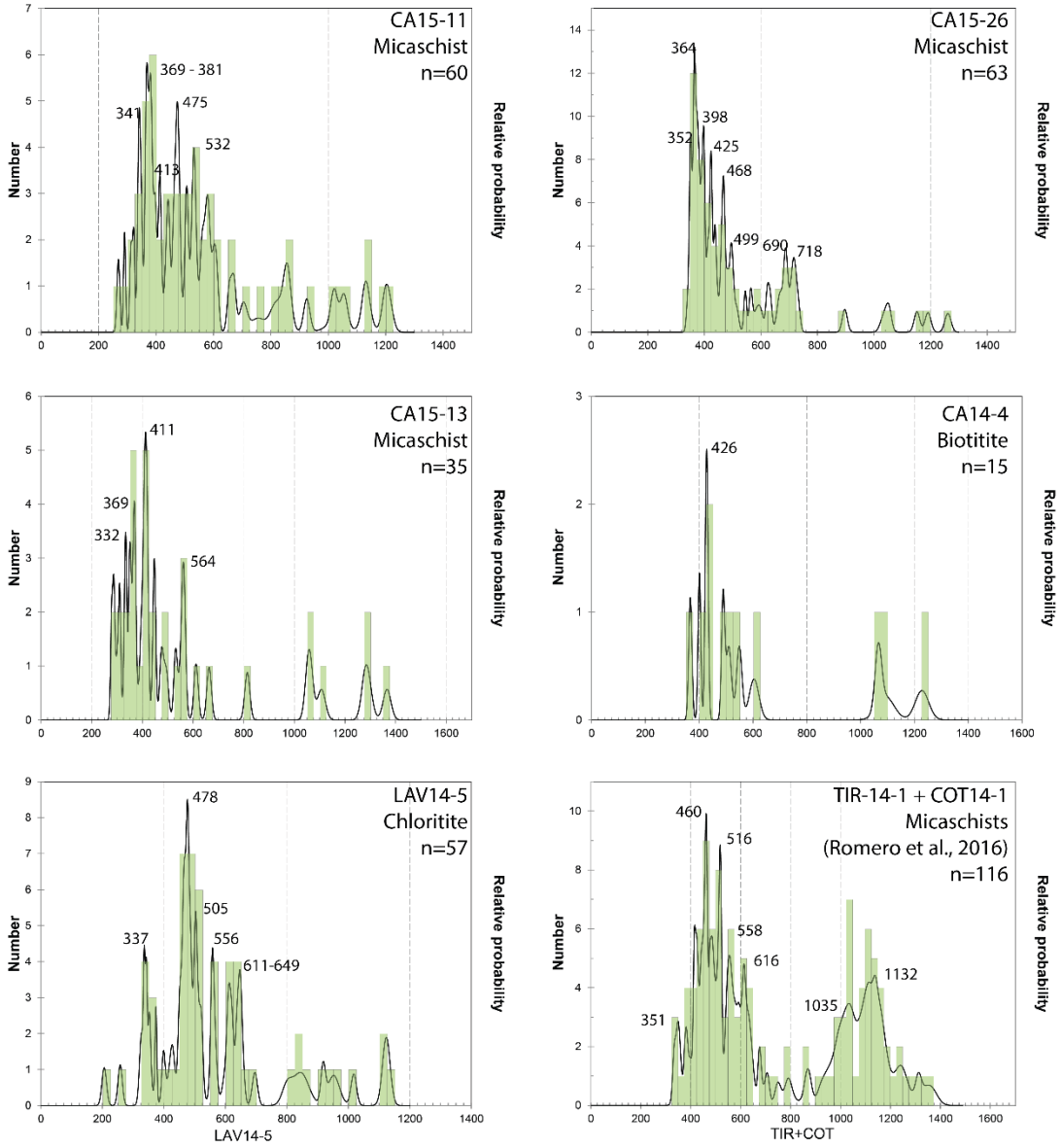

FIGURE 4. ROMERO ET AL.

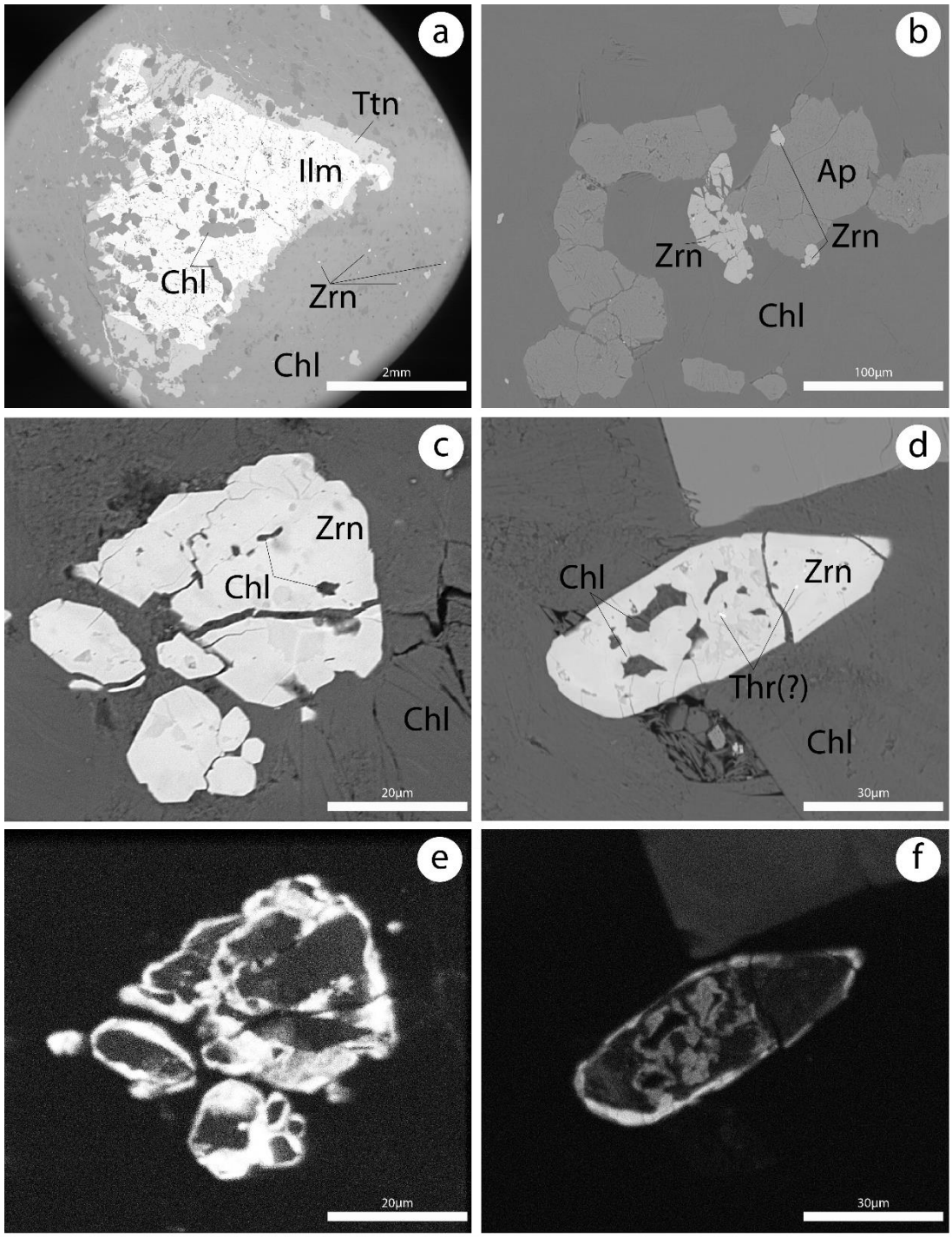

FIGURE 5. ROMERO ET AL.

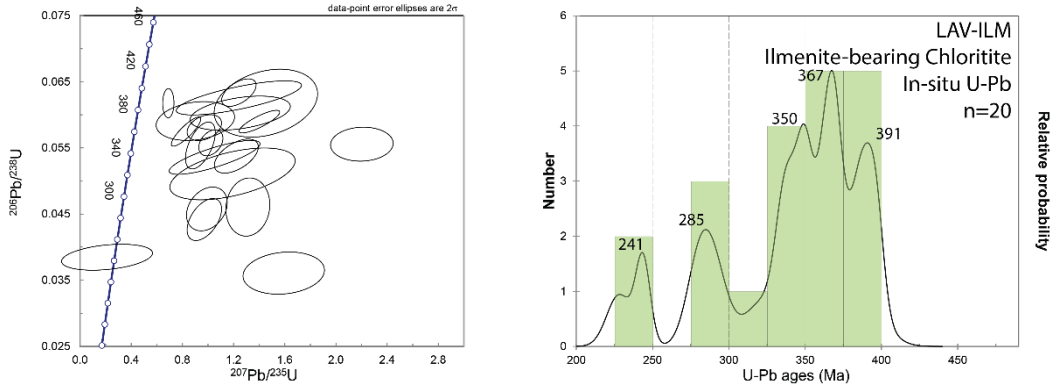

FIGURE 6. ROMERO ET AL.

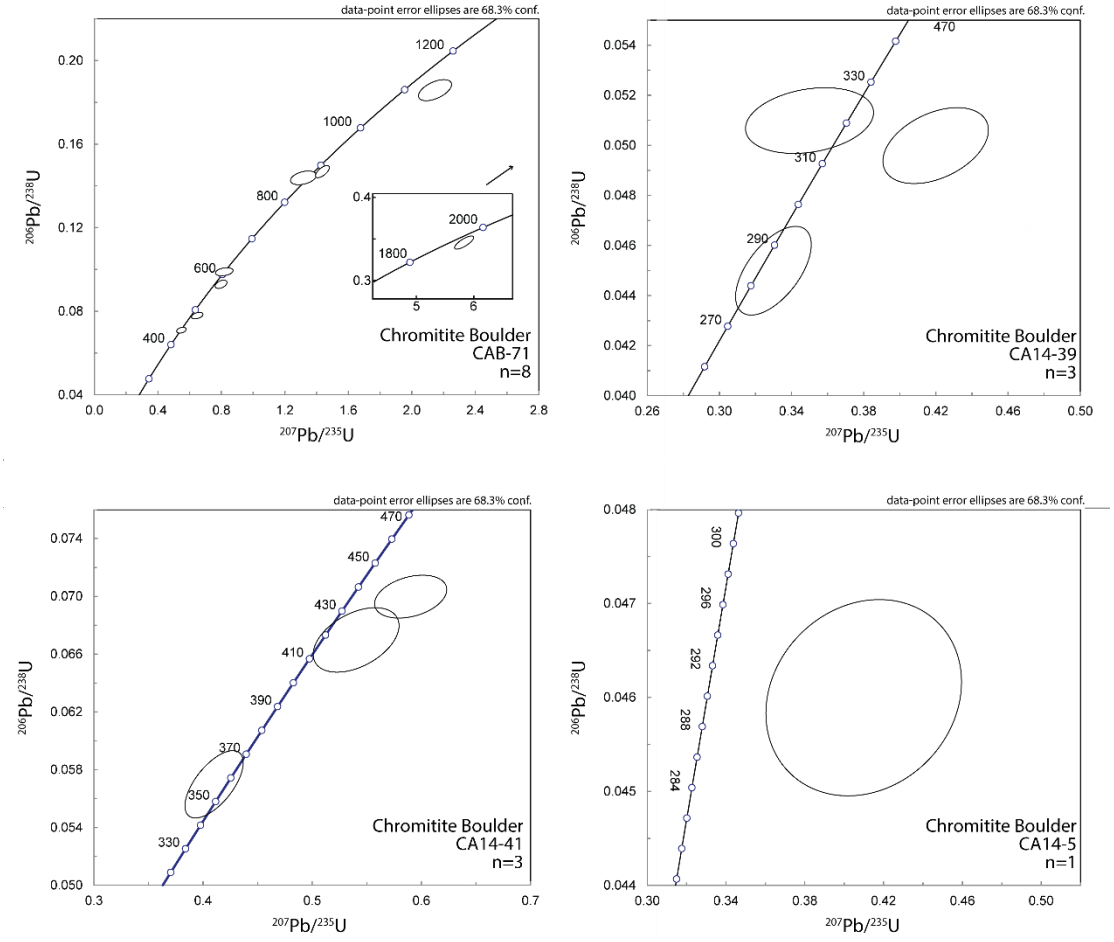

FIGURE 7. ROMERO ET AL.

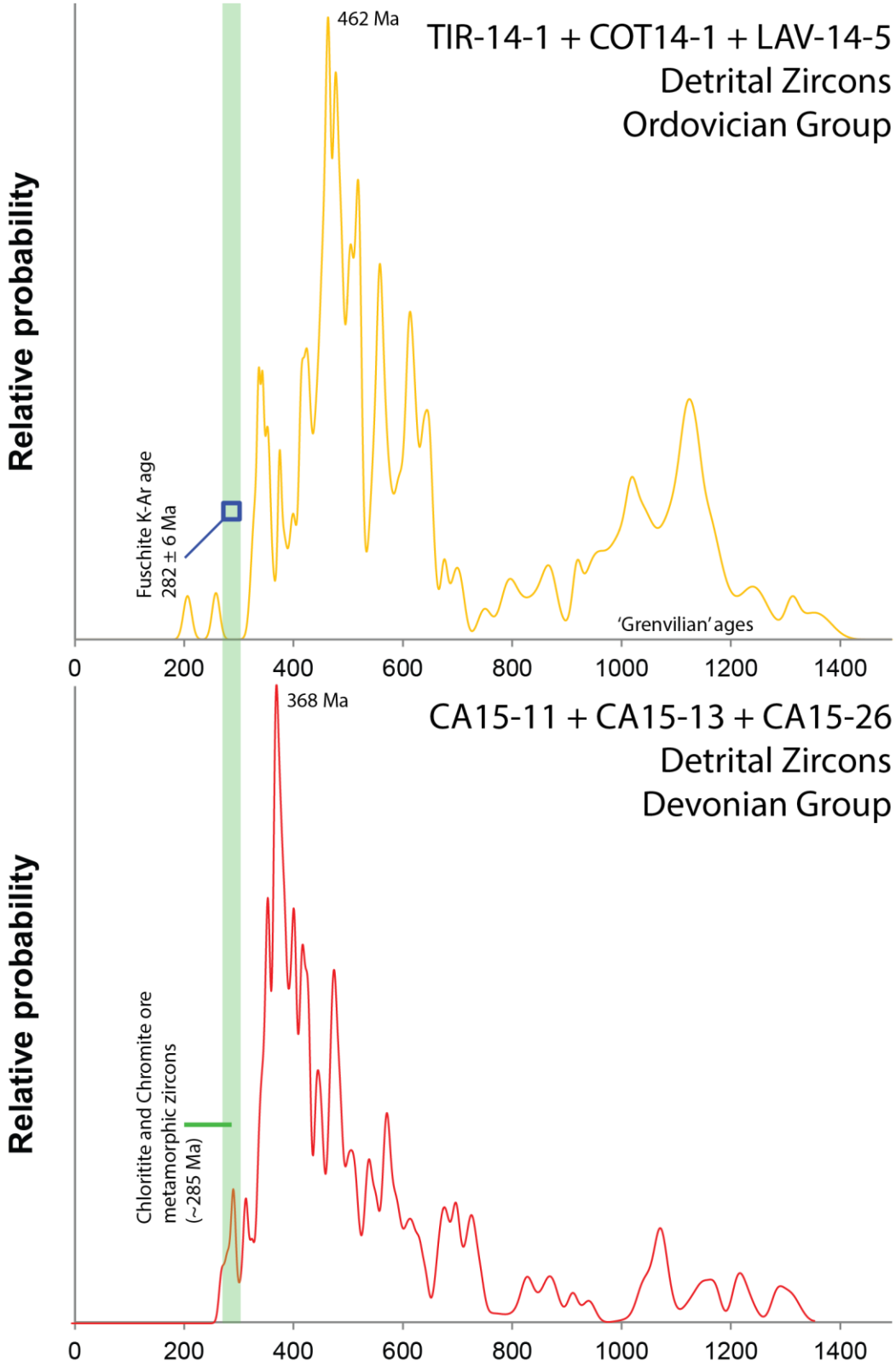

FIGURE 8. ROMERO ET AL.

4. Discusiones Generales

4.1. Caracterización de bloques del Basamento Paleozoico

Analizando la base de datos de ambos artículos en preparación, expuestos en este trabajo de tesis, es posible distinguir dos bloques dentro de las rocas metamórficas de alta presión con distinta caracterización geocronológica, que aportan tanto a la temporalidad de la formación del protolito sedimentario como a la variación paleogeográfica a la que fue sometido el margen gondwánico.

4.1.1. Serie Occidental

Es posible identificar un primer bloque representado principalmente por un patrón de circones detríticos presente en diversos complejos metamórficos del país y Argentina (Pankhurst et al., 2006; Alvarez et al., 2011; Hervé et al., 2013; Maksaev et al., 2015). Este grupo se caracteriza por edades máximas de depósito missisipianas a ordovícicas, un evidente hiato devónico, un gran contenido de circones ordovícicos (mayormente ~470 Ma) y relativa presencia de edades mesoproterozoicas (1000-1200 Ma) interpretadas como provenientes desde bloques de basamento 'grenvilliano' de Sudamérica.

El patrón mencionado representa el bloque más antiguo del presente trabajo y se encuentra en las muestras metasedimentarias desde la localidad de Yobilo hasta Tirúa, incluyendo el Complejo Piedra Santa en Argentina (Capítulo 2), como también en la cloritita de Lavaderos, interpretada como la muestra metasedimentaria más cercana al cuerpo ultramáfico de La Cabaña (Capítulo 3). Estas muestras, a excepción de Yobilo y Complejo Piedra Santa, corresponden directamente a la definición de la Serie Occidental en cuanto a la temporalidad de la formación del depósito sedimentario como el proceso metamórfico de enfriamiento al que fue sometido en el Pérmico (Hofer et al., 2001; Willner et al, 2008; Capítulo 3).

Aproximadamente al SW del cuerpo ultramáfico de La Cabaña, las muestras metasedimentarias analizadas (Capítulo 3) presentan un nuevo patrón de circones detríticos con edades máximas de depósito cercanas a las anteriores. Este patrón se caracteriza por un aporte principal de edades devónicas (360-380 Ma) las cuales no se encuentran en ninguna otra zona del complejo metamórfico. En vista que estas edades se asocian a un hiato en la actividad tectónica en el continente, manifestada por una ausencia generalizada de cuerpos magmáticos de estas edades, y que las muestras geográficamente más cercanas al margen no presentan estas edades, la proveniencia de estos circones es probablemente desde una posición más al oeste en un contexto de magmatismo oceánico.

Dado lo anterior, en el Capítulo 3 del trabajo se sugiere, a base de la variación de patrones de circones detríticos con edades de depósito similares y el origen de los cuerpos ultramáficos de La Cabaña como magmatismo de suprasubducción, un ambiente tectónico de tras-arco como es planteado por Frutos y Alfaro (1970). En este contexto (Fig. 3), las muestras que se encuentran al NE del cuerpo de La Cabaña representan aportes

continentales próximos al margen, a diferencia de al SW donde los circones provienen casi únicamente desde un posible arco oceánico desarrollado en el devónico (~360-380 Ma). Así, el magmatismo de La Cabaña y probablemente las ocurrencias de mineralización tipo VMS en las cercanías de Tirúa estarían asociadas a este proceso.

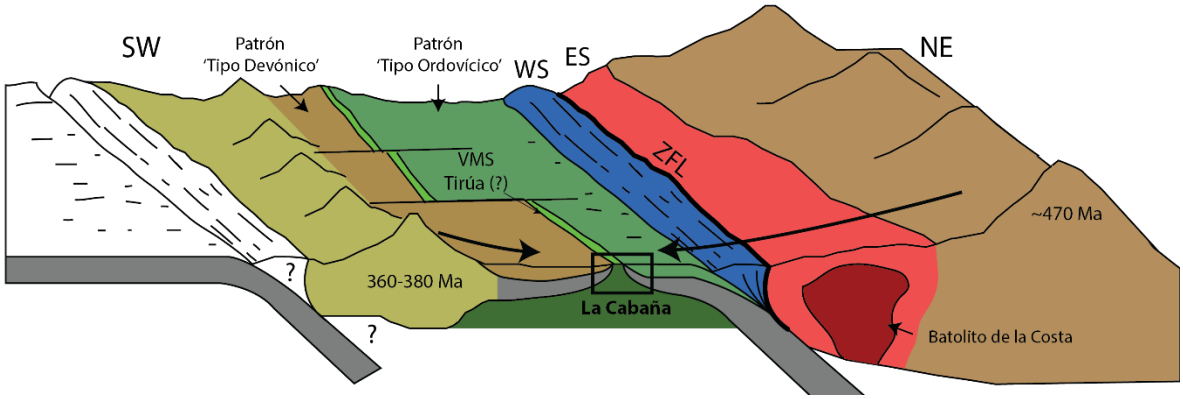

Fig. 3 Esquema de formación del Complejo Metamórfico de La Cabaña como una posible cuenca de trasarco con sus respectivas fuentes sedimentarias. Notar la Zona de Falla Lanalhue como un límite natural entre la Serie Oriental y Serie Occidental.

Como es sugerido en el Capítulo 2 y corroborado en el Capítulo 3, el área comprendida entre la Zona de Falla Lanalhue y la Zona de Falla Mocha-Villarrica (Fig. 1) denominado como Complejo Metamórfico La Cabaña, corresponde al afloramiento más continuo y completo de la Serie Occidental, donde es posible identificar tanto la transición de las edades de los sedimentos que conforman el protolito metasedimentario como fragmentos del complejo ofiolítico desarrollado en un ambiente de trasarco.

4.1.2. Complejo Metamórfico Bahía Mansa

Las muestras metasedimentarias analizadas al sur de los 39°S poseen edades de circones detríticos mucho más jóvenes que las encontradas en el Complejo Metamórfico de La Cabaña. Esta distribución se caracteriza por un alto contenido de circones de edades pérmicas (250-298 Ma) con escasos aportes de otras edades. Las edades máximas de depósito obtenidas en esta zona concuerdan con un protolito depositado incluso posteriormente a la fase de enfriamiento de la Serie Occidental (~280 Ma).

Edades plateau en micas de rocas metasedimentarias, reportadas entre los 39°30'S y 42°S, indican fases de enfriamiento de edad triásica (~240 Ma), las cuales fueron asociadas por Duhart et al. (2001) como parte del Complejo Metamórfico Bahía Mansa.

Los resultados obtenidos en este estudio, sugieren que este último complejo se extendería más al norte hasta la localidad de Gorbea (~39°S) y el contacto con el Complejo Metamórfico de La Cabaña se asociaría a la Zona de Falla Mocha-Villarrica, área donde el rasgo de la Cordillera de la Costa es atenuado aproximadamente desde los 500 a 40 msnm.

4.2. Circones en blackwall y cromititas, su significado y alcances

Los patrones de edades U-Pb en circones encontrados en La Cabaña en las zonas de reacción (blackwall) entre las metaperidotitas de La Cabaña y la roca caja metasedimentaria pueden también clasificarse en los grupos anteriormente descritos.

Para el caso de la cloritita de Lavanderos (LAV-14-5), es bastante claro que corresponde al típico patrón de circones detríticos con alto contenido de circones ordovícicos. Caso menos obvio es la biotitita (CA14-5) donde el número de circones fue menor por lo cual el patrón no es estadísticamente representativo. A pesar de ello, el rango de edades que este comprende es similar a los de la roca encajante, ya sea el patrón típico o el amplio aporte de circones devónicos. Por lo cual estos corresponderían a circones no alterados por el metasomatismo y provendrían directamente de los metasedimentos albergantes.

Sin embargo, circones metamórficos encontrados en la sección gruesa de cloritita con ilmenita, presentan claros indicios de un origen metamórfico y, en efecto, presentan edades más jóvenes que la roca encajante, llamando principalmente la atención un peak de ~285 Ma.

Paralelamente, los circones obtenidos de los podos de cromita tienen edades que varían según la morfología del circón. En general, los circones de edades carboníferas a proterozoicas tienen razones de U/Th y zonaciones en CL que sugieren un origen magmático de estos. Contrariamente, los circones con zonaciones irregulares tienen edades más jóvenes desde carboníferas a pérmicas, nuevamente se distingue un peak a los ~285 Ma.

En vista de lo anteriormente expuesto, se concluye que el origen de los circones en la cromitita es directo desde los sedimentos albergantes y el hecho de que ambos posean las mismas edades metamórficas a los ~285 Ma que, a su vez, son coincidentes con la edades K-Ar de 282±6 Ma de Hofer et al. (2001), es suficiente para afirmar que desde aproximadamente los 285 Ma, la peridotita y los esquistos llevan un proceso metamórfico en común en el canal de subducción en condiciones retrógradas.

5. Conclusión

El Basamento Metamórfico del Centro Sur de Chile, dentro del área estudiada, se conforma de dos bloques con distintas temporalidades en la formación de sus protolitos y su posterior metamorfismo pero originadas a partir de procesos sedimentarios y metamórficos muy similares.

El bloque más antiguo identificado lo conforma el denominado Complejo Metamórfico La Cabaña, entre la Zona de Falla Lanalhue y la Zona de Falla Mocha-Villarrica, donde las edades máximas de depósito en circones detríticos del protolito metasedimentario son principalmente carboníferas a ordovícicas. A este bloque también es posible asociar el Complejo Piedra Santa en Argentina, el cual posee similares patrones de edades y además es intruido por el Complejo Plutónico Chachil, con una edad bastante similar al Batolito de la Costa en territorio Chileno, sugiriendo una continuidad del basamento en dirección SE.

En el Complejo de La Cabaña, los patrones de circones detríticos varían de un patrón de proveniencia típico del continente, representado por un aporte principal desde cuerpos pertenecientes a la Orogenia Famatiniana en el Ordovícico, a una población representada mayoritariamente por circones devónicos (360-380 Ma) cuyos cuerpos magmáticos no se encuentran dentro del continente. El arreglo entre las variaciones de circones detríticos, marcado por las metaperidotitas de La Cabaña, de génesis en ambiente de suprasubducción, sugiere una paleotopografía correspondiente a una cuenca de trasarco con un magmatismo devónico en posición oceánica al SW del margen continental.

La presencia de circones metamórficos en la zona de reacción y en las cromititas presentes en La Cabaña, de ca. 285 Ma sugieren que desde ese momento los sedimentos y las rocas ultramáficas poseen una trayectoria metamórfica común al acretarse al margen continental. En este proceso, fluidos provenientes desde los metasedimentos removilizan tanto zirconio como fragmentos de circones a través de las rocas ultramáficas.

Al sur de la Zona de Falla Mocha-Villarrica se encuentra un patrón de circones detríticos con edades máximas de depósito considerablemente más jóvenes en el Pérmico Temprano a Medio. Esto coincide con la definición del Complejo Metamórfico Bahía Mansa, de edades de enfriamiento triásicas.

La actual disposición de los bloques del Basamento Metamórfico se debería por lo tanto a un movimiento dextral a través de la Zona de Falla Mocha-Villarrica, como una posible continuación del Sistema de Falla Huincul. Esta falla disloca tanto el Batolito de la Costa en las latitudes del Complejo Plutónico Chachil, como también el complejo metamórfico asociado a un paleomargen con disposición NW-SE.

6. Bibliografía

Aguirre, L., Hervé, F., Godoy, E., 1972, Distribution of metamorphic facies in Chile, an outline: Kristalinikum, v. 9, p. 7–19.

Alfaro, G., 1980. Antecedentes preliminares sobre la composición y génesis de las cromitas de La Cabaña (Cautín). Revista Geológica de Chile 11: 29-41.

Alvarez, J, Mpodozis, C., Arriagada, C., Astini, R., Morata, D., Salazar, E., Valencia, V., Vervoort, J., 2011. Detrital zircons from late Paleozoic accretionary complexes in north-central Chile (28°-32°S): Possible fingerprints of the Chilenia terrane. Jounral of South American Earth Sciences 32: 460-476.

Barra, F., Rabbia, O., Alfaro, G., Miller, H., Höfer, C., Kraus, S., 1998, Serpentinitas y cromititas de La Cabaña, Cordillera de la Costa, Chile central: Revista Geológica de Chile v. 25, p. 29-44.

Deckart, K., Hervé, F., Fanning, M., Ramírez, V., Calderón, M., y Godoy, E., 2014. U-Pb geochronology and Hf-O isotopes of zircons from the pennsylvanian coastal batholith, south central Chile. Andean Geology 41: 49-82.

Duhart, P., McDonough, M., Muñoz, J., Martin, M., y Villaneuve, M., 2001. El Complejo Metamórfico Bahía Mansa en la Cordillera de la Costa del centro-sur de Chile (39°30'-42°S): Geocronología K-Ar, 40Ar/39Ar y U-Pb e implicancias en la evolución del margen sur-occidental de Gondwana. Revista Geológica de Chile 28: 179-208.

Frutos J., Alfaro, G., 1987, Metallogenetic and tectonic characteristics of the Paleozoic ophiolitic belt of the southern Chile coast cordillera: Geologische Rundschau, v. 76, p. 343–356.

Glodny, J., Lohrmann, J., Echtler, H., Gräfe, K., Seifert, W., Collao, S., Figueroa, O., 2005, Internal dynamics of a paleoaccretionary wedge: Insights from combined isotope tectonochronology and sandbox modelling of the south-central Chilean forearc: Earth and Planetary Science Letters, v. 231, p. 23–39.

Glodny, J., Echtler, H., Collao, S., Ardiles, M., Burón, P., Figueroa, O., 2008. Differential Late Paleozoic active margin evolution in South-Central Chile (37°S-40°S) - the Lanalhue Fault Zone. Journal of South American Earth Sciences 26: 397-411.

Godoy, E., 1979, Metabasitas del basamento metamórfico, in Congreso Geológico Chileno: Actas, p. 133–144.

González-Bonorino F., 1971. Metamorphism of the crystalline basement of Central Chile. Journal of Petrology 12: 149-175.

González-Jiménez J.M., Barra, F., Walker, R., Reich, M., Gervilla, F., 2014, Geodynamic implications of ophiolitic chromitites in the La Cabaña ultramafic bodies, Central Chile: International Geology Review, v. 56, p. 1466-1483.

González-Jiménez, J.M., Barra, F., Garrido, L., Reich, M., Satsukawa, T., Romero, R., Salazar, E., Colás, V., Orellana, F., Rabbia, O., Plissart, G., Morata, D., 2016, A secondary precious and base metalmineralization in chromitites linked to the development of a Paleozoic accretionary complex in Central Chile: Ore Geology Reviews, v. 78, p. 14-40.

González-Jimenez, J.M., Plissart, G., Garrido, L., Padrón-Navarta, J., Romero, R., Marchesi, C., Reich, M., Barra, F., Morata, D., 2016. Ti-clinohumite and Ti-chondrodite in antigorite serpentinites from Central Chile: mineralogical evidence for deep and cold subduction. European Journal of Mineralogy, accepted.

Hervé, F., Godoy, E., Del Campo, M., Ojeda, J., 1976, Las metabasitas del basamento metamórfico de Chile Central y Austral. in I Congreso Geológico Chileno, Actas, p. 175–187.

Hervé, F., 1988, Late Paleozoic Subduction and Accretion in Southern Chile. Episodes, v. 11, p. 183-188.

Hervé, F., Munizaga, F., Parada, M., Brook, M., Pankhurst, R., Snelling, N., Drake, R., 1988. Granitoids of the Coast Range of central Chile: geochronology and geologic setting. Journal of South American Earth Sciences 1: 185-194.

Hervé, F., Faundez, V., Calderón, M., Massone H.J., Willner, A.P., 2007. Metamorphic and plutonic basement complexes. In: Moreno, T., Gibbons, W. (Eds). The Geology of Chile. The Geological Society, London. pp. 5-19.

Hervé, F., Calderón, M., Fanning, C.M., Pankhurst, R.J., Godoy, E., 2013. Provenance variations in the Late Paleozoic accretionary complex of central Chile as indicated by detrital zircons. Gondwana Research 23: 1122-1135.

Höfer, C., Kraus, S., Miller, H., Alfaro, G., and Barra, F., 2001, Chromite-bearing serpentinite bodies within an arc–backarc metamorphic complex near La Cabaña, south Chilean Coastal Cordillera: Journal of South American Earth Sciences, v. 14, p. 113–126. doi:10.1016/S0895-9811(01)00011-6.

Hufmann, L., Massonne, H., 2000, Ancient arc/back-arc and N-MORB volcanics incorporated in the Late Palaeozoic/Early Mesozoic metamorphic complex of the Coastal Cordillera of Chiloé, Southern Central Chile, in IX Congreso Geológico Chileno, Actas, Puerto Varas, Chile, p. 738–741.

Lucassen, F., Trumbull, R., Franz, G., Creixell, C., Vásquez, P., Romer, R., y Figueroa, O., 2004. Distinguishing crustal recycling and juvenile additions at active continental margins: the Paleozoic to recent compositional evolution of the Chilean Pacific margin. Journal of South American Earth Sciences 17: 103-119.

Maksaev, V., Arancibia, J., Munizaga, F., Tassinari, C., 2015. Detrital-zircon U-Pb geochronology of the Quebrada del Carrizo Metamorphic Complex and El Jardín Schists and spatially-related granitoids of the Sierra Castillo Batholith. Andean Geology 42: 285-312.

Miyashiro A.,1961. Evolution of metamorphic belts. Journal of Petrology 2: 277-311.

Muñoz Cristi , J., 1962. Comentarios sobre los granitos chilenos. Publ. Soc. Geol. Chile, 15-19.

Pankhurst. R., Rapela. C., Fanning, C., Márquez, M., 2006. Gondwanide continental collision ant the origin of Patagonia. Earth-Science Reviews 76: 235-257.

Rabbia, O., Hernández, L., Miller, H., Alfaro, G., 1999. Química mineral de la asociación: Turmalina-Cr, Mica-Cr, Cromita, Cuarzo, presente en el Basamento Metamórfico del centro sur de Chile. VIII Congreso Geológico Chileno (Antofagasta), Actas, pp. 1468-1472.

Rodriguez, C., Perez, Y., Moreno, H., Clayton, J., Antinao, J.L., Duhart, P., Martin, M. 1998. Geología preliminar del área Panguipulli-Riñihue, Región de Los Lagos. Mapa 12, escala 1:100.000. In SERNAGEOMIN, 1998. Estudio Geológico-Económico de la Xa Región Norte. Servicio Nacional de Geología y Minería. Informe Registrado IR-98-15, 6 Vols., 26 mapas. Santiago.

SERNAGEOMIN, 2003. Mapa Geológico de Chile: version digital. publicación geológica digital, No. 4, 2003. CDROM, versión 1.0, 2003. Base Geológica escala 1:1.000.000. Gobierno de Chile, Servicio Nacional de Geología y Minería, Subdirección Nacional de Geología.

Vergara, L. 1970. Prospección de yacimientos de cromo y hierro en La Cabaña, Cautín. Bachelor's thesis, Universidad de Chile. 96 p.

Willner A.P., 2005, Pressure-Temperature Evolution of a Late Palaeozoic Paired Metamophic Belt in North-Central Chile (34°-35°30'S): Journal of Petrology, v. 46, p. 1805-1833.

Willner, A.P., Thompson, S., Kröner, A., Wartho, J., Wijbrans, J., Hervé, F., 2005. Time markers for the evolution and exhumation history of a Late Palaeozoic Paired Metamorphic Belt in North-Central Chile (34°-35°30'S). Journal of Petrology 46: 1835-1858.

Anexo 1. Edades U-Pb: "Sedimentary provenance of detrital zircons from Late Paleozoic basement of South Central Chile and Argentina between 37°S and 40°S and its implications for the evolution of the Paleozoic Gondwana margin"

Table 1. Detrital zircon LA-MC-ICPMS U-Pb data of samples YOB-D5, COT-14-1, TIR-14-1, RRPS-2, QE-D3, GRB1-D5, LLG-14-1, DL-D4, PA-D4 and RRPS-1.

Spot	207Pb/ 235U	2σ	206Pb/ 238U	2σ	ρ	238U/ 206Pb	2σ	207Pb/ 206Pb	2σ	ρ	206Pb/ 238Pb Age (Ma)	2σ	207Pb/ 206Pb Age (Ma)	2σ	U (PPM)	Th (PPM)	U/Th Ratio
YOB-D5_1	0.93000	0.06300	0.10460	0.00420	0.98	9.56023	0.38387	0.06414	0.00270	-0.01	641	25	746.1	90	358	353	1.02
YOB-D5_2	0.66300	0.04400	0.07900	0.00310	0.99	12.65823	0.49672	0.06040	0.00260	-0.50	490	19	621.4	78	970	87	11.17
YOB-D5_3	0.67000	0.04700	0.07970	0.00330	0.99	12.54705	0.51951	0.06064	0.00260	-0.65	494	20	626	91	527	31.5	16.80
YOB-D5_4	0.65540	0.03700	0.07879	0.00280	0.81	12.69197	0.45104	0.05991	0.00260	0.30	488.9	17	600.3	94	534	37.6	14.11
YOB-D5_5	1.34430	0.08400	0.13622	0.00470	0.79	7.34107	0.25329	0.07069	0.00290	-0.08	823.2	27	948.4	84	196	211.5	0.92
YOB-D5_6	1.53850	0.10000	0.15560	0.00550	0.49	6.42674	0.22717	0.07131	0.00310	-0.22	932.1	31	966	89	337.7	85.4	3.99
YOB-D5_7	0.44490	0.02800	0.05706	0.00200	0.80	17.52541	0.61428	0.05607	0.00230	0.05	357.7	12	455	91	866	500	1.75
YOB-D5_8	0.74610	0.04800	0.08630	0.00320	-0.29	11.58749	0.42966	0.06270	0.00290	0.88	533.6	19	695	99	337	147	2.30
YOB-D5_9	1.19400	0.08000	0.12200	0.00440	0.87	8.19672	0.29562	0.07072	0.00300	-0.33	742.1	25	949.3	88	359	73	4.92
YOB-D5_10	0.78300	0.05200	0.09392	0.00340	0.66	10.64736	0.38545	0.06018	0.00260	0.34	578.7	20	609	94	168	35.22	4.75
YOB-D5_11	0.63320	0.04200	0.07860	0.00300	0.98	12.72265	0.48560	0.05805	0.00250	0.10	487.7	18	532	94	586	89	6.60
YOB-D5_12	0.59860	0.04000	0.06894	0.00250	0.96	14.50537	0.52601	0.06256	0.00270	-0.62	429.8	15	693	92	315	92.5	3.45
YOB-D5_13	0.80500	0.05400	0.09150	0.00340	0.97	10.92896	0.40610	0.06386	0.00270	-0.11	564.5	20	736.9	90	682	6.67	102.70
YOB-D5_14	0.52730	0.03500	0.06647	0.00240	0.99	15.04438	0.54320	0.05583	0.00240	0.37	414.8	15	445	93	716	193	3.88
YOB-D5_15	1.44300	0.09500	0.14640	0.00530	0.81	6.83060	0.24728	0.06998	0.00300	-0.54	880.9	30	927.8	88	204.1	36.1	5.85
YOB-D5_16	1.48000	0.09900	0.14700	0.00550	0.95	6.80272	0.25452	0.07325	0.00310	-0.88	884	31	1021	87	413	232	1.78
YOB-D5_17	0.62520	0.04100	0.08060	0.00300	0.72	12.40695	0.46180	0.05713	0.00250	0.49	499.7	18	496	95	185	62.9	3.06
YOB-D5_18	0.69080	0.04500	0.08235	0.00300	0.95	12.14329	0.44238	0.06184	0.00270	0.72	510.1	18	668.5	93	1290	120	11.52
YOB-D5_19	0.75940	0.05000	0.09376	0.00340	0.94	10.66553	0.38676	0.05940	0.00250	0.00	577.7	20	582	93	264.5	102.7	2.76

YOB-D5_20	0.57570	0.03800	0.07010	0.00250	0.88	14.26534	0.50875	0.05900	0.00250	-0.42	436.8	15	567	93	642	171	3.77
YOB-D5_21	0.60340	0.04000	0.07545	0.00270	0.84	13.25381	0.47429	0.05715	0.00240	-0.04	468.9	16	497	94	255	101.94	2.58
YOB-D5_22	0.95400	0.06600	0.09950	0.00390	0.97	10.05025	0.39393	0.06857	0.00290	-0.73	612	23	886	89	365	39	10.60
YOB-D5_23	0.76400	0.05700	0.08902	0.00320	0.97	11.23343	0.40381	0.06210	0.00330	-0.96	549.7	19	674	110	504	49.3	10.95
YOB-D5_24	0.60900	0.04700	0.07600	0.00420	0.99	13.15789	0.72715	0.05746	0.00240	0.33	472	25	509	93	1190	430	3.10
YOB-D5_25	1.37100	0.09200	0.14200	0.00520	0.87	7.04225	0.25789	0.06863	0.00300	-0.51	856	30	887	89	530	144.6	3.98
YOB-D5_26	1.73750	0.11000	0.16558	0.00580	0.38	6.03938	0.21155	0.07477	0.00310	0.44	987.7	32	1062	84	240	171.5	1.43
YOB-D5_27	0.51210	0.03400	0.06024	0.00210	0.90	16.60027	0.57869	0.06111	0.00270	-0.82	377.1	13	642	94	127.3	58.7	2.10
YOB-D5_28	0.90200	0.06200	0.10090	0.00380	0.87	9.91080	0.37325	0.06490	0.00290	-0.56	619.7	22	771	95	195	84	2.35
YOB-D5_29	0.59600	0.04100	0.07358	0.00260	0.98	13.59065	0.48024	0.05781	0.00250	-0.86	457.7	16	522	96	376	49.5	7.89
YOB-D5_30	0.70900	0.05300	0.08520	0.00400	1.00	11.73709	0.55104	0.06005	0.00260	-0.74	527	24	605	93	287.7	39.4	8.35
YOB-D5_31	0.52500	0.03600	0.06850	0.00280	0.99	14.59854	0.59673	0.05535	0.00240	-0.49	427.2	17	426	95	76	21.7	4.12
YOB-D5_32	1.17940	0.07700	0.12301	0.00430	0.81	8.12942	0.28418	0.07006	0.00300	-0.21	747.8	25	930	87	183	59.8	3.57
YOB-D5_33	0.53700	0.05800	0.06890	0.00560	1.00	14.51379	1.17964	0.05640	0.00270	-0.99	429	34	463	120	277	269	1.25
YOB-D5_34	0.51100	0.03800	0.06580	0.00300	0.99	15.19757	0.69290	0.05633	0.00240	-0.57	411	18	465	95	451	14.5	47.00
YOB-D5_35	0.58040	0.03800	0.07270	0.00280	0.99	13.75516	0.52977	0.05717	0.00240	0.09	452.5	17	498	94	243	47.2	6.38
YOB-D5_36	0.52500	0.03900	0.06480	0.00290	0.97	15.43210	0.69063	0.05787	0.00250	-0.43	405	18	524	94	275	81.9	3.94
YOB-D5_37	1.90100	0.12000	0.17515	0.00610	0.56	5.70939	0.19884	0.07884	0.00330	0.08	1040.4	34	1168	84	295	100.1	3.14
YOB-D5_38	0.56190	0.03600	0.07094	0.00250	0.64	14.09642	0.49677	0.05737	0.00240	0.31	441.8	15	505.7	93	282.8	225	1.29
YOB-D5_39	0.57140	0.03700	0.07010	0.00250	0.57	14.26534	0.50875	0.05898	0.00250	-0.22	436.8	15	566	93	274	188	1.45
YOB-D5_40	1.13300	0.07400	0.12060	0.00440	0.93	8.29187	0.30252	0.06839	0.00290	-0.44	733.9	25	880.3	87	537	112	4.95
YOB-D5_41	0.66730	0.04400	0.08135	0.00290	0.89	12.29256	0.43821	0.05917	0.00260	-0.67	504.2	18	573	98	375	152	2.49
YOB-D5_42	0.61380	0.04000	0.07770	0.00280	0.98	12.87001	0.46378	0.05738	0.00240	0.42	482.4	17	506.1	93	522	175.1	3.02
YOB-D5_43	0.56460	0.03700	0.07143	0.00270	0.79	13.99972	0.52918	0.05694	0.00240	0.27	444.7	16	489	94	203.6	21.72	9.55
YOB-D5_44	0.62300	0.05500	0.07680	0.00580	1.00	13.02083	0.98334	0.05873	0.00250	0.58	477	35	557.2	92	740	243	3.12
YOB-D5_45	0.86800	0.05900	0.09270	0.00380	0.88	10.78749	0.44221	0.06889	0.00300	0.23	571	22	895	92	207	81.5	2.62
YOB-D5_46	0.65500	0.04400	0.08460	0.00330	0.98	11.82033	0.46108	0.05617	0.00240	0.45	523.2	20	459	94	420	56.4	8.20
YOB-D5_47	0.78700	0.05200	0.09358	0.00330	-0.02	10.68604	0.37683	0.06022	0.00260	0.32	576.7	20	611	92	129.1	63.9	2.04
YOB-D5_48	0.48820	0.03200	0.05902	0.00210	0.46	16.94341	0.60287	0.05710	0.00240	0.55	369.7	13	495	95	244	67.8	3.64

YOB-D5_49	0.59530	0.03900	0.07338	0.00260	0.89	13.62769	0.48286	0.05812	0.00250	-0.85	456.5	15	534	93	338	126	2.75
YOB-D5_50	0.36900	0.09000	0.05180	0.00390	0.98	19.30502	1.45347	0.05660	0.00430	-0.42	326	24	460	180	400	9.8	33.60
YOB-D5_51	0.86500	0.07500	0.10080	0.00700	1.00	9.92064	0.68893	0.06266	0.00270	0.66	619	41	696.6	91	813	118.9	6.67
YOB-D5_52	1.42400	0.09300	0.14080	0.00510	0.98	7.10227	0.25726	0.07342	0.00310	0.53	849.2	29	1025.4	85	161	22.45	7.23
YOB-D5_53	1.43800	0.09700	0.14200	0.00540	0.61	7.04225	0.26780	0.07380	0.00330	0.19	856	30	1034	90	462	117	4.19
YOB-D5_54	0.56480	0.03800	0.07254	0.00260	0.92	13.78550	0.49410	0.05630	0.00240	0.20	451.4	16	464	94	331	40	8.41
YOB-D5_55	0.57600	0.03900	0.07180	0.00270	0.57	13.92758	0.52374	0.05831	0.00260	-0.11	447.1	16	541	97	270	3.2	83.00
YOB-D5_56	0.63090	0.04100	0.07637	0.00270	0.75	13.09415	0.46293	0.05975	0.00250	0.01	474.41	16	594	92	219	77.8	2.84
YOB-D5_57	0.70200	0.04500	0.08773	0.00310	0.51	11.39861	0.40278	0.05810	0.00250	0.46	542.1	18	533	93	176.5	61.7	2.86
YOB-D5_58	2.38800	0.17000	0.16690	0.00740	0.99	5.99161	0.26566	0.10414	0.00450	-0.26	995	41	1699	79	529	126	4.12
YOB-D5_59	0.65000	0.04400	0.07930	0.00310	0.95	12.61034	0.49296	0.05926	0.00250	-0.15	492.1	18	576.5	93	352	99.5	3.56
YOB-D5_60	1.43700	0.10000	0.14230	0.00630	1.00	7.02741	0.31112	0.07269	0.00310	1.00	858	35	1005.1	87	540	106.4	5.13
YOB-D5_61	2.13000	0.19000	0.19490	0.00870	0.97	5.13084	0.22903	0.08168	0.00350	-0.36	1148	47	1237.7	83	422	143	3.00
YOB-D5_62	0.67460	0.04400	0.08066	0.00280	0.45	12.39772	0.43037	0.06059	0.00260	0.52	500.1	17	624.6	92	154.1	77.1	1.98
YOB-D5_63	0.60400	0.04400	0.07480	0.00300	0.90	13.36898	0.53619	0.05815	0.00260	-0.62	464.7	18	535	95	222	84.6	2.62
YOB-D5_64	2.22280	0.14000	0.19980	0.00700	0.42	5.00501	0.17535	0.08085	0.00340	0.42	1174.3	38	1217.7	84	159.6	37.22	4.34
YOB-D5_65	0.82460	0.05400	0.09796	0.00340	0.82	10.20825	0.35431	0.06128	0.00260	-0.18	602.4	20	649	93	357	64.5	5.56
YOB-D5_66	0.94830	0.06200	0.11050	0.00410	0.97	9.04977	0.33578	0.06186	0.00270	0.03	675.6	24	669	93	159.5	32.2	5.05

Spot	207Pb/ 235U	2σ	206Pb/ 238U	2σ	ρ	238U/ 206Pb	2σ	207Pb/ 206Pb	2σ	ρ	206Pb/ 238Pb Age (Ma)	2σ	207Pb/ 206Pb Age (Ma)	2σ	U (PPM)	Th (PPM)	U/Th Ratio
COT14_1_1	0.71400	0.08800	0.07645	0.00140	0.93	13.08044	0.23954	0.06600	0.00720	-0.91	474.9	8.4	740.0	180.0	42	25	1.69
COT14_1_2	0.97000	0.11000	0.08810	0.00280	0.44	11.35074	0.36075	0.08290	0.00750	-0.17	544.0	17.0	1230.0	170.0	890	280	3.06
COT14_1_3	0.74260	0.03500	0.08270	0.00180	0.88	12.09190	0.26319	0.06443	0.00079	0.41	512.4	11.0	756.0	26.0	398	227	1.79
COT14_1_4	1.76000	0.15000	0.17570	0.00710	0.53	5.69152	0.22999	0.07540	0.00260	-0.14	1043.0	38.0	1072.0	78.0	304	120	2.57
COT14_1_5	1.00100	0.07200	0.10220	0.00350	0.00	9.78474	0.33509	0.07210	0.00270	0.36	627.0	20.0	983.0	79.0	540	94	6.39
COT14_1_6	0.56880	0.02600	0.07452	0.00130	-0.12	13.41922	0.23410	0.05640	0.00088	0.34	463.3	7.9	467.0	34.0	96	60	1.63
COT14_1_7	1.80000	0.12000	0.17630	0.00870	0.99	5.67215	0.27991	0.07590	0.00140	-0.94	1046.0	48.0	1091.0	38.0	155	249	0.62
COT14_1_8	0.69800	0.03400	0.08382	0.00150	-0.61	11.93033	0.21350	0.06129	0.00110	0.97	518.9	9.1	647.0	39.0	422	37	10.80
COT14_1_9	1.71600	0.09500	0.17260	0.00620	0.99	5.79374	0.20812	0.07414	0.00083	-0.93	1026.0	34.0	1045.3	23.0	349	139	2.37
COT14_1_10	1.93700	0.09500	0.18880	0.00470	0.97	5.29661	0.13185	0.07731	0.00092	-0.81	1115.0	25.0	1129.1	23.0	62	33	1.75
COT14_1_11	0.58090	0.02800	0.07080	0.00180	0.65	14.12429	0.35909	0.05972	0.00093	0.06	441.0	11.0	593.0	34.0	124	86	1.44
COT14_1_12	0.74400	0.03900	0.08450	0.00190	0.62	11.83432	0.26610	0.06290	0.00160	-0.45	522.6	11.0	729.0	73.0	729	578	1.20
COT14_1_13	0.48850	0.02300	0.06623	0.00120	0.94	15.09890	0.27357	0.05487	0.00061	-0.52	413.4	7.5	406.7	25.0	574	348	1.67
COT14_1_14	0.87400	0.06100	0.09190	0.00480	0.95	10.88139	0.56834	0.07021	0.00110	-0.44	566.0	28.0	933.0	34.0	543	47	14.80
COT14_1_15	0.39000	0.03500	0.05470	0.00370	0.41	18.28154	1.23659	0.05384	0.00120	0.63	343.0	23.0	363.0	50.0	412	339	1.22
COT14_1_16	1.10800	0.05600	0.11600	0.00300	0.99	8.62069	0.22295	0.06863	0.00093	-0.46	707.0	17.0	887.0	28.0	470	138	3.59
COT14_1_17	1.93600	0.09500	0.18710	0.00350	0.94	5.34474	0.09998	0.07691	0.00098	-0.65	1113.0	42.0	1125.0	33.0	63	71	0.92
COT14_1_18	0.50200	0.06800	0.06170	0.00770	1.00	16.20746	2.02265	0.06047	0.00080	-0.46	386.0	47.0	620.0	29.0	970	147	6.95
COT14_1_19	1.16300	0.05800	0.13060	0.00450	0.99	7.65697	0.26383	0.06585	0.00076	-0.28	791.0	26.0	801.5	24.0	331	164	2.08
COT14_1_20	1.63200	0.08400	0.14460	0.00450	0.87	6.91563	0.21522	0.08240	0.00150	0.10	870.0	25.0	1255.0	34.0	369	159	2.40
COT14_1_21	0.55960	0.02700	0.06690	0.00180	0.57	14.94768	0.40218	0.06230	0.00130	0.43	417.3	11.0	683.0	43.0	635	357	1.79
COT14_1_22	0.57750	0.02800	0.07430	0.00170	0.66	13.45895	0.30794	0.05797	0.00077	0.21	461.9	10.0	528.0	29.0	281	152	1.85
COT14_1_23	0.50300	0.03100	0.07060	0.00280	0.61	14.16431	0.56176	0.05600	0.00150	0.33	440.0	17.0	450.0	66.0	660	295	2.13

COT14_1_24	0.73100	0.05500	0.09880	0.00260	0.58	10.12146	0.26635	0.05670	0.00280	0.19	607.0	15.0	510.0	82.0	200	48	4.11
COT14_1_25	0.81000	0.03900	0.09610	0.00220	0.97	10.40583	0.23822	0.06078	0.00083	-0.37	591.7	13.0	631.0	29.0	399	85	4.60
COT14_1_26	0.72600	0.05000	0.07520	0.00520	0.98	13.29787	0.91953	0.07202	0.00120	0.69	467.0	31.0	986.0	33.0	740	116	6.48
COT14_1_27	1.39000	0.12000	0.13200	0.01000	0.99	7.57576	0.57392	0.07990	0.00096	0.10	796.0	59.0	1194.5	24.0	610	272	2.40
COT14_1_28	0.64600	0.03700	0.07210	0.00310	0.98	13.86963	0.59634	0.06601	0.00093	0.56	449.0	18.0	806.0	29.0	1085	361	3.21
COT14_1_29	0.84500	0.04400	0.09995	0.00190	0.52	10.00500	0.19019	0.06343	0.00100	-0.29	614.1	11.0	722.0	34.0	453	487	0.96
COT14_1_30	1.19200	0.06400	0.12320	0.00410	0.99	8.11688	0.27012	0.07023	0.00081	0.03	749.0	24.0	935.0	24.0	880	95	10.30
COT14_1_31	2.65100	0.13000	0.22570	0.00430	0.82	4.43066	0.08441	0.08504	0.00110	-0.39	1312.0	23.0	1316.0	24.0	406	105	3.98
COT14_1_32	1.97600	0.09300	0.19312	0.00350	0.94	5.17813	0.09385	0.07753	0.00088	-0.01	1138.3	19.0	1134.7	23.0	278	79	3.57
COT14_1_33	0.97900	0.04600	0.11044	0.00210	0.88	9.05469	0.17217	0.06473	0.00081	-0.62	675.3	12.0	765.0	26.0	510	60	8.80
COT14_1_34	0.70500	0.03600	0.09000	0.00270	1.00	11.11111	0.33333	0.05845	0.00067	-0.89	556.0	16.0	546.8	25.0	693	1270	0.53
COT14_1_35	0.57900	0.02900	0.06830	0.00160	0.42	14.64129	0.34299	0.06397	0.00110	0.17	426.0	9.8	740.0	36.0	610	460	1.63
COT14_1_36	0.77000	0.04100	0.09400	0.00250	0.95	10.63830	0.28293	0.05981	0.00068	-0.09	579.0	15.0	596.8	25.0	1215	128	9.90
COT14_1_37	0.61100	0.03200	0.07780	0.00200	0.90	12.85347	0.33042	0.05829	0.00080	0.20	483.2	12.0	540.0	30.0	696	347	2.03
COT14_1_38	0.70800	0.03600	0.09100	0.00270	1.00	10.98901	0.32605	0.05904	0.00073	-0.99	562.0	16.0	568.0	27.0	431	587	0.74
COT14_1_39	0.64500	0.03700	0.07850	0.00290	0.97	12.73885	0.47061	0.05962	0.00085	-0.08	487.0	18.0	590.0	31.0	1372	1280	1.06
COT14_1_40	0.59300	0.02900	0.07452	0.00140	-0.17	13.41922	0.25211	0.05875	0.00110	0.54	463.3	8.6	556.0	42.0	216	158	1.37
COT14_1_41	0.66100	0.03000	0.08395	0.00150	0.07	11.91185	0.21284	0.05793	0.00065	-0.14	519.7	8.6	527.2	24.0	1031	215	4.79
COT14_1_42	0.67100	0.03100	0.08340	0.00170	0.20	11.99041	0.24441	0.05861	0.00083	0.75	516.6	10.0	552.0	31.0	360	306	1.18
COT14_1_43	0.59100	0.03000	0.07350	0.00180	0.98	13.60544	0.33319	0.05804	0.00084	-0.79	457.5	11.0	531.0	32.0	525	910	0.60

Spot	207Pb/ 235U	2σ	206Pb/ 238U	2σ	ρ	238U/ 206Pb	2σ	207Pb/ 206Pb	2σ	ρ	206Pb/ 238Pb Age (Ma)	2σ	207Pb/ 206Pb Age (Ma)	2σ	U (PPM)	Th (PPM)	U/Th Ratio
TIR-14-1_1	0.62800	0.06000	0.08030	0.00350	0.99	12.45330	0.54280	0.05658	0.00480	-0.99	498	21	475	110	257	342	0.80
TIR-14-1_2	1.58400	0.14000	0.14420	0.00530	0.46	6.93481	0.25489	0.07910	0.00670	0.07	868.3	30	1172	110	345	123.3	3.00
TIR-14-1_3	0.65570	0.05100	0.08210	0.00320	0.97	12.18027	0.47475	0.05667	0.00460	0.97	508.9	19	478.6	140	724	423	1.82

TIR-14-1_4	0.61900	0.04600	0.07854	0.00300	0.97	12.73237	0.48634	0.05644	0.00390	-0.95	487.4	18	469.8	120	564	393	1.50
TIR-14-1_5	2.20200	0.18000	0.20840	0.01000	1.00	4.79846	0.23025	0.07674	0.00540	-1.00	1220	55	1114.4	120	156	80	2.08
TIR-14-1_6	0.82000	0.07100	0.10060	0.00420	0.42	9.94036	0.41501	0.05960	0.00420	-0.06	618	25	587	150	631	698	0.95
TIR-14-1_7	0.80100	0.08600	0.09920	0.00630	0.95	10.08065	0.64020	0.05895	0.00420	-0.50	609	37	563	130	442	520	0.89
TIR-14-1_8	1.83600	0.18000	0.17580	0.00940	0.97	5.68828	0.30415	0.07490	0.00560	-1.00	1043	53	1063	100	190	112	1.75
TIR-14-1_9	0.60870	0.04500	0.07752	0.00290	0.18	12.89990	0.48258	0.05689	0.00350	0.21	481.3	17	490	120	49.66	79.4	0.65
TIR-14-1_10	0.89280	0.06300	0.10512	0.00400	0.29	9.51294	0.36198	0.06193	0.00370	0.28	644.3	23	671	120	251	112	2.30
TIR-14-1_11	1.49340	0.10000	0.15368	0.00570	0.94	6.50703	0.24135	0.06946	0.00410	0.43	921.5	32	912.3	120	326	122.9	2.74
TIR-14-1_12	2.15100	0.15000	0.19444	0.00720	0.64	5.14298	0.19044	0.07784	0.00460	0.10	1145.4	39	1142.8	110	69.4	41.1	1.75
TIR-14-1_13	2.11100	0.15000	0.19610	0.00720	0.17	5.09944	0.18723	0.07746	0.00450	0.18	1154.3	39	1133.1	110	58	28.34	2.11
TIR-14-1_14	0.52240	0.03700	0.06685	0.00250	-0.02	14.95886	0.55942	0.05669	0.00340	0.52	417.2	15	477	120	550	301	2.01
TIR-14-1_15	0.53400	0.03800	0.06792	0.00250	0.23	14.72320	0.54193	0.05598	0.00330	-0.14	423.6	15	451	120	481	198.3	2.50
TIR-14-1_16	0.41270	0.02800	0.05530	0.00200	0.27	18.08318	0.65400	0.05396	0.00320	0.15	347	12	369	130	51.12	119.8	0.44
TIR-14-1_17	0.42620	0.02900	0.05676	0.00210	0.60	17.61804	0.65183	0.05467	0.00320	-0.01	355.9	13	398	130	46.3	93.7	0.51
TIR-14-1_18	0.55900	0.04600	0.07120	0.00420	0.99	14.04494	0.82849	0.05699	0.00330	-0.43	443	25	491	130	640	870	0.76
TIR-14-1_19	1.97020	0.13000	0.18720	0.00690	0.68	5.34188	0.19690	0.07601	0.00430	-0.15	1106.4	38	1095.2	110	164.5	117.2	1.45
TIR-14-1_20	2.87600	0.20000	0.23690	0.00870	0.94	4.22119	0.15502	0.08748	0.00500	-0.13	1370.3	46	1371.1	110	179.6	88.5	2.08
TIR-14-1_21	0.77240	0.05200	0.09295	0.00340	0.31	10.75847	0.39353	0.05958	0.00340	-0.11	573	20	588	120	55.24	85.6	0.68
TIR-14-1_22	2.09400	0.16000	0.19520	0.00930	0.99	5.12295	0.24408	0.07824	0.00450	0.05	1149	51	1153	110	284	126	2.32
TIR-14-1_23	2.03000	0.20000	0.19400	0.01300	1.00	5.15464	0.34541	0.07660	0.00460	-0.96	1120	87	1106	130	180	95	1.90
TIR-14-1_24	0.85600	0.06800	0.09880	0.00520	0.99	10.12146	0.53271	0.06232	0.00370	-0.97	607	30	683	120	189	310	0.70
TIR-14-1_25	0.45870	0.03300	0.06044	0.00240	0.91	16.54533	0.65700	0.05449	0.00310	-0.22	378.3	14	391	130	611	539	1.15
TIR-14-1_26	1.94760	0.13000	0.18447	0.00700	-0.15	5.42094	0.20571	0.07631	0.00440	0.44	1091.4	38	1103.1	110	40.5	21.4	1.97
TIR-14-1_27	1.93000	0.13000	0.18367	0.00700	0.35	5.44455	0.20750	0.07617	0.00440	0.22	1087	38	1099	110	22.7	8.65	2.64
TIR-14-1_28	2.15800	0.16000	0.20120	0.00870	0.93	4.97018	0.21491	0.07906	0.00450	0.04	1181	47	1173.6	110	300	306	1.00
TIR-14-1_29	0.94900	0.06600	0.10394	0.00400	0.86	9.62094	0.37025	0.06423	0.00370	-0.26	637.5	23	749	120	244.9	220	1.16
TIR-14-1_30	1.75200	0.13000	0.16990	0.00780	0.98	5.88582	0.27021	0.07465	0.00430	-0.45	1011	43	1059	120	95.5	38.2	2.53
TIR-14-1_31	1.63900	0.13000	0.15980	0.00800	0.88	6.25782	0.31328	0.07370	0.00440	-0.58	955	45	1029	130	77.5	30.5	2.55
TIR-14-1_32	2.69000	0.24000	0.22400	0.01400	0.81	4.46429	0.27902	0.08700	0.00510	-0.49	1299	77	1359	120	229	164	1.42

TIR-14-1_33	2.05400	0.16000	0.19110	0.00880	0.97	5.23286	0.24097	0.07771	0.00450	-0.85	1127	48	1139.2	110	358	97.2	3.73
TIR-14-1_34	0.74000	0.05200	0.08864	0.00320	0.47	11.28159	0.40728	0.06043	0.00350	-0.20	547.5	19	618.9	120	160.5	153.6	1.04
TIR-14-1_35	0.72220	0.05200	0.08932	0.00340	0.45	11.19570	0.42617	0.05855	0.00370	-0.27	551.54	20	550.1	130	151	132.3	1.16
TIR-14-1_36	0.52410	0.03600	0.06818	0.00260	0.34	14.66706	0.55932	0.05580	0.00330	-0.04	425.16	16	444.4	120	112	37.5	3.01
TIR-14-1_37	2.37640	0.21000	0.21202	0.00830	0.71	4.71654	0.18464	0.08181	0.00560	0.30	1239.6	44	1240.9	110	239	111.6	2.15
TIR-14-1_38	1.80100	0.14000	0.17610	0.00680	0.95	5.67859	0.21928	0.07431	0.00430	-0.11	1045.7	37	1050	100	146.5	69	2.07
TIR-14-1_39	1.76600	0.14000	0.17280	0.00690	1.00	5.78704	0.23108	0.07392	0.00500	-0.93	1027	38	1039.1	120	114.2	50	2.29
TIR-14-1_40	2.22700	0.20000	0.20074	0.00770	0.35	4.98157	0.19108	0.07737	0.00530	-0.13	1179.3	41	1130.8	110	231.2	156	1.49
TIR-14-1_41	2.07200	0.18000	0.18881	0.00730	0.58	5.29633	0.20477	0.07801	0.00500	0.51	1114.9	39	1147	100	240	132.9	1.80
TIR-14-1_42	2.14500	0.18000	0.19615	0.00760	0.78	5.09814	0.19753	0.07924	0.00520	-0.28	1154.6	41	1178	110	33.8	52.6	0.64
TIR-14-1_43	2.16500	0.18000	0.19767	0.00760	0.44	5.05894	0.19451	0.07971	0.00520	0.37	1162.8	41	1190	110	24.29	29.65	0.82
TIR-14-1_44	0.56500	0.04600	0.07334	0.00290	0.95	13.63512	0.53916	0.05628	0.00370	0.32	456.3	17	463.2	130	267	140	1.90
TIR-14-1_45	0.74300	0.05600	0.09200	0.00400	0.87	10.86957	0.47259	0.06020	0.00350	-0.18	567	23	610	120	468	144.3	3.21
TIR-14-1_46	0.72000	0.05300	0.08173	0.00320	0.38	12.23541	0.47906	0.06320	0.00390	0.26	506.4	19	711	130	327	302	1.00
TIR-14-1_47	1.98000	0.20000	0.17920	0.00740	0.58	5.58036	0.23044	0.08030	0.00660	-0.29	1062	40	1187	130	154	285	0.54
TIR-14-1_48	1.26000	0.25000	0.16340	0.00670	-0.11	6.11995	0.25094	0.05500	0.01100	0.11	976	37	380	410	37	22	1.69
TIR-14-1_49	0.39430	0.02700	0.05317	0.00200	0.31	18.80760	0.70745	0.05386	0.00310	0.10	333.9	12	365	130	827	911	0.90
TIR-14-1_50	0.50180	0.03600	0.06392	0.00250	0.16	15.64456	0.61188	0.05751	0.00330	0.58	399.4	15	511	130	158.8	127.5	1.21
TIR-14-1_51	0.65170	0.04700	0.08182	0.00320	0.72	12.22195	0.47800	0.05787	0.00340	-0.41	507	19	524.7	130	247	414	0.59
TIR-14-1_52	2.53700	0.17000	0.21492	0.00810	0.64	4.65289	0.17536	0.08512	0.00490	-0.12	1255	43	1318.2	110	104.8	65.4	1.56
TIR-14-1_53	0.66500	0.05000	0.07310	0.00310	0.67	13.67989	0.58013	0.06540	0.00410	0.45	454.5	19	783	130	650	19.4	40.00
TIR-14-1_54	0.94500	0.06800	0.11160	0.00450	0.34	8.96057	0.36131	0.06263	0.00380	0.85	682.3	26	694	120	74.6	28.8	2.52
TIR-14-1_55	0.79240	0.05700	0.09658	0.00380	0.89	10.35411	0.40739	0.05968	0.00360	-0.34	594.3	22	591.8	120	328	112	3.02
TIR-14-1_56	1.87810	0.13000	0.18258	0.00690	0.95	5.47705	0.20699	0.07551	0.00430	-0.98	1081	38	1081.9	110	161.3	70.5	2.22
TIR-14-1_57	1.89400	0.14000	0.18290	0.00800	1.00	5.46747	0.23915	0.07583	0.00430	-1.00	1083	44	1090.5	110	160.4	97.2	1.62
TIR-14-1_58	2.79300	0.20000	0.23160	0.00880	0.70	4.31779	0.16406	0.08781	0.00500	0.05	1343.1	46	1378.3	110	75.8	94.1	0.80
TIR-14-1_59	2.20100	0.15000	0.19650	0.00750	0.45	5.08906	0.19424	0.07917	0.00460	0.80	1156.7	41	1176	110	147.4	72.94	1.98
TIR-14-1_60	2.00700	0.14000	0.18710	0.00710	0.99	5.34474	0.20282	0.07858	0.00450	0.40	1105.5	39	1161.6	110	153.8	68.2	2.20
TIR-14-1_61	0.72090	0.05300	0.08793	0.00330	0.27	11.37268	0.42682	0.05898	0.00340	0.15	543.3	20	566	130	75.2	79.39	0.92

TIR-14-1_62	1.76100	0.13000	0.16780	0.00770	0.98	5.95948	0.27347	0.07519	0.00430	-0.96	1000	43	1073	110	97.7	37.5	2.54
TIR-14-1_63	1.74600	0.12000	0.16801	0.00630	0.84	5.95203	0.22319	0.07487	0.00430	0.01	1001.1	35	1064.9	120	100.9	38.6	2.55
TIR-14-1_64	2.00000	0.15000	0.19190	0.00890	0.99	5.21105	0.24168	0.07598	0.00430	-0.63	1131	48	1094.6	110	290	178.6	1.59
TIR-14-1_65	1.32000	0.19000	0.16520	0.00710	0.04	6.05327	0.26016	0.05970	0.00830	0.22	986	39	530	310	91	47	1.93
TIR-14-1_66	0.45960	0.03200	0.06126	0.00230	0.35	16.32387	0.61288	0.05470	0.00310	0.01	383.26	14	399.9	130	310	193	1.57
TIR-14-1_67	2.17300	0.15000	0.21110	0.00890	1.00	4.73709	0.19972	0.07563	0.00430	0.61	1234	47	1085.2	110	246	82.6	2.90
TIR-14-1_68	0.62800	0.05500	0.07282	0.00290	0.53	13.73249	0.54689	0.05810	0.00440	-0.34	453.1	17	525	150	323	727	0.44
TIR-14-1_69	0.61380	0.04300	0.07900	0.00310	0.97	12.65823	0.49672	0.05677	0.00320	-0.12	490.2	19	482.5	130	359	170	2.05
TIR-14-1_70	1.64600	0.11000	0.15850	0.00600	0.27	6.30915	0.23883	0.07536	0.00430	0.26	948.4	33	1077.9	120	103.5	117.4	0.88
TIR-14-1_71	1.85300	0.13000	0.17460	0.00660	0.85	5.72738	0.21650	0.07580	0.00430	0.43	1037.4	36	1090	110	89.6	70.3	1.26
TIR-14-1_72	1.69600	0.12000	0.16760	0.00690	0.99	5.96659	0.24564	0.07395	0.00420	-0.37	999	38	1039.9	120	161	82.4	1.91
TIR-14-1_73	0.88200	0.06700	0.10250	0.00500	0.97	9.75610	0.47591	0.06183	0.00350	0.48	629	29	668.2	120	751	587	1.26

Spot	207Pb/ 235U	2σ	206Pb/ 238U	2σ	ρ	238U/ 206Pb	2σ	207Pb/ 206Pb	2σ	ρ	206Pb/ 238Pb Age (Ma)	2σ	207Pb/ 206Pb Age (Ma)	2σ	U (PPM)	Th (PPM)	U/Th Ratio
RRPS_2_1	0.546600	0.00860	0.07171	0.00120	0.44	13.94506	0.23336	0.05602	0.00036	0.12	446.5	6.9	452.8	14	235	170.5	1.29
RRPS_2_2	2.653000	0.04100	0.22723	0.00360	0.17	4.40083	0.06972	0.08606	0.00048	0.22	1320.0	19	1339.4	11	342	148	2.15
RRPS_2_3	2.079000	0.03900	0.19090	0.00350	0.93	5.23835	0.09604	0.07962	0.00051	-0.74	1126.3	19	1187.5	13	195	51.8	3.53
RRPS_2_4	1.877000	0.03900	0.18160	0.00320	0.87	5.50661	0.09703	0.07610	0.00110	-0.98	1075.7	18	1095	24	118.9	39.4	2.77
RRPS_2_5	2.046000	0.03500	0.18990	0.00330	0.89	5.26593	0.09151	0.07889	0.00044	-0.36	1120.6	18	1169.4	11	204	80.3	2.38
RRPS_2_6	1.808000	0.03200	0.17660	0.00320	0.69	5.66251	0.10261	0.07497	0.00044	0.11	1048.4	18	1067.6	12	203	59.1	3.39
RRPS_2_7	0.738700	0.01400	0.09290	0.00180	0.94	10.76426	0.20856	0.05838	0.00035	-0.56	572.7	11	544	13	427	263	1.75
RRPS_2_8	2.736000	0.04200	0.23112	0.00370	0.68	4.32676	0.06927	0.08682	0.00048	0.14	1340.4	20	1356.5	11	135.3	85.7	1.64
RRPS_2_9	1.838000	0.02900	0.17581	0.00290	0.74	5.68796	0.09382	0.07578	0.00043	-0.13	1044.0	16	1089.3	11	435	128.9	3.43
RRPS_2_10	2.451000	0.04100	0.21670	0.00370	0.84	4.61468	0.07879	0.08244	0.00046	0.00	1264.6	20	1256.6	11	155	57.1	2.66
RRPS_2_11	1.871000	0.04600	0.15900	0.00350	0.97	6.28931	0.13844	0.08530	0.00061	-0.66	951.0	19	1324.4	13	274.4	93.8	2.92

RRPS_2_12	1.863400	0.02900	0.17855	0.00290	0.37	5.60067	0.09097	0.07584	0.00045	0.18	1059.0	16	1090.6	12	322	147	2.18
RRPS_2_13	2.170000	0.05300	0.19700	0.00410	0.94	5.07614	0.10565	0.08001	0.00069	-0.73	1159.0	22	1196	17	153	90.8	1.66
RRPS_2_14	2.113000	0.03500	0.19554	0.00320	0.77	5.11404	0.08369	0.07841	0.00043	0.10	1151.3	17	1157.2	11	158	44	3.38
RRPS_2_15	2.519000	0.04000	0.21786	0.00360	0.56	4.59010	0.07585	0.08404	0.00046	0.07	1270.5	19	1293.4	11	168	42.3	3.75
RRPS_2_16	1.683000	0.03600	0.16500	0.00300	0.78	6.06061	0.11019	0.07359	0.00058	-0.13	984.2	17	1030	16	58.7	20.8	2.60
RRPS_2_17	1.854000	0.03900	0.17730	0.00370	0.93	5.64016	0.11770	0.07599	0.00045	-0.21	1052.0	20	1094.6	12	141	68.7	1.95
RRPS_2_18	2.000000	0.03100	0.18872	0.00310	0.57	5.29886	0.08704	0.07688	0.00042	0.14	1114.4	17	1118.1	11	200	109.5	1.73
RRPS_2_19	2.119000	0.03400	0.19550	0.00320	0.35	5.11509	0.08373	0.07876	0.00048	-0.03	1151.1	17	1168.2	12	84.7	51.8	1.58
RRPS_2_20	1.550000	0.03000	0.15310	0.00320	0.95	6.53168	0.13652	0.07261	0.00040	-0.06	918.0	18	1003.1	11	607	358	1.66
RRPS_2_21	0.558900	0.01000	0.07090	0.00150	0.91	14.10437	0.29840	0.05655	0.00033	-0.59	441.6	9.2	474	13	593	325	1.79
RRPS_2_22	1.847000	0.03500	0.17450	0.00360	0.97	5.73066	0.11823	0.07638	0.00041	-0.15	1037.0	20	1105	11	359	113	3.14
RRPS_2_23	1.729000	0.02800	0.17160	0.00300	0.77	5.82751	0.10188	0.07323	0.00043	0.12	1020.9	16	1020.3	12	273	244	1.11
RRPS_2_24	2.115000	0.03300	0.19573	0.00320	0.51	5.10908	0.08353	0.07830	0.00044	0.16	1152.3	17	1154.5	11	129.9	106.8	1.20
RRPS_2_25	2.130000	0.04100	0.19560	0.00400	0.39	5.11247	0.10455	0.07947	0.00079	0.01	1152.0	22	1183	19	110.8	126	0.86
RRPS_2_26	1.781000	0.04200	0.17200	0.00440	0.07	5.81395	0.14873	0.07150	0.00230	0.43	1023.0	24	960	71	362	387	0.94
RRPS_2_27	2.198000	0.03700	0.19860	0.00360	0.83	5.03525	0.09127	0.08006	0.00045	0.04	1167.5	19	1198.3	11	164.8	80.4	2.05
RRPS_2_28	0.589000	0.01400	0.07371	0.00120	0.12	13.56668	0.22087	0.05740	0.00100	0.10	458.5	7.3	506	41	36	38.7	0.93
RRPS_2_29	2.297000	0.03900	0.20020	0.00340	0.65	4.99501	0.08483	0.08257	0.00058	-0.05	1176.4	18	1258.8	14	192	83.9	2.33
RRPS_2_30	2.668000	0.04100	0.22552	0.00360	0.22	4.43420	0.07078	0.08576	0.00048	-0.28	1310.9	19	1332.8	11	217.4	122.9	1.84
RRPS_2_31	2.319000	0.05300	0.20480	0.00420	0.97	4.88281	0.10014	0.08207	0.00060	-0.89	1201.0	23	1248.9	14	358	107.5	3.36
RRPS_2_32	0.903000	0.01800	0.10154	0.00180	-0.37	9.84834	0.17458	0.06430	0.00120	0.59	623.4	10	748	38	701	466	1.68
RRPS_2_33	12.935000	0.21000	0.50250	0.00810	0.50	1.99005	0.03208	0.18619	0.00099	-0.08	2624.3	35	2708.8	8.8	80.4	70.1	1.17
RRPS_2_34	1.118000	0.02200	0.12340	0.00230	0.67	8.10373	0.15104	0.06554	0.00057	0.05	750.1	13	791	18	47.5	41.9	1.14
RRPS_2_35	0.523000	0.01500	0.06598	0.00110	0.10	15.15611	0.25268	0.05830	0.00130	0.05	411.9	6.8	533	48	39.1	11.16	3.57
RRPS_2_36	2.558000	0.05500	0.21610	0.00480	0.94	4.62749	0.10279	0.08531	0.00048	-0.15	1261.0	25	1322.5	11	318	147.5	2.18
RRPS_2_37	0.597400	0.00940	0.07653	0.00120	0.48	13.06677	0.20489	0.05635	0.00033	0.06	475.4	7.4	465.8	13	337	297.5	1.19
RRPS_2_38	2.103000	0.03900	0.19180	0.00350	0.86	5.21376	0.09514	0.08049	0.00054	-0.33	1131.2	19	1209	13	254	78.76	3.33
RRPS_2_39	1.801000	0.03000	0.17641	0.00290	0.57	5.66861	0.09319	0.07399	0.00044	0.07	1047.3	16	1041	12	129	73.8	1.74
RRPS_2_40	2.091000	0.03400	0.19404	0.00310	0.27	5.15358	0.08233	0.07833	0.00054	0.02	1143.2	17	1154.9	14	69.7	28.17	2.60

RRPS_2_41	3.047000	0.08900	0.22060	0.00590	0.95	4.53309	0.12124	0.09962	0.00078	-0.59	1285.0	31	1617	15	109	73	1.60
RRPS_2_42	2.160000	0.13000	0.18300	0.00440	0.87	5.46448	0.13139	0.08370	0.00270	-0.74	1083.0	24	1272	56	78.8	31.1	2.77
RRPS_2_43	2.912000	0.04500	0.23786	0.00390	0.85	4.20415	0.06893	0.08863	0.00049	-0.16	1375.5	20	1396.2	11	595	329.5	1.95
RRPS_2_44	1.923000	0.03000	0.18120	0.00300	0.48	5.51876	0.09137	0.07655	0.00047	-0.02	1073.5	17	1109.3	12	99.2	60.7	1.76
RRPS_2_45	0.578600	0.01100	0.07277	0.00130	0.82	13.74193	0.24549	0.05784	0.00051	-0.11	452.8	7.7	525	20	294	159	2.12
RRPS_2_46	1.948000	0.03100	0.18302	0.00310	0.50	5.46388	0.09255	0.07689	0.00047	0.10	1083.4	17	1118.2	12	136	135.3	1.09
RRPS_2_47	1.670000	0.02700	0.16500	0.00290	-0.22	6.06061	0.10652	0.07359	0.00041	0.64	984.6	16	1030.2	11	220.3	123.5	1.97
RRPS_2_48	1.759000	0.03500	0.16400	0.00290	0.64	6.09756	0.10782	0.07672	0.00066	-0.13	979.1	16	1116	16	74.1	18.31	4.40
RRPS_2_49	0.726200	0.01200	0.08990	0.00180	0.93	11.12347	0.22272	0.05863	0.00043	-0.96	554.9	11	553	16	829	73.9	14.20
RRPS_2_50	2.633000	0.04500	0.22320	0.00400	0.89	4.48029	0.08029	0.08575	0.00047	-0.08	1298.6	21	1332.4	11	180.7	197.9	0.99
RRPS_2_51	1.861000	0.04100	0.17490	0.00470	0.71	5.71755	0.15364	0.07543	0.00063	0.37	1044.0	28	1080	17	658	238	2.99
RRPS_2_52	1.971000	0.03200	0.18530	0.00330	0.73	5.39665	0.09611	0.07731	0.00045	0.10	1095.6	18	1130.1	12	159	128	1.33
RRPS_2_53	0.564500	0.00940	0.07318	0.00130	0.82	13.66494	0.24275	0.05629	0.00032	-0.08	455.3	7.8	463.7	13	538	209.8	2.73
RRPS_2_54	2.584000	0.04100	0.21670	0.00370	0.83	4.61468	0.07879	0.08616	0.00047	0.09	1264.4	20	1341.8	11	252	81.7	3.33
RRPS_2_55	3.017000	0.06700	0.23850	0.00570	0.92	4.19287	0.10021	0.09107	0.00058	0.31	1379.0	30	1447.9	12	73.8	52.1	1.50
RRPS_2_56	2.653000	0.04700	0.22940	0.00420	0.92	4.35920	0.07981	0.08407	0.00052	-0.17	1332.0	22	1294.1	12	253	116	2.81
RRPS_2_57	1.603000	0.04400	0.16710	0.00440	0.94	5.98444	0.15758	0.06989	0.00044	-0.22	996.0	25	925	13	109	54.3	2.12
RRPS_2_58	2.462700	0.03800	0.21400	0.00350	0.58	4.67290	0.07643	0.08357	0.00046	0.01	1250.1	18	1283.1	10	245	130.5	1.98
RRPS_2_59	2.818000	0.04600	0.23400	0.00390	0.74	4.27350	0.07123	0.08749	0.00053	-0.10	1355.3	20	1371.1	12	100.2	107.7	0.99
RRPS_2_60	2.705000	0.06700	0.22880	0.00470	0.87	4.37063	0.08978	0.08613	0.00062	-0.52	1328.0	25	1340.9	14	48.1	34.2	1.49
RRPS_2_61	2.335000	0.04500	0.20780	0.00440	0.69	4.81232	0.10190	0.08231	0.00049	-0.16	1217.0	23	1252.8	12	592	6.6	107.00
RRPS_2_62	1.840000	0.03200	0.17630	0.00310	0.09	5.67215	0.09974	0.07631	0.00086	0.26	1046.5	17	1103	22	221	120	1.91
RRPS_2_63	0.632000	0.03100	0.07291	0.00120	0.59	13.71554	0.22574	0.06340	0.00280	-0.55	453.6	7.1	690	86	581	226	2.73
RRPS_2_64	2.176000	0.03900	0.20078	0.00330	0.65	4.98058	0.08186	0.07903	0.00056	-0.19	1179.5	18	1172.7	14	137	190	0.72
RRPS_2_65	1.994000	0.03400	0.18650	0.00310	0.82	5.36193	0.08913	0.07757	0.00048	-0.06	1102.1	17	1135.6	12	243	478	0.54
RRPS_2_66	1.825000	0.03600	0.17360	0.00380	0.98	5.76037	0.12609	0.07645	0.00043	-0.07	1032.0	21	1106.9	11	686.3	353.8	2.04
RRPS_2_67	1.743000	0.04600	0.16610	0.00630	0.86	6.02047	0.22835	0.07670	0.00055	-0.82	989.0	35	1106	24	412	320	1.90
RRPS_2_68	1.029000	0.07000	0.07595	0.00150	0.36	13.16656	0.26004	0.09810	0.00590	-0.20	471.9	8.7	1570	120	850	677	1.36
RRPS_2_69	1.964600	0.03000	0.18558	0.00300	0.52	5.38851	0.08711	0.07689	0.00042	-0.13	1097.4	16	1118.2	11	276	118.1	2.43

RRPS_2_70	0.691000	0.01500	0.08590	0.00180	0.99	11.64144	0.24394	0.05844	0.00032	0.20	531.1	11	546.3	12	946	47.1	21.10
RRPS_2_71	2.061000	0.03300	0.19014	0.00310	0.67	5.25928	0.08575	0.07904	0.00043	-0.30	1122.1	17	1173.1	11	219	85.2	2.61
RRPS_2_72	1.719000	0.03000	0.16740	0.00310	0.77	5.97372	0.11062	0.07411	0.00041	-0.25	998.0	17	1044.3	11	420	156	2.85
RRPS_2_73	1.878100	0.02900	0.18084	0.00300	0.43	5.52975	0.09173	0.07573	0.00045	0.09	1071.5	16	1088	12	306	187	1.69
RRPS_2_74	0.575400	0.00900	0.07393	0.00120	0.47	13.52631	0.21955	0.05650	0.00032	-0.02	459.8	7.2	472.9	12	415	235	1.70
RRPS_2_75	1.762000	0.06100	0.15120	0.00280	-0.22	6.61376	0.12248	0.08410	0.00290	0.45	907.8	15	1286	66	942	179	5.56
RRPS_2_76	0.868000	0.02200	0.10180	0.00220	0.95	9.82318	0.21229	0.06159	0.00045	-0.59	624.9	13	662	15	275	245	1.15
RRPS_2_77	1.500000	0.03000	0.14380	0.00330	0.89	6.95410	0.15959	0.07452	0.00043	-0.90	866.0	19	1055.5	12	491	239	2.13
RRPS_2_78	0.554500	0.00920	0.07123	0.00130	0.81	14.03903	0.25622	0.05649	0.00035	-0.19	443.6	7.7	471.4	14	376	479	0.78
RRPS_2_79	12.750000	0.23000	0.50600	0.00990	0.71	1.97629	0.03867	0.18233	0.00110	0.65	2639.0	43	2674.1	10	107.1	44	2.37
RRPS_2_80	0.573700	0.00990	0.07389	0.00120	0.64	13.53363	0.21979	0.05660	0.00038	-0.20	459.6	7.3	475.4	15	196	137.6	1.35
RRPS_2_81	0.945000	0.01500	0.10929	0.00180	0.49	9.14997	0.15070	0.06281	0.00036	0.24	668.6	10	701.8	12	320	198.9	1.51
RRPS_2_82	1.896000	0.03200	0.17940	0.00320	0.74	5.57414	0.09943	0.07682	0.00051	-0.42	1063.7	17	1116.2	13	162	42.1	3.63
RRPS_2_83	1.889000	0.03400	0.18016	0.00290	0.20	5.55062	0.08935	0.07633	0.00058	0.00	1067.8	16	1103	15	46.8	14.11	3.00
RRPS_2_84	1.990000	0.03500	0.18120	0.00330	-0.28	5.51876	0.10051	0.08050	0.00150	0.64	1073.4	18	1208	36	424	193	2.34
RRPS_2_85	0.546600	0.00840	0.07064	0.00120	0.65	14.15629	0.24048	0.05611	0.00034	-0.06	440.0	7	456.6	13	446	163.5	2.51
RRPS_2_86	2.318600	0.03600	0.20804	0.00330	0.29	4.80677	0.07625	0.08110	0.00044	0.27	1218.4	18	1223.8	11	185	103.2	1.65
RRPS_2_87	0.573800	0.00920	0.07376	0.00120	0.82	13.55748	0.22057	0.05658	0.00034	0.18	458.8	7.5	474.9	13	598	424	1.32
RRPS_2_88	0.568800	0.00910	0.07255	0.00120	-0.57	13.78360	0.22799	0.05664	0.00031	0.85	451.5	7.2	477.6	12	1168	992	1.06
RRPS_2_89	0.557500	0.01100	0.07120	0.00170	0.96	14.04494	0.33534	0.05677	0.00035	0.15	443.5	10	482.3	13	473	276	1.50
RRPS_2_90	0.582100	0.00980	0.07490	0.00140	0.86	13.35113	0.24955	0.05660	0.00034	0.02	465.6	8.1	475.8	13	634	308.7	1.85
RRPS_2_91	2.824000	0.04400	0.23487	0.00380	-0.11	4.25767	0.06889	0.08752	0.00052	0.27	1360.0	20	1371.7	11	109.2	58.1	1.66
RRPS_2_92	2.490000	0.05500	0.18970	0.00530	-0.36	5.27148	0.14728	0.09710	0.00310	0.83	1119.0	29	1555	57	87.8	32.4	2.34

Spot	207Pb/ 235U	2σ	206Pb/ 238U	2σ	ρ	238U/ 206Pb	2σ	207Pb/ 206Pb	2σ	ρ	206Pb/ 238Pb Age (Ma)	2σ	207Pb/ 206Pb Age (Ma)	2σ	U (PPM)	Th (PPM)	U/Th Ratio
QE-D3_1	0.72900	0.04400	0.08710	0.00240	0.85	11.48106	0.31636	0.06199	0.00230	0.14	538.2	14	672	79	465	215.7	2.40
QE-D3_2	0.78500	0.05000	0.09520	0.00280	0.95	10.50420	0.30895	0.06095	0.00220	-0.72	586.4	16	637	79	56.7	1.14	53.00
QE-D3_3	0.57950	0.03500	0.07460	0.00210	0.99	13.40483	0.37735	0.05706	0.00200	-0.99	463.7	12	494	79	351	124.1	3.14
QE-D3_4	0.89800	0.05700	0.09610	0.00630	0.51	10.40583	0.68217	0.06770	0.00440	0.85	591	37	830	120	406	91.9	4.99
QE-D3_5	0.97200	0.06600	0.11520	0.00440	0.98	8.68056	0.33155	0.06191	0.00240	-0.94	703	25	669	91	411	197	2.31
QE-D3_6	0.78500	0.07300	0.08730	0.00290	0.39	11.45475	0.38051	0.06340	0.00440	-0.03	539	17	850	160	404	139	3.16
QE-D3_7	0.67000	0.50000	0.08020	0.00590	0.52	12.46883	0.91728	0.05800	0.04400	-0.46	497	35	-100	950	67	38	2.02
QE-D3_8	0.60100	0.03900	0.07690	0.00230	0.92	13.00390	0.38893	0.05799	0.00220	-0.80	477.8	14	528	79	719	399	2.02
QE-D3_9	0.39000	0.06600	0.05110	0.00270	0.11	19.56947	1.03400	0.05700	0.01000	0.13	321	17	370	370	750	143	6.90
QE-D3_10	0.61510	0.03600	0.07945	0.00200	0.84	12.58653	0.31684	0.05686	0.00200	-0.05	492.8	12	486	77	680	558	1.35
QE-D3_11	0.93900	0.10000	0.10130	0.00350	-0.75	9.87167	0.34107	0.06890	0.00820	0.82	622	21	830	200	334	167	2.69
QE-D3_12	0.72600	0.04300	0.09070	0.00270	0.91	11.02536	0.32821	0.05865	0.00210	0.36	559.7	16	554	77	274	124.7	2.43
QE-D3_13	0.88940	0.05200	0.10640	0.00270	0.95	9.39850	0.23850	0.06131	0.00210	0.12	651.8	16	650.2	75	221	139.3	1.78
QE-D3_14	0.79970	0.04700	0.09818	0.00250	0.98	10.18537	0.25935	0.05986	0.00210	0.08	603.7	14	598.6	75	483	47.3	11.39
QE-D3_15	0.75000	0.04400	0.09370	0.00240	0.97	10.67236	0.27336	0.05899	0.00210	-0.57	577.2	14	566.6	76	301	102.2	3.27
QE-D3_16	0.67300	0.04000	0.08090	0.00270	0.86	12.36094	0.41254	0.06077	0.00220	0.67	501	16	630	77	575	421	1.52
QE-D3_17	0.47300	0.08100	0.06190	0.00410	0.78	16.15509	1.07005	0.05530	0.00850	-0.71	387	25	380	320	500	222	2.73
QE-D3_18	1.04100	0.06400	0.11660	0.00350	0.99	8.57633	0.25744	0.06578	0.00230	-0.78	711	20	799.1	74	266.2	74.4	4.00
QE-D3_19	0.96400	0.08000	0.09475	0.00240	-0.01	10.55409	0.26733	0.07500	0.00540	0.18	583.5	14	1030	140	142	147	1.12
QE-D3_20	0.33790	0.02000	0.04161	0.00100	0.94	24.03268	0.57757	0.05914	0.00210	-0.30	262.8	6.4	572	77	1246	660	2.10
QE-D3_21	0.61000	0.25000	0.10120	0.00780	0.93	9.88142	0.76161	0.03900	0.01700	-0.92	620	46	-280	640	153	50	3.26
QE-D3_22	1.39700	0.08500	0.14540	0.00400	0.99	6.87758	0.18920	0.07045	0.00250	-0.82	875	23	941	72	210	88	2.65
QE-D3_23	0.31190	0.01800	0.04351	0.00110	0.99	22.98322	0.58105	0.05249	0.00180	0.22	274.5	6.9	306.7	79	749	646	1.26
QE-D3_24	0.67700	0.05300	0.08360	0.00470	0.95	11.96172	0.67249	0.05940	0.00250	-0.81	517	28	576	98	711	638	1.21
QE-D3_25	0.35200	0.04000	0.04950	0.00330	0.97	20.20202	1.34680	0.04950	0.00480	-0.95	312	20	180	200	770	133	6.50

QE-D3_26	0.79100	0.06700	0.06760	0.00320	0.68	14.79290	0.70026	0.08590	0.00370	-0.20	422	19	1332	88	880	267	3.82
QE-D3_27	0.35160	0.02000	0.04840	0.00120	0.93	20.66116	0.51226	0.05330	0.00190	-0.62	304.7	7.2	341.3	79	470	600	0.89
QE-D3_28	0.64600	0.04200	0.08250	0.00300	0.98	12.12121	0.44077	0.05762	0.00210	-0.97	511	18	515	78	602	473	1.43
QE-D3_29	0.97000	0.17000	0.09800	0.00420	0.55	10.20408	0.43732	0.07500	0.01400	-0.80	602	25	960	310	194	75	2.80
QE-D3_30	1.34100	0.08200	0.14110	0.00410	0.99	7.08717	0.20593	0.06986	0.00240	-0.71	851	23	924	72	283	114.6	2.75
QE-D3_31	0.70800	0.07700	0.09460	0.00430	0.89	10.57082	0.48049	0.05490	0.00380	-0.67	583	26	400	150	405	81	5.25
QE-D3_32	1.79870	0.10000	0.17736	0.00420	0.93	5.63825	0.13352	0.07417	0.00260	-0.05	1052.5	23	1045.9	70	272	143.8	2.14
QE-D3_33	0.80600	0.07900	0.09010	0.00240	0.53	11.09878	0.29564	0.06860	0.00700	-0.71	556	14	810	170	578	277	2.36
QE-D3_34	0.35000	0.12000	0.05160	0.00530	0.97	19.37984	1.99057	0.04700	0.01200	-0.91	324	33	40	470	550	66	9.90
QE-D3_35	0.40680	0.02400	0.05541	0.00140	1.00	18.04728	0.45599	0.05360	0.00190	-1.00	347.6	8.4	354.2	79	831	592	1.57
QE-D3_36	0.77200	0.05100	0.08700	0.00240	0.68	11.49425	0.31708	0.06490	0.00270	-0.50	537.5	14	765	84	202	265	0.86
QE-D3_37	0.72700	0.04500	0.08690	0.00240	0.98	11.50748	0.31781	0.06104	0.00230	-1.00	536.9	14	638	78	245	564	0.51
QE-D3_38	0.38110	0.02300	0.05106	0.00130	0.77	19.58480	0.49863	0.05423	0.00190	-0.22	321	8	385	90	208.7	223.3	1.04
QE-D3_39	0.70170	0.04100	0.08769	0.00210	0.90	11.40381	0.27310	0.05825	0.00200	0.22	541.9	13	538.9	76	331	141.4	2.61
QE-D3_40	1.34600	0.07900	0.14450	0.00370	0.98	6.92042	0.17720	0.06787	0.00240	-0.10	869.9	21	864.6	72	440.3	220.1	2.24
QE-D3_41	1.35700	0.07900	0.14560	0.00360	0.99	6.86813	0.16982	0.06804	0.00240	-0.98	876.2	20	869.6	72	297	123	2.68
QE-D3_42	0.81600	0.04900	0.09630	0.00350	0.24	10.38422	0.37741	0.06078	0.00220	0.80	592	21	630	75	258	981	0.30
QE-D3_43	0.64700	0.03900	0.07580	0.00210	0.81	13.19261	0.36549	0.06237	0.00220	-0.10	470.7	13	686	75	722	477.7	1.69
QE-D3_44	0.67500	0.03900	0.07530	0.00220	-0.24	13.28021	0.38800	0.06610	0.00280	0.95	468	13	806	87	400	336	1.33
QE-D3_45	0.71070	0.04100	0.08857	0.00220	0.96	11.29050	0.28045	0.05849	0.00200	-0.11	547	13	548.1	76	316	352	1.07
QE-D3_46	1.17310	0.06800	0.12944	0.00310	0.88	7.72559	0.18502	0.06597	0.00230	-0.06	784.7	18	805.3	73	259.3	135.2	2.15
QE-D3_47	1.20880	0.07000	0.13400	0.00330	0.97	7.46269	0.18378	0.06579	0.00230	0.06	810.8	19	799.8	73	275	126	2.50
QE-D3_48	0.19300	0.06000	0.04490	0.00630	0.45	22.27171	3.12498	0.02400	0.01900	0.25	283	39	-860	720	125	9.7	15.40
QE-D3_49	0.59200	0.03800	0.07620	0.00260	0.92	13.12336	0.44778	0.05616	0.00200	-0.59	473	16	458	83	846	607	1.61
QE-D3_50	0.69100	0.04100	0.08680	0.00250	0.94	11.52074	0.33182	0.05788	0.00200	-0.52	536.3	15	525.2	77	415	61.4	7.48
QE-D3_51	0.79900	0.05100	0.09720	0.00330	1.00	10.28807	0.34929	0.05977	0.00210	-1.00	598	19	595	79	620	429	1.63
QE-D3_52	0.85900	0.05000	0.09930	0.00270	0.69	10.07049	0.27382	0.06302	0.00220	0.37	610.1	16	709	75	316	360.6	0.99
QE-D3_53	1.07700	0.06900	0.12680	0.00430	1.00	7.88644	0.26744	0.06220	0.00220	-0.66	769	25	681	75	384	231	1.86
QE-D3_54	0.44510	0.02700	0.05930	0.00180	0.99	16.86341	0.51187	0.05465	0.00190	0.36	371.3	11	398	78	762	257.5	3.40

QE-D3_55	0.83400	0.05000	0.10020	0.00280	0.98	9.98004	0.27888	0.06048	0.00210	-0.28	615.8	17	620.8	75	419	168.9	2.80
QE-D3_56	0.38900	0.02700	0.05360	0.00190	0.78	18.65672	0.66134	0.05180	0.00220	-0.30	336.2	12	275	97	660	79	9.52
QE-D3_57	0.92100	0.05500	0.11060	0.00310	0.98	9.04159	0.25343	0.06088	0.00210	-0.95	676.3	18	635	76	187	140	1.52
QE-D3_58	0.86780	0.05100	0.10328	0.00250	0.87	9.68242	0.23437	0.06094	0.00210	-0.07	633.6	15	636.9	75	142	118.9	1.39
QE-D3_59	0.60000	0.06500	0.07620	0.00330	0.93	13.12336	0.56833	0.05900	0.00350	-0.90	473	20	540	130	760	106	8.15
QE-D3_60	0.84400	0.05700	0.10130	0.00410	0.97	9.87167	0.39954	0.06046	0.00220	-0.22	622	24	620	78	581	460	1.55
QE-D3_61	0.72400	0.04400	0.07690	0.00280	0.93	13.00390	0.47348	0.06895	0.00240	0.57	478	17	897	74	887	346	3.00
QE-D3_62	0.63840	0.03700	0.08078	0.00200	0.95	12.37930	0.30649	0.05746	0.00200	-0.17	500.8	12	509.2	77	599	363	1.93
QE-D3_63	0.53100	0.03300	0.06746	0.00180	0.60	14.82360	0.39553	0.05630	0.00230	-0.17	420.8	11	459	90	777	402	2.24
QE-D3_64	0.59200	0.03800	0.07570	0.00290	0.98	13.21004	0.50606	0.05681	0.00200	0.08	470	18	484	78	573	168.7	4.09
QE-D3_65	0.94900	0.06400	0.11140	0.00430	1.00	8.97666	0.34650	0.06168	0.00220	-0.87	681	25	666	83	215	260	1.01
QE-D3_66	0.87500	0.05100	0.10510	0.00270	0.99	9.51475	0.24443	0.06035	0.00210	-0.29	644.3	16	616	75	424.6	431	1.15
QE-D3_67	0.75300	0.04700	0.09171	0.00230	0.82	10.90394	0.27346	0.06000	0.00230	-0.71	565.6	13	601	79	108.2	114.9	1.08
QE-D3_68	0.71600	0.08400	0.07970	0.00250	0.76	12.54705	0.39357	0.06540	0.00620	-0.68	494	15	740	160	399	445	1.04
QE-D3_69	0.79010	0.04600	0.09484	0.00230	0.90	10.54407	0.25571	0.06037	0.00210	-0.29	584.1	14	616.8	75	111.3	57.6	2.27
QE-D3_70	0.85900	0.05200	0.10420	0.00320	0.99	9.59693	0.29472	0.05972	0.00210	-0.83	639	18	593.3	75	627	264	2.78

Spot	207Pb/ 235U	2σ	206Pb/ 238U	2σ	ρ	238U/ 206Pb	2σ	207Pb/ 206Pb	2σ	ρ	206Pb/ 238Pb Age (Ma)	2σ	207Pb/ 206Pb Age (Ma)	2σ	U (PPM)	Th (PPM)	U/Th Ratio
GRB1-D5_1	0.32950	0.02000	0.04484	0.00180	0.75	22.30152	0.89524	0.05415	0.00260	0.51	282.8	11	377	110	580	217	2.76
GRB1-D5_2	0.37970	0.02500	0.05049	0.00210	0.61	19.80590	0.82377	0.05497	0.00270	-0.21	317.5	13	409	110	372	125	3.42
GRB1-D5_3	0.76800	0.05000	0.08481	0.00340	0.70	11.79106	0.47270	0.06610	0.00350	-0.64	524.8	20	804	100	131	72.5	1.86
GRB1-D5_4	0.59600	0.07400	0.06460	0.00290	0.00	15.47988	0.69492	0.06610	0.00850	0.02	403.3	18	860	250	425	178	2.44
GRB1-D5_5	0.38900	0.02600	0.04950	0.00220	0.69	20.20202	0.89787	0.05730	0.00300	-0.33	311.3	13	496	110	332	128	2.73
GRB1-D5_6	0.49190	0.03200	0.06520	0.00300	0.92	15.33742	0.70571	0.05571	0.00270	0.02	407.3	18	440	110	417	32.1	16.10
GRB1-D5_7	0.41000	0.03000	0.05010	0.00250	0.83	19.96008	0.99601	0.06070	0.00320	-0.48	314.9	16	638	130	408	135	3.39

GRB1-D5_8	0.79800	0.07200	0.09690	0.00810	0.99	10.31992	0.86266	0.06220	0.00300	0.24	595	47	680	100	430	126.5	3.71
GRB1-D5_9	0.72850	0.04500	0.09125	0.00360	0.83	10.95890	0.43235	0.05849	0.00280	0.23	562.9	21	547.9	110	281	141	2.13
GRB1-D5_10	0.54900	0.04200	0.07270	0.00470	0.99	13.75516	0.88926	0.05696	0.00280	0.33	452	28	489	110	300	122	2.79
GRB1-D5_11	0.62150	0.03900	0.08051	0.00330	0.76	12.42082	0.50911	0.05729	0.00280	-0.04	499.2	19	502.5	110	151	82	1.74
GRB1-D5_12	0.45630	0.03000	0.06320	0.00290	0.93	15.82278	0.72605	0.05450	0.00260	-0.85	394.8	17	391.7	110	484	376	1.16
GRB1-D5_13	0.38600	0.03000	0.04900	0.00240	0.97	20.40816	0.99958	0.05870	0.00310	-0.85	308.2	15	552	110	409	96.1	4.33
GRB1-D5_14	0.51300	0.03700	0.06930	0.00310	0.86	14.43001	0.64550	0.05536	0.00270	-0.55	431.9	18	426	110	392	152	2.44
GRB1-D5_15	0.77700	0.05600	0.09720	0.00520	0.97	10.28807	0.55039	0.05953	0.00290	-0.72	598	31	586	110	492	150	3.13
GRB1-D5_16	0.60000	0.05500	0.07950	0.00460	0.93	12.57862	0.72782	0.05700	0.00320	-0.70	498	27	482	130	319	47.8	7.30
GRB1-D5_17	0.34290	0.02200	0.04716	0.00190	0.95	21.20441	0.85429	0.05274	0.00260	-0.92	297	12	317	110	260.1	79.8	3.13
GRB1-D5_18	0.59270	0.03600	0.07569	0.00310	0.90	13.21178	0.54111	0.05644	0.00270	-0.76	470.3	19	469.4	110	256.7	54.1	4.86
GRB1-D5_19	0.33720	0.02200	0.04570	0.00220	0.90	21.88184	1.05339	0.05318	0.00260	-0.01	288.3	13	335	110	231	112	2.33
GRB1-D5_20	0.40370	0.02700	0.05110	0.00240	0.60	19.56947	0.91911	0.05700	0.00300	-0.03	321.3	15	487	110	266.7	117.8	2.41
GRB1-D5_21	0.65900	0.04700	0.08210	0.00440	0.99	12.18027	0.65278	0.05938	0.00290	-0.67	508	26	581	110	287.5	103.6	2.90
GRB1-D5_22	0.54020	0.03300	0.06978	0.00280	0.99	14.33075	0.57504	0.05450	0.00370	-1.00	434.8	17	390	150	218	50.8	4.48
GRB1-D5_23	0.44180	0.02700	0.05693	0.00230	0.33	17.56543	0.70965	0.05584	0.00280	0.20	356.9	14	445	110	263	109.3	2.60
GRB1-D5_24	0.36100	0.02500	0.04700	0.00230	0.90	21.27660	1.04120	0.05659	0.00290	-0.04	296.3	14	472	110	494	146	3.81
GRB1-D5_25	0.51880	0.03200	0.06686	0.00270	0.97	14.95663	0.60399	0.05551	0.00270	-0.94	417.2	16	432.8	110	313	94	3.86
GRB1-D5_26	0.36710	0.02300	0.04902	0.00200	0.71	20.39984	0.83231	0.05464	0.00270	-0.24	308.5	12	397	110	424	273	1.75
GRB1-D5_27	0.36060	0.02300	0.04661	0.00190	0.77	21.45462	0.87457	0.05551	0.00280	-0.55	293.7	11	431	110	118.2	63.7	1.80
GRB1-D5_28	0.25670	0.01600	0.03196	0.00130	0.67	31.28911	1.27271	0.05781	0.00290	-0.38	202.8	8.1	521	110	421	460	0.87
GRB1-D5_29	0.32710	0.02000	0.04439	0.00170	0.78	22.52760	0.86274	0.05287	0.00260	-0.13	280	11	322.9	110	606	303	1.93
GRB1-D5_30	0.48970	0.03100	0.06098	0.00260	0.83	16.39882	0.69920	0.05718	0.00280	-0.21	381.6	16	497	110	88.8	57.8	1.47
GRB1-D5_31	0.71500	0.07000	0.04716	0.00190	0.73	21.20441	0.85429	0.10650	0.00920	-0.65	297	12	1680	170	253	311	0.81
GRB1-D5_32	0.48270	0.03000	0.06268	0.00260	0.87	15.95405	0.66178	0.05492	0.00270	-0.22	391.9	15	409	110	310	111.9	2.74
GRB1-D5_33	0.34080	0.02200	0.04512	0.00190	-0.31	22.16312	0.93329	0.05350	0.00290	0.55	284.5	12	344	100	410	65	8.16
GRB1-D5_34	0.38900	0.04000	0.05360	0.00300	0.97	18.65672	1.04422	0.05040	0.00420	-0.97	336	18	220	170	970	335	2.98
GRB1-D5_35	0.54800	0.04200	0.07240	0.00420	0.97	13.81215	0.80126	0.05621	0.00280	-0.99	451	26	459	110	827	170.2	4.97
GRB1-D5_36	1.68500	0.10000	0.16290	0.00650	0.97	6.13874	0.24495	0.07362	0.00350	-0.84	973.1	36	1030.8	97	257.8	217.2	1.16

GRB1-D5_37	0.36870	0.02400	0.04812	0.00210	0.98	20.78138	0.90692	0.05469	0.00280	-1.00	302.9	13	396	110	507	259	2.11
GRB1-D5_38	0.35020	0.02100	0.04693	0.00190	0.75	21.30833	0.86269	0.05300	0.00260	0.28	295.6	12	329	110	432	215	2.10
GRB1-D5_39	0.71520	0.04400	0.08786	0.00350	0.83	11.38174	0.45340	0.05837	0.00280	-0.19	542.9	21	543.4	110	553	250.8	2.29
GRB1-D5_40	0.64000	0.04100	0.08010	0.00340	0.66	12.48439	0.52992	0.05777	0.00290	0.28	496.7	20	520	100	766	128.1	6.22
GRB1-D5_41	0.30810	0.02000	0.04216	0.00180	0.99	23.71917	1.01268	0.05235	0.00250	-0.99	266.2	11	300	110	1911	144.5	13.76
GRB1-D5_42	0.25190	0.01500	0.03488	0.00140	0.80	28.66972	1.15073	0.05259	0.00260	-0.02	221	8.7	311	110	387	277	1.47
GRB1-D5_43	0.32010	0.02000	0.04436	0.00180	0.70	22.54283	0.91472	0.05255	0.00260	-0.11	279.8	11	309	110	524	383	1.33
GRB1-D5_44	0.36960	0.02400	0.05076	0.00210	0.50	19.70055	0.81503	0.05456	0.00270	-0.27	319.2	13	393	110	584	298	1.96
GRB1-D5_45	0.32290	0.02000	0.04474	0.00190	0.98	22.35136	0.94921	0.05201	0.00250	-0.83	282.1	12	285	110	1260	820	1.57
GRB1-D5_46	0.47490	0.03000	0.06217	0.00250	0.42	16.08493	0.64681	0.05657	0.00280	0.21	388.8	15	474	110	920	257	3.59
GRB1-D5_47	0.51200	0.04700	0.04590	0.00190	0.69	21.78649	0.90184	0.08120	0.00540	-0.50	289.3	12	1212	130	1420	933	1.48
GRB1-D5_48	0.34590	0.02300	0.04794	0.00190	0.36	20.85941	0.82672	0.05480	0.00280	0.06	301.9	12	401	110	940	405	2.36
GRB1-D5_49	0.34900	0.02900	0.04433	0.00180	0.43	22.55809	0.91596	0.05690	0.00440	-0.34	279.6	11	470	150	466	216.7	2.17
GRB1-D5_50	0.77500	0.06700	0.09900	0.00530	0.96	10.10101	0.54076	0.05880	0.00340	-0.90	609	31	554	140	931	451	2.19
GRB1-D5_51	0.72500	0.04600	0.09335	0.00380	0.89	10.71237	0.43607	0.05891	0.00290	-0.71	575.3	22	563	100	722	352	2.10
GRB1-D5_52	0.31900	0.02400	0.04426	0.00200	0.82	22.59376	1.02096	0.05360	0.00290	-0.69	279.2	12	345	120	835	739	1.11
GRB1-D5_53	0.34250	0.02200	0.04881	0.00200	0.86	20.48760	0.83948	0.05232	0.00250	-0.65	307.2	12	299	110	1597	1297	1.24
GRB1-D5_54	0.33950	0.02200	0.04755	0.00200	0.69	21.03049	0.88456	0.05321	0.00260	-0.12	299.5	12	342	100	637	456	1.34
GRB1-D5_55	0.32760	0.02000	0.04480	0.00180	0.90	22.32143	0.89684	0.05289	0.00260	-0.44	282.5	11	323.8	110	791	781	1.01
GRB1-D5_56	0.37610	0.02400	0.05284	0.00210	0.74	18.92506	0.75213	0.05319	0.00260	-0.43	332	13	336.9	110	1205	563	2.05
GRB1-D5_57	0.34580	0.02100	0.04694	0.00190	0.73	21.30379	0.86232	0.05344	0.00260	-0.02	295.7	12	347	110	292	197	1.51
GRB1-D5_58	0.43500	0.02900	0.05544	0.00240	0.96	18.03752	0.78084	0.05957	0.00290	0.36	347.8	15	587	110	1593	737	2.15
GRB1-D5_59	0.65840	0.04200	0.08630	0.00380	0.95	11.58749	0.51023	0.05654	0.00270	-0.23	533.5	23	473.6	110	498	12.1	44.10
GRB1-D5_60	0.37180	0.02400	0.05050	0.00230	0.84	19.80198	0.90187	0.05400	0.00270	-0.55	317.6	14	369	110	615	312	2.58
GRB1-D5_61	0.40600	0.03400	0.04725	0.00200	0.40	21.16402	0.89583	0.06490	0.00440	-0.11	297.6	12	750	130	1141	811	1.35
GRB1-D5_62	0.31100	0.02400	0.04428	0.00200	0.93	22.58356	1.02003	0.04760	0.00550	-0.97	279.3	12	110	220	227	226	1.00
GRB1-D5_63	0.59000	0.04100	0.07970	0.00390	0.95	12.54705	0.61397	0.05654	0.00270	-0.81	494	23	473	110	787	356	2.07

Spot	207Pb/ 235U	2σ	206Pb/ 238U	2σ	ρ	238U/ 206Pb	2σ	207Pb/ 206Pb	2σ	ρ	206Pb/ 238Pb Age (Ma)	2σ	207Pb/ 206Pb Age (Ma)	2σ	U (PPM)	Th (PPM)	U/Th Ratio
LLG_1_1	0.45560	0.01400	0.05963	0.00130	0.79	16.77008	0.36561	0.05503	0.00098	-0.15	373.3	7.9	413	39	281.1	184	1.62
LLG_1_2	0.52400	0.01600	0.05120	0.00140	-0.55	19.53125	0.53406	0.07450	0.00290	0.88	322	8.5	1050	80	1256	284	4.63
LLG_1_3	0.60500	0.03800	0.06900	0.00170	0.12	14.49275	0.35707	0.06370	0.00390	0.12	430.2	10	720	120	701	310	2.39
LLG_1_4	0.45210	0.01100	0.06043	0.00096	0.62	16.54807	0.26289	0.05426	0.00077	-0.05	378.2	6.2	382	32	143.4	82.3	1.78
LLG_1_5	0.34620	0.00840	0.04715	0.00053	0.51	21.20891	0.23840	0.05265	0.00080	-0.15	297	4.8	313	34	139	57.47	2.20
LLG_1_6	0.29300	0.00940	0.04004	0.00067	0.77	24.97502	0.41791	0.05308	0.00080	-0.29	253.1	4.2	332	34	521	1410	0.33
LLG_1_7	1.46000	0.12000	0.04200	0.00140	0.70	23.80952	0.79365	0.25200	0.01700	-0.46	265.4	8.9	3190	110	869	222	3.31
LLG_1_8	0.31470	0.00760	0.04058	0.00065	0.38	24.64268	0.39472	0.05613	0.00079	-0.05	256.42	4	457	31	945	679	1.25
LLG_1_9	0.30970	0.00770	0.04210	0.00096	0.08	23.75297	0.54164	0.05322	0.00073	0.60	265.8	4.2	338	31	822	293	2.76
LLG_1_10	0.32120	0.00870	0.04196	0.00027	0.01	23.83109	0.15334	0.05518	0.00087	0.51	264.98	4.3	419	35	623	500.5	1.35
LLG_1_11	0.29840	0.00690	0.04191	0.00079	0.79	23.86065	0.44977	0.05172	0.00066	0.18	264.6	4.5	275	27	458	550	1.00
LLG_1_12	0.53120	0.01500	0.07000	0.00130	0.72	14.28571	0.26531	0.05549	0.00075	-0.17	436.2	7.3	432	30	429.8	95.3	4.93
LLG_1_13	0.37670	0.00940	0.05197	0.00095	0.94	19.24187	0.35174	0.05267	0.00064	0.15	326.6	6	314.4	28	795	6.56	116.50
LLG_1_14	0.32970	0.00790	0.04571	0.00071	0.94	21.87705	0.33981	0.05218	0.00064	0.22	288.1	5.6	293.3	28	288	211	1.33
LLG_1_15	0.31980	0.00820	0.04015	0.00088	0.99	24.90660	0.54590	0.05779	0.00086	-0.95	253.8	5.5	521	33	771	316	2.53
LLG_1_16	0.44530	0.01100	0.05964	0.00097	0.88	16.76727	0.27271	0.05411	0.00066	0.11	373.4	5.9	375.7	27	593	407	1.54
LLG_1_17	0.47730	0.01200	0.06367	0.00110	0.91	15.70598	0.27135	0.05433	0.00068	-0.20	397.9	6.7	384.6	28	643	439	1.54
LLG_1_18	0.30790	0.00750	0.04288	0.00069	0.28	23.32090	0.37527	0.05168	0.00068	0.26	270.6	4.3	271	30	630	483	1.40
LLG_1_19	0.30940	0.00740	0.04294	0.00068	0.79	23.28831	0.36879	0.05173	0.00063	0.15	271.1	4.2	273.3	28	1285	1180	1.13
LLG_1_20	0.34260	0.01000	0.04241	0.00068	0.21	23.57934	0.37807	0.05811	0.00120	0.17	267.7	4.2	533	45	576	424	1.44
LLG_1_21	0.30700	0.00840	0.04272	0.00083	0.91	23.40824	0.45479	0.05184	0.00069	0.09	269.7	5.1	278	31	590	173	3.47
LLG_1_22	0.50300	0.01600	0.05081	0.00110	-0.53	19.68117	0.42608	0.07250	0.00260	0.82	319.5	6.8	993	72	876	117	7.67
LLG_1_23	0.78300	0.02400	0.07265	0.00120	0.22	13.76462	0.22736	0.07740	0.00280	0.03	452.1	7.3	1128	70	1010	399	2.54
LLG_1_24	0.63000	0.02700	0.04270	0.00093	0.27	23.41920	0.51007	0.10480	0.00260	0.36	269.5	5.8	1711	46	702	740	1.00
LLG_1_25	0.38800	0.01400	0.04130	0.00089	-0.73	24.21308	0.52178	0.06650	0.00290	0.90	260.9	5.5	819	90	902	513	1.83

LLG_1_26	0.60400	0.02000	0.07055	0.00110	0.71	14.17434	0.22100	0.06070	0.00140	0.16	439.4	6.8	627	48	229	22.9	10.48
LLG_1_27	0.38120	0.00940	0.05169	0.00083	0.36	19.34610	0.31065	0.05286	0.00069	0.25	324.9	5.1	323	30	383	236.9	1.50
LLG_1_28	0.45160	0.01400	0.05825	0.00110	0.86	17.16738	0.32419	0.05570	0.00130	-0.18	367.6	11	439	50	464	59.9	7.86
LLG_1_29	0.34500	0.01800	0.04459	0.00079	0.95	22.42655	0.39733	0.05610	0.00220	-0.92	281.2	4.8	448	87	551.4	247	2.19
LLG_1_30	0.33200	0.01300	0.04453	0.00090	0.47	22.45677	0.45388	0.05400	0.00150	-0.33	280.8	5.6	366	60	640	450	1.66
LLG_1_31	0.36510	0.00990	0.04384	0.00087	-0.08	22.81022	0.45267	0.05950	0.00110	0.32	276.6	5.4	585	40	434	397	1.13
LLG_1_32	0.30330	0.00750	0.04208	0.00071	0.80	23.76426	0.40097	0.05210	0.00066	-0.05	265.7	4.4	289.5	29	358	165	2.25
LLG_1_33	0.77900	0.02000	0.08756	0.00150	-0.41	11.42074	0.19565	0.06400	0.00130	0.78	541.1	8.7	741	41	207	259.8	0.79
LLG_1_34	0.73000	0.02600	0.07685	0.00120	0.62	13.01236	0.20319	0.06800	0.00190	-0.49	477.3	7.2	868	58	149.9	22.02	6.73
LLG_1_35	0.64200	0.03000	0.02364	0.00063	0.76	42.30118	1.12732	0.19510	0.00690	0.26	150.6	4	2783	57	542	420	1.23
LLG_1_36	0.53620	0.01500	0.07000	0.00160	0.93	14.28571	0.32653	0.05529	0.00073	0.04	436	9.4	424	29	264	75	3.55
LLG_1_37	0.75800	0.06400	0.03120	0.00110	0.97	32.05128	1.13001	0.17250	0.01000	-0.88	198.1	6.7	2576	93	435	236.3	1.81
LLG_1_38	0.77700	0.02200	0.08951	0.00160	0.30	11.17194	0.19970	0.06208	0.00100	0.09	552.7	9.3	676	35	154	10	15.10
LLG_1_39	0.35230	0.00880	0.04759	0.00079	0.69	21.01282	0.34882	0.05300	0.00067	0.15	299.7	4.9	329	29	473	420	1.18
LLG_1_40	0.89200	0.07000	0.05110	0.00180	0.92	19.56947	0.68934	0.12350	0.00630	-0.82	321.2	11	2004	90	377.3	129.7	3.14
LLG_1_41	0.51930	0.01500	0.06795	0.00140	0.93	14.71670	0.30321	0.05549	0.00072	-0.28	423.8	8.5	432	29	87.2	1.339	58.30
LLG_1_42	0.49200	0.04200	0.04580	0.00250	0.34	21.83406	1.19182	0.07980	0.00690	0.42	288	15	1160	170	246	73	2.91
LLG_1_43	0.34950	0.00830	0.04803	0.00077	0.81	20.82032	0.33378	0.05272	0.00064	-0.09	302.4	4.8	316.5	27	759	596	1.15
LLG_1_44	0.64160	0.01600	0.08153	0.00130	0.51	12.26542	0.19557	0.05696	0.00077	0.04	505.2	7.7	490	30	151.9	69.9	2.03
LLG_1_45	0.33410	0.00810	0.04474	0.00071	0.80	22.35136	0.35470	0.05263	0.00066	-0.74	282.12	4.4	312.7	29	312	184.27	1.61

Spot	207Pb/ 235U	2σ	206Pb/ 238U	2σ	ρ	238U/ 206Pb	2σ	207Pb/ 206Pb	2σ	ρ	206Pb/ 238Pb Age (Ma)	2σ	207Pb/ 206Pb Age (Ma)	2σ	U (PPM)	Th (PPM)	U/Th Ratio
DL-D4_1	0.43130	0.05800	0.05866	0.00190	0.94	17.04739	0.55217	0.05477	0.00470	-0.24	367.4	11	402.5	190	457.0	36.7	15.20
DL-D4_2	0.47700	0.07200	0.06110	0.00230	0.69	16.36661	0.61609	0.05850	0.00590	-0.42	382.6	14	590	230	504.0	26.3	19.47
DL-D4_3	0.30950	0.04100	0.04329	0.00130	0.80	23.10002	0.69369	0.05251	0.00450	-0.25	273.2	8.2	307.4	190	746.0	197.0	3.89

DL-D4_4	1.55000	0.27000	0.06460	0.00270	0.89	15.47988	0.64699	0.17600	0.02100	-0.83	404	16	2580	200	170.0	115.0	1.42
DL-D4_5	0.45000	0.19000	0.04530	0.00420	0.94	22.07506	2.04669	0.06900	0.02700	-0.97	285	26	470	850	410.0	152.0	2.93
DL-D4_6	0.74000	0.17000	0.04740	0.00260	0.93	21.09705	1.15722	0.11200	0.02400	-0.95	298	16	1500	630	500.0	149.0	3.62
DL-D4_7	0.49630	0.06700	0.06855	0.00220	0.87	14.58789	0.46817	0.05467	0.00470	-0.38	427.4	13	404	220	359.0	110.0	3.24
DL-D4_8	1.15000	0.28000	0.05820	0.00210	-0.06	17.18213	0.61997	0.15000	0.03000	0.20	365	13	2130	440	99.9	26.3	3.76
DL-D4_9	0.83900	0.13000	0.08120	0.00400	-0.10	12.31527	0.60666	0.08040	0.01100	0.52	503	24	1110	250	372.0	40.2	8.28
DL-D4_10	0.37500	0.05300	0.04836	0.00150	-0.60	20.67825	0.64138	0.05810	0.00530	0.85	304.4	9.4	525	180	690.0	352.0	1.98
DL-D4_11	-0.12500	0.10000	0.04970	0.00450	0.90	20.12072	1.82180	-0.03000	0.02000	-0.95	312	28	-2900	770	74.6	28.4	6.20
DL-D4_12	0.32170	0.04600	0.04634	0.00150	0.31	21.57963	0.69852	0.05271	0.00460	0.00	292	9	315	180	532.0	295.0	1.73
DL-D4_13	0.50900	0.11000	0.04662	0.00160	0.75	21.45002	0.73617	0.08300	0.01600	-1.00	293.7	10	1110	340	314.0	205.0	1.57
DL-D4_14	0.45300	0.06900	0.04766	0.00160	0.62	20.98196	0.70439	0.07210	0.00710	-0.30	300.1	9.8	975	190	383.0	104.0	3.52
DL-D4_15	0.37900	0.06300	0.04604	0.00160	0.82	21.72024	0.75483	0.06060	0.00650	-0.71	290.2	10	610	230	431.0	188.0	2.13
DL-D4_16	0.35500	0.04900	0.04576	0.00140	0.31	21.85315	0.66858	0.05750	0.00510	-0.12	288.4	8.8	502	190	115.2	54.4	2.02
DL-D4_17	0.47270	0.06200	0.06470	0.00220	0.98	15.45595	0.52555	0.05378	0.00460	-0.01	405.3	14	361.8	190	369.3	17.7	20.50
DL-D4_18	0.29050	0.04200	0.04690	0.00140	0.12	21.32196	0.63648	0.04686	0.00400	0.05	295.5	8.9	42	190	655.0	263.0	2.26
DL-D4_19	0.46980	0.06900	0.07126	0.00210	0.80	14.03312	0.41355	0.04989	0.00430	0.12	443.8	13	190	200	323.0	56.9	5.04
DL-D4_20	0.59300	0.08100	0.07550	0.00300	0.98	13.24503	0.52629	0.05844	0.00490	-0.36	469	18	546	190	260.0	404.0	0.78
DL-D4_21	0.49300	0.06900	0.06335	0.00210	0.73	15.78532	0.52327	0.05770	0.00510	-0.55	396	13	506	180	208.0	257.0	0.85
DL-D4_22	0.38040	0.05200	0.05427	0.00180	0.92	18.42639	0.61116	0.05233	0.00450	-0.18	340.7	11	299	200	230.0	111.2	1.99
DL-D4_23	0.47700	0.06400	0.06222	0.00210	0.78	16.07200	0.54245	0.05589	0.00480	-0.32	389.1	13	454	170	70.8	35.1	1.99
DL-D4_24	0.35690	0.04700	0.04962	0.00160	0.15	20.15316	0.64984	0.05329	0.00460	0.62	312.2	9.8	339	190	440.0	172.3	2.51
DL-D4_25	0.35140	0.05200	0.04655	0.00140	0.21	21.48228	0.64608	0.05690	0.00510	0.04	293.3	8.7	484	180	760.0	446.0	1.66
DL-D4_26	0.33860	0.04500	0.04764	0.00150	0.72	20.99076	0.66092	0.05253	0.00450	-0.39	300	9.2	307	190	338.0	150.0	2.22
DL-D4_27	0.48480	0.06700	0.06710	0.00220	0.54	14.90313	0.48863	0.05417	0.00460	0.22	418.9	14	377	190	549.0	221.0	2.49
DL-D4_28	0.47200	0.07400	0.04900	0.00170	0.47	20.40816	0.70804	0.07240	0.00810	-0.32	308.7	11	960	210	307.0	185.0	1.57
DL-D4_29	0.38100	0.05300	0.04753	0.00150	0.42	21.03934	0.66398	0.06060	0.00550	-0.01	299.4	9.2	611	190	611.0	251.0	2.35
DL-D4_30	0.34730	0.04600	0.04847	0.00150	0.77	20.63132	0.63848	0.05296	0.00450	-0.12	305.1	9	326.8	190	283.0	224.0	1.32
DL-D4_31	0.56500	0.08900	0.07590	0.00470	0.97	13.17523	0.81586	0.05450	0.00540	-0.98	471	29	380	230	523.0	374.0	1.35
DL-D4_32	0.43820	0.06200	0.06203	0.00190	0.70	16.12123	0.49380	0.05388	0.00460	0.12	387.9	12	365	190	469.0	264.0	1.62

DL-D4_33	0.32770	0.04500	0.04783	0.00150	0.91	20.90738	0.65568	0.05161	0.00440	-0.19	301.2	9.5	268	200	244.0	145.0	1.60
DL-D4_34	0.31000	0.04200	0.04422	0.00140	0.67	22.61420	0.71596	0.05123	0.00440	0.10	278.9	8.8	249	200	88.1	35.3	2.39
DL-D4_35	0.41700	0.06200	0.04240	0.00210	0.78	23.58491	1.16812	0.07270	0.00780	-0.60	268	13	960	220	760.0	470.0	1.88
DL-D4_36	5.55000	0.88000	0.09270	0.00650	0.71	10.78749	0.75640	0.44900	0.04700	-0.09	571	38	4067	150	1.8	0.8	2.40
DL-D4_37	0.31390	0.03800	0.04564	0.00120	0.86	21.91060	0.57609	0.05162	0.00440	-0.51	287.7	7.7	268	200	228.0	283.0	0.76
DL-D4_38	0.32060	0.05800	0.04713	0.00130	-0.25	21.21791	0.58526	0.05202	0.00450	0.28	296.9	7.8	284	190	396.0	223.0	1.63
DL-D4_39	0.63000	0.12000	0.05290	0.00210	0.73	18.90359	0.75043	0.09000	0.01300	-0.61	332.1	13	1360	270	245.0	147.0	1.49
DL-D4_40	0.60600	0.09800	0.06290	0.00230	-0.65	15.89825	0.58134	0.07360	0.01000	0.78	393	14	970	260	607.0	332.0	1.50
DL-D4_41	0.50300	0.07700	0.06650	0.00240	-0.63	15.03759	0.54271	0.05750	0.00540	0.79	414.8	14	498	180	411.0	259.0	1.41
DL-D4_42	0.57700	0.09400	0.06918	0.00220	0.06	14.45504	0.45969	0.06240	0.00850	0.06	431.2	13	610	200	631.0	142.2	3.62
DL-D4_43	0.39400	0.05600	0.04964	0.00160	0.48	20.14504	0.64932	0.05950	0.00590	-0.33	312.3	9.9	548	190	217.0	101.6	1.78
DL-D4_44	0.22470	0.03200	0.05007	0.00150	0.86	19.97204	0.59832	0.03417	0.00290	-0.16	315	9.4	-455	110	297.0	56.9	3.99
DL-D4_45	0.28700	0.04100	0.04958	0.00160	-0.16	20.16942	0.65089	0.04380	0.00470	0.35	311.9	11	-70	190	579.0	137.6	3.11
DL-D4_46	0.37800	0.05600	0.07020	0.00300	0.45	14.24501	0.60876	0.04080	0.00380	0.00	437	18	-214	130	420.0	35.6	12.20
DL-D4_47	0.22400	0.06400	0.04560	0.00320	0.97	21.92982	1.53894	0.03800	0.00800	-0.95	287	20	-310	310	760.0	96.0	6.77
DL-D4_48	0.36100	0.05700	0.04511	0.00170	0.80	22.16803	0.83542	0.05860	0.00630	-0.91	284.4	10	520	230	950.0	800.0	1.25
DL-D4_49	0.38000	0.07900	0.05120	0.00370	0.90	19.53125	1.41144	0.05310	0.00670	-0.79	322	23	360	290	690.0	480.0	1.80
DL-D4_50	0.36800	0.06300	0.04525	0.00170	0.56	22.09945	0.83026	0.05830	0.00750	-0.39	285.3	10	520	280	801.0	770.0	1.04
DL-D4_51	0.36050	0.05200	0.05367	0.00140	0.98	18.63238	0.48603	0.04892	0.00350	-0.92	337	8.7	144.1	130	1033.0	98.1	9.71
DL-D4_52	0.42600	0.06500	0.04788	0.00170	0.85	20.88555	0.74155	0.06700	0.00690	-0.74	301.5	11	740	230	400.0	282.0	1.51
DL-D4_53	0.31270	0.03600	0.04792	0.00160	0.56	20.86811	0.69677	0.04843	0.00330	0.50	301.8	10	120	130	370.0	157.0	2.34
DL-D4_54	0.35530	0.06300	0.05512	0.00170	0.48	18.14224	0.55954	0.04943	0.00340	0.39	345.9	11	168	130	525.0	172.0	2.83
DL-D4_55	0.43500	0.05600	0.04510	0.00160	0.78	22.17295	0.78662	0.07210	0.00630	-0.84	284.4	10	950	220	740.0	103.0	6.27
DL-D4_56	0.49400	0.07400	0.06740	0.00300	0.89	14.83680	0.66039	0.05500	0.00520	-0.85	420	18	403	210	517.0	84.0	5.78
DL-D4_57	0.58400	0.11000	0.05780	0.00190	0.00	17.30104	0.56872	0.07720	0.01100	0.23	362.1	11	1030	250	246.0	68.7	3.63

Spot	207Pb/ 235U	2σ	206Pb/ 238U	2σ	ρ	238U/ 206Pb	2σ	207Pb/ 206Pb	2σ	ρ	206Pb/ 238Pb Age (Ma)	2σ	207Pb/ 206Pb Age (Ma)	2σ	U (PPM)	Th (PPM)	U/Th Ratio
PA-D4_1	0.70500	0.04000	0.05080	0.00190	0.28	19.68504	0.73625	0.09840	0.00830	0.59	320	12	1550	150	619	141	4.55
PA-D4_2	0.52200	0.03100	0.05352	0.00110	0.59	18.68460	0.38403	0.05850	0.00420	-0.32	336.1	6.9	580	130	727	322	2.25
PA-D4_3	0.57800	0.04600	0.05040	0.00240	0.62	19.84127	0.94482	0.07060	0.00360	-0.28	317	15	949	90	640	221	3.13
PA-D4_4	0.51000	0.06300	0.05690	0.00360	0.90	17.57469	1.11193	0.05280	0.00330	-0.67	356	22	310	140	560	128	3.83
PA-D4_5	1.09000	0.37000	0.07150	0.00280	0.79	13.98601	0.54770	0.08600	0.02800	-0.73	445	17	1010	420	373	174	2.126
PA-D4_6	0.48900	0.02000	0.05726	0.00110	0.85	17.46420	0.33550	0.05546	0.00071	0.46	358.9	6.9	431	28	696	343	1.957
PA-D4_7	1.22000	0.11000	0.06110	0.00340	0.94	16.36661	0.91074	0.11890	0.00530	-0.95	382	21	1931	79	422	364	1.25
PA-D4_8	0.47900	0.02300	0.05470	0.00140	0.95	18.28154	0.46790	0.05650	0.00270	-1.00	343.5	8.6	458	85	735	381	1.93
PA-D4_9	0.44000	0.02000	0.05268	0.00088	0.36	18.98254	0.31710	0.05577	0.00093	-0.15	331	5.4	442	36	268	103	2.34
PA-D4_10	0.36100	0.02300	0.04040	0.00200	0.89	24.75248	1.22537	0.05130	0.00130	-0.58	255	12	250	58	660	409	1.576
PA-D4_11	0.41700	0.01900	0.04370	0.00190	0.90	22.88330	0.99493	0.05388	0.00077	-0.73	276	12	366	32	299	233.1	1.282
PA-D4_12	0.41200	0.02000	0.04220	0.00150	0.93	23.69668	0.84230	0.05700	0.00160	-0.61	266.7	9.3	484	58	430	235	1.78
PA-D4_13	0.39700	0.01600	0.04140	0.00110	0.91	24.15459	0.64179	0.05930	0.00210	-0.62	261.5	6.7	567	79	702	635	1.066
PA-D4_14	0.37500	0.03100	0.03760	0.00180	0.93	26.59574	1.27320	0.05860	0.00400	-0.72	238	11	520	150	670	620	1.061
PA-D4_15	0.35400	0.01600	0.04200	0.00120	0.84	23.80952	0.68027	0.05530	0.00190	-0.79	265	7.6	424	75	351.1	279	1.33
PA-D4_16	0.34700	0.03400	0.04090	0.00180	0.82	24.44988	1.07603	0.04850	0.00290	-0.62	258	11	180	160	570	219	3.02
PA-D4_17	0.57200	0.03800	0.05410	0.00170	0.65	18.48429	0.58084	0.06250	0.00420	-0.71	339.5	10	660	120	555	348	1.6
PA-D4_18	0.50900	0.03600	0.04730	0.00140	0.30	21.14165	0.62576	0.06470	0.00280	0.01	298.2	8.6	754	86	427	131	3.66
PA-D4_19	0.39220	0.01500	0.04534	0.00079	-0.65	22.05558	0.38429	0.05567	0.00081	0.00	285.8	4.9	438	32	387	254	1.637
PA-D4_20	0.46500	0.02300	0.04770	0.00170	0.51	20.96436	0.74716	0.06240	0.00370	0.11	300.5	10	670	120	910	59	19
PA-D4_21	1.14000	0.30000	0.05330	0.00310	0.87	18.76173	1.09121	0.11700	0.02400	-0.72	334	19	1740	400	523	176	2.79
PA-D4_22	0.56400	0.02300	0.05630	0.00170	0.98	17.76199	0.53633	0.05700	0.00170	-0.80	353.3	10	487	62	829	252.3	3.35
PA-D4_23	0.63000	0.05300	0.06730	0.00390	0.99	14.85884	0.86106	0.05770	0.00390	-0.98	420	23	510	160	777	90.1	8.68
PA-D4_24	0.53100	0.05100	0.05530	0.00210	0.86	18.08318	0.68670	0.05790	0.00310	-0.62	347	13	510	110	560	140	4.11
PA-D4_25	0.34520	0.01200	0.03984	0.00083	0.53	25.10040	0.52293	0.05171	0.00062	-0.80	251.8	5.2	272.7	28	830	504	1.66

PA-D4_26	0.39870	0.01400	0.04947	0.00098	0.74	20.21427	0.40044	0.05411	0.00077	-0.67	311.3	6	380	35	167	146	1.35
PA-D4_27	0.33830	0.01300	0.03880	0.00140	0.85	25.77320	0.92996	0.05221	0.00063	0.21	245.1	8.6	294.4	28	351	313	1.209
PA-D4_28	0.84000	0.24000	0.04300	0.00260	0.89	23.25581	1.40617	0.11900	0.02900	-0.78	271	16	1600	490	764	680	1.127
PA-D4_29	0.37120	0.01300	0.04620	0.00110	0.65	21.64502	0.51536	0.05294	0.00070	-0.72	291.1	6.9	326	30	491	308	1.522
PA-D4_30	0.44900	0.06000	0.04540	0.00210	0.96	22.02643	1.01884	0.06400	0.00730	-0.93	286	13	670	210	567	346	1.583
PA-D4_31	0.35370	0.01400	0.04450	0.00130	-0.21	22.47191	0.65648	0.05309	0.00100	0.49	280.6	7.9	330	40	500	403	1.53
PA-D4_32	0.48860	0.01700	0.05362	0.00120	0.85	18.64976	0.41738	0.05526	0.00100	-0.88	336.7	7.2	420	40	579	121.1	4.89
PA-D4_33	0.33560	0.01300	0.04233	0.00084	0.27	23.62391	0.46879	0.05262	0.00079	0.10	267.2	5.2	311	32	365	258.3	1.377
PA-D4_34	0.42120	0.01500	0.04405	0.00110	0.63	22.70148	0.56689	0.05283	0.00068	-0.13	277.9	6.9	321	29	606	136	4.02
PA-D4_35	0.39500	0.02300	0.04040	0.00130	0.89	24.75248	0.79649	0.05279	0.00070	-0.41	255	8	320	30	622	158	3.5
PA-D4_36	0.38600	0.02000	0.04250	0.00140	0.84	23.52941	0.77509	0.05250	0.00069	-0.79	268.2	8.9	307	30	713	374	1.87
PA-D4_37	0.49000	0.01900	0.05406	0.00100	0.83	18.49797	0.34217	0.05740	0.00130	-0.64	339.4	6.2	503	50	279	110.6	2.489
PA-D4_38	0.53400	0.03500	0.05140	0.00210	0.85	19.45525	0.79486	0.05820	0.00200	-0.60	323	13	529	82	470	100	4.99

Spot	207Pb/ 235U	2σ	206Pb/ 238U	2σ	ρ	238U/ 206Pb	2σ	207Pb/ 206Pb	2σ	ρ	206Pb/ 238Pb Age (Ma)	2σ	207Pb/ 206Pb Age (Ma)	2σ	U (PPM)	Th (PPM)	U/Th Ratio
RRPS1_1	0.347600	0.00850	0.04783	0.00095	0.78	20.90738	0.41526	0.05318	0.00064	-0.33	301.2	5.8	336	27	267.9	112	2.13
RRPS1_2	0.350600	0.00830	0.04774	0.00083	0.66	20.94680	0.36418	0.05392	0.00071	-0.31	300.6	5.1	372	29	184	57.2	2.88
RRPS1_3	0.346900	0.00740	0.04840	0.00083	0.30	20.66116	0.35431	0.05279	0.00059	0.04	304.7	5.1	319	25	219	82.57	2.40
RRPS1_4	0.343500	0.00760	0.04755	0.00082	0.13	21.03049	0.36267	0.05301	0.00065	0.17	299.4	5.1	331	29	137	41.3	3.06
RRPS1_5	0.347800	0.00750	0.04765	0.00083	0.04	20.98636	0.36555	0.05371	0.00063	0.21	300.1	5.1	358	26	176	58.6	2.67
RRPS1_6	0.353800	0.00780	0.04801	0.00083	0.20	20.82899	0.36009	0.05423	0.00070	0.09	302.3	5.1	380	29	233	83.1	2.56
RRPS1_7	0.370600	0.00890	0.04747	0.00082	0.08	21.06594	0.36389	0.05695	0.00089	0.07	299.0	5	487	34	160	100.4	1.48
RRPS1_8	0.332200	0.00740	0.04630	0.00080	0.38	21.59827	0.37319	0.05235	0.00065	-0.06	291.8	4.9	300	29	238	81	3.28
RRPS1_9	0.338100	0.00710	0.04668	0.00081	0.60	21.42245	0.37173	0.05317	0.00057	0.08	294.1	5	335.8	24	548	207.5	2.71
RRPS1_10	0.341100	0.00720	0.04739	0.00080	0.32	21.10150	0.35622	0.05314	0.00058	0.20	298.5	4.9	334.6	25	394	178.8	2.36

RRPS1_11	0.375800	0.01200	0.04885	0.00086	0.41	20.47083	0.36039	0.05720	0.00130	-0.33	307.5	5.3	506	48	264	84.3	3.30
RRPS1_12	0.321700	0.00680	0.04405	0.00076	-0.48	22.70148	0.39167	0.05467	0.00061	0.66	277.9	4.7	399	25	741.7	142.6	5.37
RRPS1_13	0.343200	0.00720	0.04761	0.00080	0.32	21.00267	0.35289	0.05299	0.00060	0.10	299.9	4.9	328	26	333	122.8	2.57
RRPS1_14	0.343100	0.00730	0.04688	0.00080	-0.08	21.33106	0.36401	0.05387	0.00062	0.37	295.3	4.9	367	25	281	131.9	2.07
RRPS1_15	0.339200	0.00720	0.04750	0.00085	0.32	21.05263	0.37673	0.05290	0.00057	0.03	299.2	5.2	324.5	24	579	178	3.48
RRPS1_16	0.333600	0.00720	0.04632	0.00083	0.31	21.58895	0.38685	0.05323	0.00063	-0.03	291.9	5.1	338	27	198	112.4	1.91
RRPS1_17	0.337100	0.00730	0.04717	0.00085	0.58	21.19992	0.38202	0.05271	0.00058	-0.22	297.1	5.3	316	25	349	159.8	2.39
RRPS1_18	0.341000	0.00740	0.04751	0.00084	-0.05	21.04820	0.37214	0.05237	0.00063	0.35	299.2	5.1	304	26	203	106.8	2.11
RRPS1_19	0.362200	0.00860	0.04746	0.00081	0.12	21.06993	0.35959	0.05598	0.00085	-0.11	298.9	5	449	33	185	104.5	1.88
RRPS1_20	0.335000	0.00770	0.04630	0.00080	0.07	21.60014	0.37325	0.05309	0.00067	0.08	291.7	4.9	332	29	264	80	3.18
RRPS1_21	0.355900	0.00750	0.04861	0.00084	0.16	20.57190	0.35549	0.05358	0.00061	0.21	306.1	5	353	26	265	111.1	2.44
RRPS1_22	0.350200	0.00910	0.04708	0.00082	0.27	21.24044	0.36995	0.05390	0.00097	-0.15	296.5	5	363	37	203	109.5	1.91
RRPS1_23	0.366200	0.00940	0.04908	0.00085	-0.14	20.37490	0.35287	0.05430	0.00083	0.35	308.9	5.2	382	34	100.9	69.1	1.61
RRPS1_24	0.353000	0.00790	0.04881	0.00084	0.02	20.48760	0.35258	0.05266	0.00072	0.21	307.2	5.2	313	31	144.2	64.5	1.89
RRPS1_25	0.343900	0.00780	0.04796	0.00082	-0.05	20.85071	0.35650	0.05244	0.00068	0.16	302.0	5	304	29	210	71.7	2.45
RRPS1_26	0.359500	0.00870	0.04730	0.00082	0.63	21.14165	0.36651	0.05532	0.00081	-0.54	297.9	5.1	428	34	263	72.1	3.05
RRPS1_27	0.350400	0.00760	0.04750	0.00082	0.31	21.05130	0.36339	0.05376	0.00064	-0.03	299.2	5	360	27	208	47.1	4.00
RRPS1_28	0.340300	0.00750	0.04722	0.00086	0.69	21.17747	0.38570	0.05272	0.00058	0.05	297.4	5.3	318.2	23	206.2	102.3	2.24
RRPS1_29	0.353200	0.00770	0.04882	0.00086	0.33	20.48341	0.36083	0.05294	0.00062	0.18	307.3	5.3	326	27	186	74.7	2.81
RRPS1_30	0.354600	0.00800	0.04934	0.00085	0.31	20.26753	0.34916	0.05299	0.00066	0.01	310.5	5.2	328	28	230	138.7	1.83
RRPS1_31	0.371600	0.00840	0.05040	0.00087	0.00	19.84127	0.34250	0.05421	0.00070	0.31	317.0	5.3	379	29	342	139.7	2.40
RRPS1_32	0.351100	0.00790	0.04871	0.00086	0.43	20.52967	0.36246	0.05277	0.00067	-0.09	306.6	5.3	318	29	165	52.1	3.04
RRPS1_33	0.349000	0.00740	0.04866	0.00084	0.29	20.55161	0.35479	0.05259	0.00059	-0.18	306.3	5.1	311	25	252	119.8	2.14
RRPS1_34	0.348600	0.00760	0.04831	0.00084	0.88	20.69965	0.35992	0.05281	0.00065	-0.91	304.2	5.2	320	28	483	154.8	3.22
RRPS1_35	0.360000	0.00780	0.04950	0.00089	0.45	20.20202	0.36323	0.05299	0.00064	0.26	311.4	5.5	330	28	181.3	97.14	1.97
RRPS1_36	0.363700	0.00800	0.04934	0.00085	0.30	20.26630	0.34911	0.05352	0.00068	-0.09	310.5	5.2	350	28	199	86.1	2.28
RRPS1_37	0.393100	0.00930	0.05197	0.00090	-0.03	19.24187	0.33322	0.05417	0.00085	0.00	326.6	5.5	376	36	55.2	31.4	1.70
RRPS1_38	0.360500	0.00790	0.04933	0.00085	0.30	20.27205	0.34931	0.05328	0.00064	-0.20	310.4	5.2	343	26	159.7	54.04	2.68
RRPS1_39	0.355000	0.00770	0.04867	0.00085	0.30	20.54654	0.35884	0.05341	0.00063	0.13	306.3	5.2	345	27	157.8	56.51	2.60

RRPS1_40	0.359900	0.00790	0.04937	0.00086	0.29	20.25522	0.35284	0.05299	0.00062	0.10	310.7	5.3	328	27	246.2	89.7	2.73
RRPS1_41	0.342400	0.00740	0.04774	0.00082	-0.06	20.94680	0.35979	0.05194	0.00063	0.39	300.7	5.1	284	29	135.4	62.32	2.07

Anexo 2. Edades U-Pb: "Timing of the tectonic emplacement of ultramafic rocks and metasediments in the southern section of the coastal accretionary complex of Central Chile"

Table 1. Detrital zircon LA-MC-ICPMS U-Pb data of CA15-11, CA15-13 and CA15-26 metapelites (host rock).

CA15-11 Spot	207Pb/ 235U	2σ	206Pb/ 238U	2σ	ρ	238U/ 206Pb	2σ	207Pb/ 206Pb	2σ	ρ	206Pb/ 238Pb Age (Ma)	2σ	207Pb/ 206Pb Age (Ma)	2σ	U (PPM)	Th (PPM)	U/Th Ratio
Ca1511_0	0.47500	0.01900	0.05470	0.00180	0.94	18.28154	0.60159	0.06290	0.00160	-0.97	343.2	11.0	701.0	55.0	217	96	2.18
Ca1511_1	0.39200	0.01400	0.04608	0.00120	-0.59	21.70139	0.56514	0.06140	0.00220	0.77	290.4	7.6	650.0	74.0	811	269	2.83
Ca1511_2	0.65480	0.01500	0.08186	0.00200	0.30	12.21598	0.29846	0.05766	0.00073	-0.03	507.2	12.0	515.0	28.0	136	68	1.84
Ca1511_3	0.49000	0.01000	0.05592	0.00150	0.83	17.88269	0.47969	0.06351	0.00071	0.42	350.8	8.9	724.0	24.0	723	280	2.45
Ca1511_4	0.68100	0.02600	0.05970	0.00260	0.57	16.75042	0.72950	0.08190	0.00210	0.46	374.0	16.0	1237.0	49.0	284	288	1.12
Ca1511_5	1.44000	0.11000	0.12430	0.00910	1.00	8.04505	0.58898	0.08405	0.00110	-0.77	755.0	52.0	1293.0	26.0	224	51	5.38
Ca1511_6	1.75900	0.03600	0.17150	0.00430	0.86	5.83090	0.14620	0.07426	0.00078	-0.03	1020.5	23.0	1047.6	21.0	268	77	3.89
Ca1511_7	0.71460	0.01500	0.08640	0.00230	0.88	11.57407	0.30811	0.05992	0.00064	0.56	534.2	14.0	599.5	23.0	474	105	4.11
Ca1511_8	0.73130	0.01400	0.09069	0.00220	0.67	11.02657	0.26749	0.05820	0.00059	-0.44	559.6	13.0	536.5	22.0	626	274	2.56
Ca1511_9	2.20500	0.04300	0.20421	0.00490	0.28	4.89692	0.11750	0.07859	0.00110	-0.01	1197.9	26.0	1161.0	28.0	91	30	3.57
Ca1511_10	1.41800	0.06800	0.13910	0.00680	0.99	7.18907	0.35144	0.07372	0.00077	0.40	839.0	39.0	1032.7	21.0	242	72	3.95
Ca1511_11	1.29400	0.05100	0.11530	0.00450	0.72	8.67303	0.33850	0.08100	0.00180	0.20	703.0	26.0	1220.0	46.0	310	59	6.07
Ca1511_12	0.43680	0.01200	0.05818	0.00160	0.89	17.18804	0.47269	0.05447	0.00084	-0.59	364.5	9.9	389.0	35.0	221	182	1.39
Ca1511_13	0.64980	0.01300	0.08170	0.00190	0.56	12.23990	0.28465	0.05759	0.00066	-0.26	506.2	12.0	513.0	25.0	282	151	1.78
Ca1511_14	0.60490	0.01200	0.07644	0.00190	0.57	13.08216	0.32517	0.05719	0.00063	0.31	474.8	11.0	498.0	24.0	103	158	0.64
Ca1511_15	0.46400	0.02400	0.04976	0.00150	0.34	20.09646	0.60580	0.06790	0.00340	-0.11	313.1	9.0	854.0	97.0	516	141	3.39
Ca1511_16	4.78600	0.10000	0.31650	0.00800	0.69	3.15956	0.07986	0.10966	0.00120	-0.43	1775.0	41.0	1792.8	20.0	40	38	1.03
Ca1511_17	0.56000	0.01600	0.07060	0.00220	0.88	14.16431	0.44138	0.05744	0.00063	-0.73	440.0	13.0	507.0	24.0	449	746	0.85
Ca1511_18	1.97000	0.14000	0.16800	0.01600	0.88	5.95238	0.56689	0.08250	0.00260	-0.94	1029.0	72.0	1251.0	66.0	498	240	2.95
Ca1511_19	0.80800	0.07000	0.08350	0.00630	0.97	11.97605	0.90358	0.06970	0.00140	-0.94	517.0	38.0	924.0	38.0	370	125	3.78

Ca1511_20	0.57200	0.01500	0.06200	0.00200	0.68	16.12903	0.52029	0.06756	0.00120	0.36	387.8	12.0	852.0	37.0	492	124	4.86
Ca1511_21	0.50770	0.01100	0.06038	0.00170	0.84	16.56178	0.46630	0.06073	0.00080	-0.52	377.9	10.0	628.0	28.0	574	39	46.60
Ca1511_22	0.40900	0.02300	0.04260	0.00170	0.96	23.47418	0.93676	0.06990	0.00380	-0.98	268.8	10.0	910.0	110.0	269	85	10.26
Ca1511_23	0.48710	0.01100	0.06030	0.00210	0.80	16.58375	0.57754	0.05790	0.00160	-0.70	377.1	13.0	521.0	65.0	820	288	5.83
Ca1511_24	0.51530	0.01100	0.06655	0.00160	0.80	15.02630	0.36126	0.05599	0.00066	-0.41	415.3	10.0	451.0	26.0	383	50	12.22
Ca1511_25	0.38060	0.00790	0.05453	0.00130	0.43	18.33853	0.43719	0.05062	0.00064	0.05	342.3	8.1	222.0	29.0	110	27	4.96
Ca1511_26	0.47490	0.01300	0.05876	0.00160	0.89	17.01838	0.46340	0.05918	0.00076	-0.58	368.1	9.5	572.0	28.0	502	149	2.72
Ca1511_27	0.62040	0.01300	0.07710	0.00230	0.47	12.97017	0.38692	0.05900	0.00081	-0.08	478.8	14.0	572.0	33.0	369	158	2.07
Ca1511_28	0.92600	0.02300	0.10710	0.00290	0.70	9.33707	0.25282	0.06199	0.00075	-0.42	656.1	17.0	673.0	26.0	740	186	5.00
Ca1511_29	0.51600	0.02400	0.05860	0.00190	0.93	17.06485	0.55330	0.06350	0.00150	-0.67	367.3	11.0	720.0	49.0	448	57	7.32
Ca1511_30	2.14300	0.04700	0.20680	0.00540	0.95	4.83559	0.12627	0.07566	0.00079	0.43	1212.0	29.0	1085.0	21.0	162	123	1.24
Ca1511_31	1.98000	0.06000	0.19220	0.00670	0.93	5.20291	0.18137	0.07480	0.00077	-0.58	1133.0	36.0	1062.2	21.0	121	48	2.49
Ca1511_32	2.01190	0.03800	0.19180	0.00470	0.00	5.21376	0.12776	0.07594	0.00085	0.67	1130.9	25.0	1092.0	22.0	336	162	2.41
Ca1511_33	0.76280	0.01500	0.08579	0.00220	0.70	11.65637	0.29892	0.06422	0.00078	0.29	530.6	13.0	748.0	26.0	710	94	8.89
Ca1511_34	0.45750	0.00930	0.06121	0.00150	0.14	16.33720	0.40036	0.05433	0.00067	-0.08	383.0	8.9	383.0	28.0	217	103	2.37
Ca1511_35	0.62300	0.01700	0.07650	0.00240	0.85	13.07190	0.41010	0.05922	0.00100	-0.21	475.4	14.0	573.0	38.0	130	123	1.17
Ca1511_36	1.00360	0.02100	0.10981	0.00280	0.81	9.10664	0.23221	0.06594	0.00069	0.07	671.7	16.0	803.3	22.0	575	73	8.52
Ca1511_37	1.49100	0.03700	0.14230	0.00420	0.74	7.02741	0.20741	0.07512	0.00078	0.38	857.0	24.0	1070.6	21.0	273	198	1.47
Ca1511_38	0.49670	0.00990	0.06590	0.00160	0.79	15.17451	0.36843	0.05461	0.00057	-0.08	411.4	9.8	395.2	24.0	457	179	2.45
Ca1511_39	1.51600	0.03400	0.15440	0.00410	0.97	6.47668	0.17198	0.07079	0.00072	-0.61	925.0	23.0	950.3	21.0	455	92	4.75
Ca1511_40	0.57500	0.02400	0.06370	0.00280	0.97	15.69859	0.69005	0.06550	0.00082	0.18	398.0	17.0	789.0	26.0	382	183	2.00
Ca1511_41	1.91300	0.04300	0.17770	0.00460	0.78	5.62746	0.14567	0.07739	0.00092	-0.14	1054.2	25.0	1130.0	24.0	48	67	0.70
Ca1511_42	0.47800	0.01300	0.05380	0.00150	0.33	18.58736	0.51824	0.06480	0.00140	-0.04	337.8	9.1	762.0	44.0	249	146	1.54
Ca1511_43	1.49400	0.04400	0.14260	0.00540	0.75	7.01262	0.26556	0.07666	0.00085	-0.81	859.0	31.0	1111.0	22.0	511	220	2.00
Ca1511_44	0.84040	0.01800	0.09948	0.00240	0.23	10.05227	0.24252	0.06120	0.00068	-0.02	611.4	14.0	645.0	24.0	303	51	5.14
Ca1511_45	0.78600	0.01600	0.09480	0.00250	0.73	10.54852	0.27818	0.06068	0.00062	-0.10	583.6	15.0	627.1	22.0	566	500	1.04
Ca1511_46	0.58280	0.01200	0.07403	0.00180	0.57	13.50804	0.32844	0.05675	0.00064	0.08	460.4	11.0	481.0	25.0	349	180	2.92
Ca1511_47	0.74000	0.03400	0.08770	0.00450	0.99	11.40251	0.58508	0.06096	0.00068	0.52	542.0	27.0	637.0	24.0	680	270	3.85
Ca1511_48	0.76880	0.01700	0.09402	0.00240	0.85	10.63603	0.27150	0.05909	0.00061	0.09	579.3	14.0	569.6	22.0	539	100	7.58

Ca1511_49	0.54810	0.01300	0.06360	0.00170	0.80	15.72327	0.42028	0.06193	0.00085	0.20	397.4	10.0	670.0	29.0	410	279	1.72
Ca1511_50	0.89900	0.03200	0.08560	0.00330	0.93	11.68224	0.45037	0.07587	0.00110	0.18	529.0	20.0	1090.0	30.0	324	213	1.40
Ca1511_51	0.62700	0.01600	0.07140	0.00200	0.76	14.00560	0.39231	0.06383	0.00080	0.62	444.5	12.0	735.0	27.0	305	171	1.47
Ca1511_52	1.51700	0.03900	0.13430	0.00630	0.61	7.44602	0.34929	0.08223	0.00110	-0.34	812.0	36.0	1250.0	26.0	513	424	0.94
Ca1511_53	0.59200	0.01300	0.07525	0.00190	0.18	13.28904	0.33554	0.05686	0.00063	-0.09	467.7	11.0	485.0	24.0	402	205	1.63
Ca1511_54	0.40300	0.01300	0.05129	0.00130	0.26	19.49698	0.49417	0.05700	0.00150	0.02	322.4	8.1	488.0	57.0	195	45	3.66
Ca1511_55	0.64300	0.03900	0.06950	0.00370	0.78	14.38849	0.76601	0.06600	0.00170	-0.01	433.0	23.0	800.0	48.0	519	102	4.94
Ca1511_56	0.66500	0.02600	0.07700	0.00330	0.96	12.98701	0.55659	0.06214	0.00066	-0.94	478.0	20.0	677.8	23.0	960	220	4.09
Ca1511_57	0.93100	0.04500	0.09510	0.00570	0.93	10.51525	0.63025	0.07221	0.00100	-0.97	586.0	33.0	991.0	29.0	381	122	3.03
Ca1511_58	0.86800	0.02700	0.09755	0.00240	-0.24	10.25115	0.25221	0.06470	0.00170	0.33	600.0	14.0	761.0	56.0	611	495	1.15
Ca1511_59	0.82990	0.01600	0.09247	0.00220	0.61	10.81432	0.25729	0.06521	0.00070	-0.43	570.1	13.0	780.2	23.0	757	65	11.30

CA15-13																	
Spot	**207Pb/ 235U**	**2σ**	**206Pb/ 238U**	**2σ**	**ρ**	**238U/ 206Pb**	**2σ**	**207Pb/ 206Pb**	**2σ**	**ρ**	**206Pb/ 238Pb Age (Ma)**	**2σ**	**207Pb/ 206Pb Age (Ma)**	**2σ**	**U (PPM)**	**Th (PPM)**	**U/Th Ratio**
CA15_13_1	3.02200	0.08000	0.23600	0.00580	0.33	4.23729	0.10414	0.0934	0.0012	0.23	1366.0	31.0	1494.0	24.0	194	82	2.55
CA15_13_2	0.44660	0.01100	0.05917	0.00150	0.75	16.90046	0.42844	0.05462	0.00032	0.05	370.5	9.0	396.6	13.0	385	419	1.01
CA15_13_3	0.49980	0.01400	0.06553	0.00170	-0.40	15.26019	0.39588	0.05532	0.0004	0.38	409.2	10.0	425.0	16.0	241	240	1.12
CA15_13_4	0.75190	0.01900	0.09137	0.00220	-0.18	10.94451	0.26352	0.05976	0.00039	0.55	563.6	13.0	595.0	14.0	267.1	734	0.39
CA15_13_5	1.85100	0.04900	0.17910	0.00480	0.97	5.58347	0.14964	0.07504	0.00041	-0.67	1062.0	26.0	1069.6	11.0	483	535	0.96
CA15_13_6	0.73700	0.02800	0.09120	0.00320	0.98	10.96491	0.38473	0.05903	0.00035	-0.73	562.4	18.0	567.9	13.0	399	117	3.54
CA15_13_7	0.52400	0.01800	0.06706	0.00190	0.86	14.91202	0.42250	0.05648	0.0007	-0.61	418.4	12.0	469.0	27.0	486	246	1.94
CA15_13_9	1.86400	0.04900	0.17780	0.00480	0.83	5.62430	0.15184	0.07567	0.00038	0.04	1055.0	26.0	1086.1	10.0	67	32.4	1.91
CA15_13_11	0.63600	0.03100	0.06600	0.00310	0.76	15.15152	0.71166	0.0702	0.0011	-0.28	412.0	19.0	931.0	31.0	306	277	1.05
CA15_13_12	0.39700	0.01200	0.05279	0.00180	0.81	18.94298	0.64591	0.05424	0.00037	0.55	331.6	11.0	380.0	15.0	522	221.5	2.38
CA15_13_13	0.51050	0.01400	0.06687	0.00180	0.94	14.95439	0.40254	0.0552	0.00029	-0.08	417.2	11.0	419.9	12.0	162.8	62.6	2.54
CA15_13_14	0.68900	0.01900	0.08588	0.00240	0.71	11.64415	0.32541	0.05788	0.00031	0.12	531.1	14.0	525.1	12.0	196	43.3	4.81

CA15_13_15	0.43110	0.01200	0.05820	0.00160	0.40	17.18213	0.47236	0.05361	0.00038	-0.02	364.6	9.6	354.0	16.0	87.3	50.4	1.80
CA15_13_16	0.42000	0.01400	0.04420	0.00140	0.53	22.62443	0.71661	0.069	0.0012	0.31	278.9	8.9	892.0	37.0	310	160.6	1.93
CA15_13_17	0.63000	0.04600	0.06327	0.00210	0.60	15.80528	0.52459	0.0718	0.0042	-0.42	395.5	13.0	940.0	110.0	192	161	1.28
CA15_13_18	0.51500	0.07200	0.07660	0.00250	0.01	13.05483	0.42607	0.0482	0.0058	0.03	475.5	15.0	130.0	230.0	402	98	5.20
CA15_13_19	2.05400	0.06300	0.18740	0.00580	0.95	5.33618	0.16515	0.07938	0.00037	0.28	1107.0	31.0	1181.6	9.1	198.3	28.3	7.02
CA15_13_21	2.43500	0.06300	0.21960	0.00570	0.90	4.55373	0.11820	0.08005	0.00036	-0.03	1279.0	30.0	1198.3	8.9	82.4	86.7	1.03
CA15_13_22	0.39710	0.01100	0.05333	0.00140	0.90	18.75117	0.49225	0.05348	0.00039	0.25	334.9	8.6	351.0	17.0	103	155	0.69
CA15_13_23	0.72700	0.02900	0.08970	0.00350	0.32	11.14827	0.43499	0.05913	0.00038	0.48	554.0	20.0	572.0	14.0	269	230	1.36
CA15_13_24	0.49690	0.01600	0.06520	0.00220	-0.83	15.33742	0.51752	0.05543	0.00032	0.98	407.1	14.0	429.3	13.0	97.8	72.3	1.56
CA15_13_25	1.35900	0.03500	0.13464	0.00350	0.34	7.42721	0.19307	0.07341	0.00037	0.18	814.3	20.0	1025.2	10.0	220	116.3	2.04
CA15_13_26	0.44120	0.01200	0.04939	0.00140	0.27	20.24701	0.57392	0.0647	0.0011	0.02	310.8	8.8	759.0	35.0	423	83.2	5.07
CA15_13_27	0.39000	0.02600	0.04780	0.00250	0.42	20.92050	1.09417	0.0583	0.0017	-0.42	301.0	15.0	526.0	65.0	207	116	1.75
CA15_13_28	2.61900	0.07200	0.22200	0.00620	0.74	4.50451	0.12580	0.08556	0.00041	-0.08	1292.5	33.0	1328.2	9.3	161	110	1.47
CA15_13_29	0.42000	0.01200	0.05579	0.00180	0.55	17.92436	0.57831	0.05467	0.00048	0.34	350.3	11.0	398.0	19.0	277	229	1.14
CA15_13_30	0.56000	0.07100	0.05930	0.00290	0.56	16.86341	0.82469	0.069	0.0045	-0.58	371.0	18.0	840.0	140.0	640	72.4	12.00
CA15_13_33	0.56500	0.02200	0.07160	0.00200	0.09	13.96648	0.39013	0.0543	0.0026	0.23	445.8	12.0	370.0	110.0	510	162	3.12
CA15_13_34	0.91500	0.02800	0.09960	0.00280	0.98	10.04016	0.28225	0.0663	0.00048	-0.84	612.0	17.0	816.0	15.0	368	79.8	5.21
CA15_13_35	0.36160	0.01300	0.04561	0.00140	0.67	21.92502	0.67299	0.05796	0.00078	-0.03	287.5	8.3	529.0	30.0	890	108	8.62
CA15_13_36	0.62500	0.02800	0.07960	0.00320	0.36	12.56281	0.50504	0.0553	0.0015	-0.39	493.4	19.0	437.0	49.0	680	216	3.47
CA15_13_37	0.41890	0.01300	0.05609	0.00180	0.87	17.82849	0.57214	0.05394	0.00029	0.02	351.8	11.0	368.1	12.0	284	121	2.23
CA15_13_38	0.56510	0.01400	0.07203	0.00190	0.89	13.88310	0.36621	0.05649	0.00031	-0.19	448.4	11.0	473.5	11.0	457	395	1.21
CA15_13_39	0.92040	0.02600	0.10839	0.00310	-0.90	9.22594	0.26387	0.06159	0.00035	0.99	663.4	18.0	659.5	12.0	217	177	1.25
CA15_13_31	4.28000	0.42000	0.30380	0.01000	-0.21	3.29164	0.10835	0.1009	0.0095	0.28	1709.0	50.0	1520.0	290.0	206	71	3.68

CA15-26 Spot	207Pb/ 235U	2σ	206Pb/ 238U	2σ	ρ	238U/ 206Pb	2σ	207Pb/ 206Pb	2σ	ρ	206Pb/ 238Pb Age (Ma)	2σ	207Pb/ 206Pb Age (Ma)	2σ	U (PPM)	Th (PPM)	U/Th Ratio
CA1526_0	0.49700	0.02500	0.05629	0.00140	0.54	17.76514	0.44184	0.06300	0.00250	-0.33	353	8.8	697	77	391	50	8.90
CA1526_1	9.42000	0.35000	0.39910	0.00830	0.87	2.50564	0.05211	0.17318	0.00350	-0.57	2165	38	2587.8	34	127	54	2.46
CA1526_2	0.58800	0.02100	0.06985	0.00150	0.41	14.31639	0.30744	0.06180	0.00160	-0.04	435.2	9.3	664	55	519	325	1.65
CA1526_3	0.47050	0.01500	0.06089	0.00120	0.55	16.42306	0.32366	0.05530	0.00110	0.15	381	7.1	423.2	45	497	19	27.20
CA1526_4	0.46140	0.01700	0.05814	0.00120	0.72	17.19986	0.35500	0.05860	0.00160	-0.57	364.3	7.4	550	58	206	1	160.00
CA1526_5	1.10500	0.03700	0.11270	0.00240	0.83	8.87311	0.18896	0.07029	0.00150	-0.85	688.2	14	935	42	277	37	7.43
CA1526_6	1.55900	0.05700	0.14920	0.00320	0.86	6.70241	0.14375	0.07566	0.00160	-0.30	896.5	18	1085	42	80	28	2.86
CA1526_7	1.86500	0.06100	0.17730	0.00350	0.84	5.64016	0.11134	0.07590	0.00150	0.14	1052.1	19	1091.5	40	104	49	2.13
CA1526_8	0.43780	0.01400	0.05857	0.00110	0.83	17.07359	0.32066	0.05390	0.00110	-0.31	366.9	6.9	365.7	46	234	74	3.30
CA1526_9	0.64100	0.02100	0.07880	0.00180	0.40	12.69036	0.28988	0.05920	0.00160	0.36	488.9	11	561	49	197	59	3.13
CA1526_10	0.52000	0.02100	0.06401	0.00140	0.73	15.62256	0.34169	0.05874	0.00150	-0.33	400	8.4	553	55	214	6	49.00
CA1526_11	0.75600	0.03100	0.08819	0.00170	0.58	11.33915	0.21858	0.06120	0.00170	-0.40	544.8	10	641	54	183	88	2.01
CA1526_12	0.44050	0.01600	0.05630	0.00150	0.88	17.76199	0.47323	0.05591	0.00120	0.48	353.1	9.3	453	45	306	20	58.00
CA1526_13	0.56100	0.02900	0.05790	0.00160	0.53	17.27116	0.47727	0.06990	0.00310	-0.40	363	9.8	914	85	352	51	7.80
CA1526_14	0.63000	0.02300	0.07553	0.00160	0.60	13.23977	0.28047	0.05971	0.00140	-0.15	469.4	9.4	591	52	412	16	25.40
CA1526_15	0.46190	0.01700	0.05972	0.00140	0.55	16.74481	0.39254	0.05602	0.00130	-0.17	373.9	8.4	451	49	677	24	37.30
CA1526_16	0.59900	0.02500	0.07140	0.00190	0.39	14.00560	0.37270	0.06160	0.00190	0.23	444.6	11	654	64	95	2	59.00
CA1526_17	0.49610	0.01800	0.06330	0.00160	-0.02	15.79779	0.39931	0.05720	0.00170	0.36	395.6	9.4	480	53	104	0	440.00
CA1526_18	1.23200	0.04200	0.11780	0.00250	0.82	8.48896	0.18016	0.07467	0.00160	-0.39	717.7	14	1058	42	301	28	10.81
CA1526_19	1.18600	0.04200	0.12000	0.00260	0.88	8.33333	0.18056	0.07044	0.00140	-0.34	730.4	15	940	42	153	17	9.38
CA1526_20	0.86040	0.02800	0.10314	0.00200	0.05	9.69556	0.18801	0.06105	0.00130	0.05	632.8	12	640	44	123	65	1.96
CA1526_21	0.62440	0.02100	0.07740	0.00150	0.54	12.91990	0.25039	0.05715	0.00120	0.04	480.6	9.3	496	47	177	17	10.53
CA1526_22	0.59700	0.01900	0.07444	0.00140	0.30	13.43364	0.25265	0.05643	0.00120	0.40	462.9	8.6	468	45	362	24	15.21

CA1526_23	1.08500	0.05600	0.10940	0.00480	0.91	9.14077	0.40106	0.06966	0.00160	-0.12	669	28	921	43	159	23	7.17
CA1526_24	1.23400	0.06300	0.11290	0.00420	0.85	8.85740	0.32950	0.07740	0.00190	-0.03	693	25	1120	32	391	29	14.30
CA1526_25	1.13600	0.04700	0.11730	0.00370	0.96	8.52515	0.26891	0.06944	0.00140	0.16	715	22	910.8	42	1020	185	6.73
CA1526_26	0.57880	0.01800	0.06767	0.00140	0.24	14.77760	0.30573	0.05921	0.00130	0.37	422.1	8.2	573	48	290	85	3.21
CA1526_27	0.49810	0.01700	0.06043	0.00120	0.61	16.54807	0.32861	0.05735	0.00140	-0.15	378.2	7.4	502	51	1425	82	17.10
CA1526_28	0.95020	0.03000	0.10140	0.00200	0.26	9.86193	0.19452	0.06471	0.00130	-0.18	622.6	11	764	44	225	47	4.76
CA1526_29	0.59100	0.02500	0.06600	0.00130	0.22	15.15152	0.29844	0.06140	0.00230	-0.05	412	8.2	648	76	762	6	137.00
CA1526_30	0.67900	0.02600	0.07539	0.00160	0.14	13.26436	0.28151	0.06210	0.00180	0.07	468.5	9.3	673	60	838	292	3.05
CA1526_31	0.50060	0.01700	0.06232	0.00120	0.15	16.04621	0.30898	0.05472	0.00130	0.01	389.7	7.2	398	53	336	89	4.11
CA1526_32	0.52250	0.01800	0.05830	0.00150	-0.01	17.15266	0.44132	0.06100	0.00190	0.34	365.2	9.2	633	65	641	45	33.00
CA1526_33	0.97100	0.05200	0.09440	0.00420	0.98	10.59322	0.47131	0.07143	0.00160	-0.15	581	25	968	45	342	48	7.99
CA1526_34	1.01760	0.03200	0.11242	0.00230	0.66	8.89521	0.18199	0.06425	0.00130	-0.10	686.8	13	748.9	42	1022	241	4.72
CA1526_35	1.17600	0.04300	0.11660	0.00300	0.94	8.57633	0.22066	0.06974	0.00150	-0.53	711	17	919	44	867	135	7.10
CA1526_36	0.49000	0.01900	0.05930	0.00150	0.56	16.86341	0.42656	0.05667	0.00130	0.18	371.3	9.4	477	52	715	4	350.00
CA1526_37	0.58900	0.03400	0.06590	0.00240	0.16	15.17451	0.55264	0.06110	0.00210	0.19	411	14	635	66	227	19	12.60
CA1526_38	0.91200	0.03400	0.07976	0.00160	0.68	12.53761	0.25151	0.08167	0.00190	-0.34	494.7	9.3	1236	45	271	44	5.00
CA1526_39	2.38400	0.07500	0.20280	0.00400	0.47	4.93097	0.09726	0.08430	0.00170	-0.07	1190.5	21	1298.5	39	99	70	1.16
CA1526_40	0.60100	0.02800	0.05573	0.00120	0.59	17.94366	0.38637	0.07490	0.00220	-0.35	349.6	7	1076	68	252	56	3.60
CA1526_41	0.58970	0.02000	0.07550	0.00170	0.34	13.24503	0.29823	0.05604	0.00120	0.59	469.2	10	452	47	153	212	0.64
CA1526_42	1.07500	0.04500	0.10900	0.00310	0.92	9.17431	0.26092	0.07005	0.00150	-0.21	667	18	929	43	456	57	11.29
CA1526_43	0.85790	0.02800	0.08073	0.00170	0.54	12.38697	0.26084	0.07478	0.00180	-0.20	500.4	10	1068	52	139	12	15.89
CA1526_44	2.18600	0.07100	0.19560	0.00380	0.23	5.11247	0.09932	0.07935	0.00170	-0.04	1151.6	20	1180	41	62	27	2.78
CA1526_45	0.46840	0.01500	0.05971	0.00120	0.78	16.74761	0.33658	0.05590	0.00130	-0.73	373.8	7.1	447	50	320	1	400.00
CA1526_46	0.54090	0.01800	0.07030	0.00130	-0.22	14.22475	0.26305	0.05513	0.00120	0.38	438	8.1	416	49	185	110	1.57
CA1526_47	0.48800	0.01800	0.05460	0.00180	0.63	18.31502	0.60379	0.06450	0.00200	0.73	342.8	11	753	66	771	109	6.73
CA1526_48	0.48400	0.01600	0.06357	0.00130	0.49	15.73069	0.32169	0.05490	0.00110	0.21	397.3	8	407	46	628	462	1.54
CA1526_49	0.75120	0.02400	0.09142	0.00180	0.36	10.93853	0.21537	0.05895	0.00120	-0.08	563.9	11	564.1	44	334	571	0.67
CA1526_50	0.43450	0.01400	0.05788	0.00110	0.51	17.27713	0.32835	0.05483	0.00120	-0.43	362.7	6.8	404	47	558	5	139.00
CA1526_51	0.61500	0.02600	0.07343	0.00160	0.72	13.61841	0.29674	0.05940	0.00180	-0.49	457.9	10	578	62	533	69	8.65

CA1526_52	0.56900	0.02000	0.06760	0.00180	0.84	14.79290	0.39389	0.06045	0.00140	0.50	421.6	11	618	49	481	186	2.99
CA1526_53	0.73300	0.03600	0.08280	0.00270	0.41	12.07729	0.39382	0.06200	0.00160	-0.19	513	16	671	50	409	64	9.30
CA1526_54	0.48350	0.01500	0.06147	0.00130	0.83	16.26810	0.34405	0.05522	0.00110	-0.19	384.5	7.8	419.9	45	639	99	5.28
CA1526_55	2.72100	0.08600	0.21608	0.00410	0.19	4.62792	0.08781	0.08738	0.00180	0.29	1261.1	22	1369.8	43	78	38	1.68
CA1526_56	0.56340	0.01900	0.06829	0.00140	-0.49	14.64343	0.30020	0.05690	0.00140	0.84	425.8	8.7	472	38	258	59	4.37
CA1526_57	0.53600	0.02000	0.06377	0.00150	0.88	15.68135	0.36886	0.05868	0.00130	-0.63	398.5	9	553	48	259	67	3.04
CA1526_58	0.47700	0.01800	0.05624	0.00150	0.29	17.78094	0.47424	0.06010	0.00230	0.32	352.7	8.9	612	84	376	26	13.00
CA1526_59	0.54300	0.02700	0.05890	0.00320	0.94	16.97793	0.92240	0.06701	0.00160	-0.05	369	20	836	49	830	502	1.37
CA1526_60	0.57500	0.02200	0.06806	0.00140	0.77	14.69292	0.30223	0.05880	0.00180	-0.62	424.4	8.1	555	63	207	3	62.00
CA1526_61	0.90800	0.04400	0.09720	0.00380	0.96	10.28807	0.40221	0.06597	0.00150	-0.23	598	22	803	48	205	49	4.00
CA1526_62	1.85400	0.06900	0.17410	0.00450	0.96	5.74383	0.14846	0.07533	0.00150	0.09	1035	25	1076.4	41	170	24	6.33
CA1526_63	0.49100	0.01800	0.06250	0.00190	0.80	16.00000	0.48640	0.05552	0.00120	-0.22	391	11	432	47	472	8	53.30

Table 2. Zircon mount SHRIMP U-Pb data of CA14-4 biotitite-albitite (blackwall).

Spot	(1) 207Pb* /235U	1σ	(1) 206Pb* /238U	1σ	ρ	(1) 238U /206Pb*	1σ	(1) 207Pb* /206Pb*	1σ	ρ	(2) 206Pb /238U Age (Ma)	1σ	(1) 207Pb /206Pb Age (Ma)	1σ	U (ppm)	Th (ppm)	232Th /238U
CA14-4z11	0.47000	0.02068	0.05900	0.00100	0.36	16.94915	0.28814	0.05800	0.00238	0.02	367	6	518	90	587	528	0.93
CA14-4z12	0.46000	0.01426	0.06400	0.00083	0.43	15.62500	0.20313	0.05200	0.00146	-0.01	401	5	299	64	548	179	0.34
CA14-4z10r	0.56000	0.02352	0.06900	0.00083	0.31	14.49275	0.17391	0.05900	0.00236	-0.02	426	5	564	86	523	89	0.18
CA14-4z9	0.52000	0.01092	0.06900	0.00083	0.65	14.49275	0.17391	0.05500	0.00088	-0.11	430	5	415	37	529	288	0.56
CA14-4z1r	0.62000	0.01178	0.07900	0.00095	0.61	12.65823	0.15190	0.05700	0.00086	0.02	489	6	494	32	525	173	0.34
CA14-4z6	0.66000	0.02904	0.08200	0.00156	0.46	12.19512	0.23171	0.05800	0.00226	-0.04	510	10	544	86	269	213	0.82
CA14-4z1c	0.76000	0.02812	0.08900	0.00169	0.50	11.23596	0.21348	0.06100	0.00195	0.01	549	10	654	69	862	485	0.58

CA14-4z4r	0.85000	0.03145	0.09900	0.00297	0.82	10.10101	0.30303	0.06300	0.00132	-0.02	604	18	705	45	654	439	0.69
CA14-4z4c	1.81000	0.02534	0.18000	0.00216	0.77	5.55556	0.06667	0.07300	0.00066	0.13	1066	12	1016	18	721	410	0.59
CA14-4z3c	2.03000	0.17255	0.18500	0.00574	0.37	5.40541	0.16757	0.07900	0.00624	0.00	1093	32	1183	156	39	93	2.46
CA14-4z5	2.37000	0.06399	0.21000	0.00441	0.75	4.76190	0.10000	0.08200	0.00148	0.05	1228	25	1243	35	80	105	1.36
CA14-4z7	4.37000	0.13984	0.30200	0.00695	0.73	3.31126	0.07616	0.10500	0.00231	-0.01	1697	38	1716	41	543	319	0.61
CA14-4z8r	4.46000	0.08920	0.30700	0.00553	0.89	3.25733	0.05863	0.10500	0.00095	0.02	1725	31	1721	16	310	204	0.68
CA14-4z8c	4.55000	0.06825	0.31100	0.00404	0.88	3.21543	0.04180	0.10600	0.00074	-0.04	1749	23	1730	14	321	288	0.93
CA14-4z2	14.99000	0.23984	0.53100	0.00850	0.98	1.88324	0.03013	0.20500	0.00062	0.09	2693	48	2866	5	1902	60	0.03

Table 3. In-situ LA-ICPMS-MC thick section U-Pb data of LAV-14-5 ilmenite-bearing chloritite (blackwall).

Spot	207Pb/ 235U	2σ	206Pb/ 238U	2σ	ρ	238U/ 206Pb	2σ	207Pb/ 206Pb	2σ	ρ	206Pb/ 238Pb Age (Ma)	2σ	207Pb/ 206Pb Age (Ma)	2σ	U (PPM)	Th (PPM)	U/Th Ratio
LAV-ILM_3	0.21000	0.29000	0.03850	0.00160	0.32	25.97403	1.07944	0.07000	0.01800	-0.37	243.7	9.6	570.0	620.0	460	275	1.92
LAV-ILM_4	1.31000	0.14000	0.04610	0.00360	-0.08	21.69197	1.69395	0.20300	0.02900	0.61	291.0	22.0	2660.0	310.0	209	271	0.88
LAV-ILM_5	0.93900	0.09500	0.05540	0.00290	0.55	18.05054	0.94488	0.12230	0.01000	-0.30	347.0	18.0	1910.0	140.0	432	640	0.93
LAV-ILM_6	1.05000	0.29000	0.05360	0.00210	0.80	18.65672	0.73095	0.15100	0.03000	-0.81	337.0	13.0	2290.0	340.0	143	143	1.54
LAV-ILM_7	0.82700	0.09400	0.05750	0.00180	0.86	17.39130	0.54442	0.09440	0.00460	-0.60	360.6	11.0	1510.0	80.0	688	872	0.90
LAV-ILM_8	1.24000	0.40000	0.06260	0.00210	0.74	15.97444	0.53588	0.12500	0.03500	-0.78	391.0	13.0	1550.0	920.0	108	223	0.59
LAV-ILM_9	0.99000	0.13000	0.04580	0.00270	0.28	21.83406	1.28716	0.14800	0.01600	-0.11	288.0	17.0	2150.0	210.0	406	880	0.59
LAV-ILM_10	1.45000	0.33000	0.06180	0.00420	0.28	16.18123	1.09970	0.13800	0.03300	-0.09	391.0	25.0	1820.0	550.0	210	1720	0.16
LAV-ILM_11	0.97000	0.11000	0.04420	0.00260	0.49	22.62443	1.33085	0.15400	0.01300	-0.09	279.0	16.0	2340.0	150.0	361	209	1.67
LAV-ILM_12	1.22000	0.14000	0.05380	0.00210	0.54	18.58736	0.72553	0.16600	0.01800	-0.07	337.0	13.0	2400.0	170.0	386	370	1.33
LAV-ILM_13	0.90000	0.25000	0.05910	0.00240	0.21	16.92047	0.68713	0.09400	0.01800	-0.08	370.0	14.0	1270.0	410.0	470	920	0.58
LAV-ILM_14	1.25000	0.32000	0.06030	0.00210	0.39	16.58375	0.57754	0.11100	0.02000	-0.11	377.0	13.0	1620.0	360.0	370	530	0.70
LAV-ILM_15	1.19000	0.40000	0.05110	0.00320	0.51	19.56947	1.22549	0.15000	0.03200	0.14	321.0	20.0	1810.0	590.0	370	530	0.75

LAV-ILM_16	1.24000	0.11000	0.06340	0.00170	-0.54	15.77287	0.42293	0.14000	0.01100	0.62	396.5	10.0	2180.0	140.0	514	413	1.24
LAV-ILM_17	1.40000	0.13000	0.05900	0.00140	-0.84	16.94915	0.40218	0.16500	0.01600	0.60	369.5	8.6	2430.0	170.0	266	224	1.35
LAV-ILM_18	2.20000	0.20000	0.05560	0.00210	0.05	17.98561	0.67931	0.27800	0.03000	0.27	349.0	13.0	3220.0	240.0	660	990	0.77
LAV-ILM_19	1.59000	0.26000	0.03610	0.00260	-0.14	27.70083	1.99507	0.30500	0.05300	0.29	228.0	16.0	3280.0	280.0	300	241	1.27
LAV-ILM_21	1.02100	0.07700	0.05580	0.00160	0.35	17.92115	0.51387	0.13720	0.00800	-0.02	350.2	9.9	2154.0	97.0	689	950	0.65
LAV-ILM_22	0.97000	0.11000	0.05810	0.00160	0.35	17.21170	0.47399	0.11800	0.01200	-0.39	364.3	9.8	1790.0	230.0	442	720	0.64
LAV-ILM_23	0.68900	0.03600	0.06180	0.00180	0.02	16.18123	0.47130	0.08020	0.00430	0.04	386.7	11.0	1160.0	140.0	810	970	0.84

Table 4. Zircon mount LA-MC-ICPMS U-Pb data of LAV-14-5 chloritite (blackwall).

Spot	207Pb/ 235U	2σ	206Pb/ 238U	2σ	ρ	238U/ 206Pb	2σ	207Pb/ 206Pb	2σ	ρ	206Pb/ 238Pb Age (Ma)	2σ	207Pb/ 206Pb Age (Ma)	2σ	U (PPM)	Th (PPM)	U/Th Ratio
LAV14_2	0.59500	0.03700	0.07710	0.00420	-0.31	12.97017	0.70655	0.05594	0.00069	0.44	479	25	449.0	28.0	420	215	1.97
LAV14_3	1.93000	0.12000	0.16030	0.00670	0.97	6.23830	0.26074	0.08670	0.00240	-0.98	958.0	37.0	1350.0	53.0	451	198	2.28
LAV14_4	1.38300	0.09700	0.13730	0.00810	1.00	7.28332	0.42968	0.07321	0.00095	-0.94	829.0	46.0	1019.0	26.0	469	252	1.94
LAV14_5	0.66900	0.02800	0.07980	0.00380	0.97	12.53133	0.59673	0.06091	0.00076	-0.02	502.0	26.0	643.0	30.0	615	321	1.92
LAV14_6	0.48100	0.01800	0.04080	0.00230	-0.88	24.50980	1.38168	0.08500	0.00600	0.98	258.0	14.0	1300.0	140.0	785	306	2.59
LAV14_7	0.58540	0.01300	0.07550	0.00170	0.86	13.24503	0.29823	0.05691	0.00045	0.71	469.3	10.0	488.0	17.0	819	365	2.28
LAV14_8	0.63500	0.02400	0.08120	0.00190	0.21	12.31527	0.28817	0.05657	0.00033	0.28	503.3	12.0	474.9	13.0	1130	526	2.17
LAV14_9	0.54500	0.02600	0.06710	0.00320	0.99	14.90313	0.71073	0.05966	0.00056	-0.38	419.0	19.0	591.0	20.0	806	403	2.13
LAV14_10	0.84230	0.02000	0.10128	0.00180	0.77	9.87362	0.17548	0.06131	0.00040	0.32	621.9	11.0	650.2	14.0	276	210.9	1.32
LAV14_11	1.78400	0.04200	0.17100	0.00320	0.88	5.84795	0.10944	0.07502	0.00051	0.20	1017.6	18.0	1068.9	14.0	712	142.8	4.81
LAV14_12	0.60750	0.01400	0.07654	0.00130	0.48	13.06506	0.22190	0.05747	0.00042	0.28	475.4	7.8	510.0	16.0	1082	999	1.07
LAV14_13	0.81700	0.03200	0.09060	0.00320	0.98	11.03753	0.38985	0.06560	0.00051	-0.13	559.0	19.0	794.0	16.0	741	191	3.92
LAV14_14	0.90800	0.02900	0.10520	0.00210	0.96	9.50570	0.18975	0.06272	0.00081	-0.86	644.7	13.0	698.0	28.0	681	112	6.10
LAV14_15	0.54400	0.01700	0.06880	0.00220	0.91	14.53488	0.46478	0.05741	0.00087	-0.89	429.0	14.0	506.0	31.0	475	205	2.20

LAV14_16	0.49200	0.01700	0.06380	0.00190	0.99	15.67398	0.46678	0.05579	0.00036	-0.49	398.9	11.0	444.0	14.0	299	164.2	1.75
LAV14_17	0.58640	0.01600	0.07260	0.00190	-0.06	13.77410	0.36048	0.05830	0.00110	0.39	451.9	11.0	539.0	39.0	487	312	1.58
LAV14_18	0.39390	0.00890	0.05355	0.00090	0.99	18.67414	0.31385	0.05327	0.00033	-0.30	336.3	5.5	340.0	14.0	849	83.7	9.85
LAV14_19	0.85300	0.02300	0.09930	0.00190	0.90	10.07049	0.19269	0.06230	0.00054	-0.17	610.2	11.0	684.0	18.0	301	163	2.05
LAV14_20	0.58270	0.01400	0.07503	0.00140	0.80	13.32800	0.24869	0.05680	0.00041	0.05	466.4	8.3	484.0	16.0	445	276	1.77
LAV14_21	0.73900	0.02400	0.09180	0.00260	0.99	10.89325	0.30852	0.05867	0.00035	0.26	566.0	15.0	554.8	13.0	508	333	1.57
LAV14_22	0.63700	0.01500	0.08123	0.00160	0.92	12.31072	0.24249	0.05711	0.00037	0.14	503.5	9.3	495.6	14.0	572	52.11	10.85
LAV14_23	1.06500	0.03500	0.11400	0.00290	0.99	8.77193	0.22315	0.06799	0.00056	-0.88	696.0	17.0	868.0	17.0	337	167.9	1.97
LAV14_24	0.74100	0.01700	0.09030	0.00150	0.70	11.07420	0.18396	0.05981	0.00034	0.13	557.3	8.9	596.6	12.0	613	80.6	7.47
LAV14_25	0.60860	0.01500	0.07716	0.00130	1.00	12.96008	0.21835	0.05748	0.00038	-0.83	479.1	7.8	509.9	14.0	657	266.7	2.47
LAV14_27	0.40190	0.00970	0.05465	0.00092	0.67	18.29826	0.30804	0.05331	0.00046	-0.28	343.0	5.6	342.0	19.0	158	109	1.45
LAV14_28	1.65400	0.07100	0.15820	0.00620	1.00	6.32111	0.24773	0.07651	0.00042	-0.23	947.0	35.0	1108.4	11.0	723	209	3.27
LAV14_29	0.60400	0.06600	0.07440	0.00430	0.68	13.44086	0.77682	0.06250	0.00390	0.21	462.0	26.0	680.0	120.0	1440	180	7.93
LAV14_30	0.63800	0.02400	0.07970	0.00310	0.99	12.54705	0.48803	0.05879	0.00045	0.68	494.0	18.0	559.0	17.0	1490	833	1.73
LAV14_31	1.41800	0.09400	0.14260	0.00820	1.00	7.01262	0.40325	0.07208	0.00063	-0.91	859.0	46.0	988.0	18.0	551	166	3.25
LAV14_32	1.48400	0.03500	0.15306	0.00270	1.00	6.53339	0.11525	0.07044	0.00041	-0.75	918.1	15.0	941.2	12.0	362	35.44	10.18
LAV14_33	0.82200	0.03000	0.09760	0.00340	0.99	10.24590	0.35693	0.06108	0.00035	-0.02	600.0	20.0	641.9	12.0	363	264.1	1.40
LAV14_34	1.97400	0.06100	0.19010	0.00470	0.98	5.26039	0.13006	0.07496	0.00045	0.00	1122.0	26.0	1067.3	12.0	265	143	1.84
LAV14_35	0.69500	0.01900	0.08220	0.00280	0.96	12.16545	0.41439	0.06170	0.00100	0.97	509.0	17.0	662.0	35.0	1014	298	3.44
LAV14_36	0.61660	0.01700	0.07660	0.00180	0.94	13.05483	0.30677	0.05874	0.00048	0.42	475.8	11.0	557.0	18.0	354	200	1.87
LAV14_37	1.37500	0.05800	0.13220	0.00570	0.99	7.56430	0.32615	0.07561	0.00063	0.46	800.0	32.0	1085.0	17.0	472	157	3.15
LAV14_38	1.98200	0.05100	0.19090	0.00440	0.97	5.23835	0.12074	0.07591	0.00046	0.49	1126.0	24.0	1092.7	12.0	233	111	2.06
LAV14_39	0.87200	0.02700	0.10000	0.00240	0.77	10.00000	0.24000	0.06270	0.00110	0.35	614.0	14.0	696.0	36.0	546	214	2.52
LAV14_40	0.48300	0.04900	0.05620	0.00480	1.00	17.79359	1.51974	0.06230	0.00120	-0.86	352.0	29.0	695.0	35.0	770	52.3	14.33
LAV14_41	0.68200	0.02900	0.08330	0.00330	1.00	12.00480	0.47558	0.05956	0.00033	0.06	516.0	20.0	587.5	12.0	755	115	6.63
LAV14_42	0.45300	0.01000	0.05978	0.00100	0.96	16.72800	0.27983	0.05554	0.00041	0.22	374.3	6.1	434.0	16.0	1462	1041	1.40
LAV14_43	0.72200	0.01900	0.09050	0.00220	0.98	11.04972	0.26861	0.05798	0.00032	0.29	558.4	13.0	529.1	12.0	518	170	3.11
LAV14_44	0.62400	0.01900	0.07720	0.00200	0.96	12.95337	0.33558	0.05877	0.00031	0.12	479.6	12.0	558.5	12.0	1400	454	2.99
LAV14_45	2.02900	0.07200	0.19020	0.00450	0.82	5.25762	0.12439	0.07710	0.00110	-0.35	1122.0	24.0	1123.0	29.0	379	209.8	1.80

LAV14_46	0.70000	0.02100	0.08430	0.00180	0.92	11.86240	0.25329	0.06085	0.00057	-0.20	522.0	11.0	634.0	20.0	269	95.4	2.73
LAV14_47	0.61600	0.02700	0.07300	0.00230	0.87	13.69863	0.43160	0.06140	0.00120	-0.43	454.0	14.0	650.0	41.0	585	261	2.19
LAV14_48	0.66550	0.01600	0.07844	0.00140	0.97	12.74860	0.22754	0.06182	0.00041	0.32	486.8	8.2	667.8	14.0	928	250	3.73
LAV14_49	0.90900	0.07000	0.10230	0.00570	0.90	9.77517	0.54466	0.06450	0.00210	-0.25	628.0	34.0	757.0	67.0	1023	64	16.80
LAV14_50	0.43400	0.03900	0.05180	0.00200	0.82	19.30502	0.74537	0.06040	0.00350	-0.57	326.0	12.0	610.0	120.0	320	14.1	20.40
LAV14_51	0.89180	0.02100	0.10580	0.00180	0.99	9.45180	0.16081	0.06128	0.00040	-0.06	648.3	10.0	649.0	14.0	381	203	1.87
LAV14_52	0.57730	0.01400	0.07443	0.00150	0.92	13.43544	0.27077	0.05665	0.00036	0.32	462.8	8.9	477.9	14.0	1106	844	1.30
LAV14_53	0.70400	0.03500	0.07590	0.00550	0.97	13.17523	0.95473	0.06660	0.00140	0.76	472.0	33.0	825.0	44.0	700	195	3.54
LAV14_54	0.45100	0.02500	0.05340	0.00310	0.99	18.72659	1.08712	0.06142	0.00057	0.58	335.0	19.0	654.0	20.0	586	160	3.73
LAV14_55	1.42800	0.07900	0.14030	0.00780	0.99	7.12758	0.39626	0.07375	0.00067	0.38	846.0	44.0	1034.0	18.0	376	106.7	3.68
LAV14_56	0.41800	0.02100	0.03250	0.00230	0.90	30.76923	2.17752	0.09500	0.00470	-0.60	206.0	15.0	1512.0	93.0	980	480	2.65
LAV14_57	0.87900	0.02300	0.10700	0.00220	0.88	9.34579	0.19216	0.05996	0.00050	0.19	655.4	13.0	602.0	18.0	106	211	0.52
LAV14_58	0.44640	0.01100	0.05631	0.00130	0.37	17.75884	0.40999	0.05780	0.00130	0.10	353.2	8.2	522.0	49.0	228	247	1.03
LAV14_59	0.87200	0.02000	0.10398	0.00180	0.83	9.61723	0.16648	0.06109	0.00038	0.41	637.7	11.0	644.4	14.0	370	127	2.94

Table 5. U-Pb SHRIMP data for zircons from La Cabaña chromitite ores.

Spot	(1) 207Pb* /235U	1σ	(1) 206Pb* /238U	1σ	ρ	(1) 238U /206Pb*	1σ	(1) 207Pb* /206Pb*	1σ	ρ	(2) 206Pb /238U Age (Ma)	1σ	(1) 207Pb /206Pb Age (Ma)	1σ	U (ppm)	Th (ppm)	232Th /238U
CAB-71z6	2.150	0.069	0.186	0.003	0.537	5.3763	0.0968	0.0840	0.0023	0.0298	1090	19	1287	52	154	37	0.25
CAB-71z8	0.820	0.037	0.099	0.001	0.295	10.1010	0.1313	0.0600	0.0026	-0.0063	607	8	621	94	550	8	0.01
CAB-71z9c	1.320	0.054	0.144	0.002	0.376	6.9444	0.1042	0.0660	0.0025	-0.0105	871	13	810	79	293	329	1.16
CAB-71z9r	0.650	0.024	0.078	0.001	0.397	12.8205	0.1667	0.0610	0.0021	-0.0498	481	6	637	73	459	5	0.01
CAB-71z10	1.440	0.029	0.147	0.002	0.662	6.8027	0.0884	0.0710	0.0011	-0.0154	881	11	965	30	378	117	0.32

CAB-71z11	0.800	0.025	0.093	0.001	0.430	10.7527	0.1505	0.0620	0.0017	0.0242	572	8	691	60	304	453	1.54
CAB-71z12	5.830	0.111	0.346	0.005	0.775	2.8902	0.0434	0.1220	0.0015	0.0222	1907	28	1985	22	271	154	0.59
CAB-71z13r	0.550	0.020	0.071	0.001	0.330	14.0845	0.1831	0.0570	0.0019	0.0328	442	6	473	75	399	5	0.01
CA14-5z6	0.410	0.033	0.046	0.001	0.160	21.7391	0.3261	0.0640	0.0051	0.0278	287	4	755	167	319	8	0.03
CA14-39z1	0.420	0.019	0.050	0.001	0.409	20.0000	0.4000	0.0610	0.0026	0.0286	309	6	629	90	430	6	0.01
CA14-39z2	0.350	0.023	0.051	0.001	0.243	19.6078	0.3333	0.0490	0.0032	0.0113	324	5	153	152	470	240	0.53
CA14-39z2dup1	0.330	0.014	0.045	0.001	0.588	22.2222	0.5778	0.0540	0.0018	0.0385	281	7	374	76	848	24	0.03
CA14-41z8	0.540	0.026	0.067	0.001	0.445	14.9254	0.3284	0.0590	0.0025	0.0153	418	9	557	95	351	58	0.17
CA14-41z11r	0.590	0.022	0.070	0.001	0.328	14.2857	0.2000	0.0610	0.0021	0.0531	431	6	639	75	808	331	0.42
CA14-41z12c	0.410	0.018	0.057	0.002	0.641	17.5439	0.4737	0.0530	0.0017	-0.0174	355	9	315	75	535	149	0.29